Design, Modeling, Fabrication and Testing of a Piezoresistive-Based Tactile Sensor for Minimally Invasive Surgery Applications

Ahmad Atieh

A Thesis

in

the Department

of

Mechanical and Industrial Engineering

Presented in Partial Fulfillment of the Requirements

for the Degree of

Master of Applied Science in Mechanical Engineering at

Concordia University

Montreal, Quebec, Canada.

February 2012

CONCORDIA UNIVERSITY
School of Graduate Studies

This is to certify that the thesis prepared

By: Ahmad Atieh

Entitled: Design, Modeling, Fabrication and Testing of a Piezoresistive-Based Tactile Sensor for Minimally Invasive Surgery Applications

and submitted in partial fulfillment of the requirements for the degree of

Master of Applied Science in Mechanical Engineering

complies with the regulations of the University and meets the accepted standards with respect to originality and quality.

Signed by the final examining committee:

Dr. A. Dolatabadi	Chair
Dr. S. Narayanswamy	Examiner
Dr. A. Bagchi	Examiner
Dr. J. Dargahi, and Dr. M. Pakirisamy	Supervisor

Approved by _____

Chair of Department or Graduate Program Director

_____

Dean of Faculty

Date   April 15, 2012

ABSTRACT

Design, Modeling, Fabrication and Testing of a Piezoresistive-Based Tactile Sensor for Minimally Invasive Surgery Applications

Ahmad Atieh

Minimally invasive surgery (MIS) has become a preferred method for surgeons for the last two decades, thanks to its crucial advantages over classical open surgeries. Although MIS has some advantages, it has a few drawbacks. Since MIS technology includes performing surgery through small incisions using long slender tools, one of the main drawbacks of MIS becomes the loss of direct contact with the patient's body in the site of operation. Therefore, the surgeon loses the sense of touch during the operation which is one of the important tools for safe manipulation of tissue and also to determine the hardness of contact tissue in order to investigate its health condition. This Thesis presents a novel piezoresistive-based multifunctional tactile sensor that is able to measure the contact force and the relative hardness of the contact object or tissue at the same time. A prototype of the designed sensor has been simulated, analyzed, fabricated, and tested both numerically and experimentally. The experiments have been performed on hyperelastic materials, which are silicone rubber samples with different hardness values that resemble different biological tissues. The ability of the sensor to measure the contact force and relative hardness of the contact objects is tested with several experiments. A finite element (FE) model has been built in COMSOL Multiphysics (v3.4) environment to simulate both the mechanical behavior of the silicone rubber samples, and the interaction

between the sensor and the silicone rubbers. Both numerical and experimental analysis proved the capability of the sensor to measure the applied force and distinguish among different silicone-rubber samples. The sensor has the potential for integration with commercially available endoscopic grasper.

Dedicated to

My Beautiful Beloved Parents

ACKNOWLEDGEMENT

My first and last thank and grateful goes to the Almighty Allah who is no god but he of this universe, whom I submit my continuous gratitude hoping that it would be accepted.

Since who does not thank people does not thank God, I would like to thank my supervisors for their invaluable support, patience, and smooth guidance. Furthermore, I would like to thank the Faculty of Engineering and Computer Science for their financial supports.

The greatest thanks and grateful combined with the deep love and feelings that words are not enough to describe them are presented to my great parents. Their love, supports physically and spiritually was the reason behind my efforts, strength and smile. They always have been the source of happiness in my world. May Allah bless them and help me to award and satisfy them for the rest of my life.

The big thanks and warm feelings are given to the important people but the closest, adorable and appreciated ones. Those, who gave me love, supports, help, and all their other helpful feelings and actions. And for the unforgettable moments that I had with them through my life, ups and downs.

Furthermore, my thanks are extended to my sisters, brothers and family members in U.S.A, U.A.E, Jordan, and Palestine. They stand beside me to share the hard times as well as the happy ones with their warm feelings, words, and actions.

Moreover, special appreciation and thanks are presented to my friends, lab mates and my people in Montreal especially, and out of Canada generally. Without them, I wasn't be

able to keep on going. I am grateful for the grate time we had, pleasant, fun, and for the continuous help and support.

Finally, I am happy to have the chance to pursuing my M.A.Sc at Concordia University within the research groups of tactile sensing and medical robotics Laboratory, Optical-Bio Microsystems Laboratory, and ConSiM (Concordia Silicon Microfabrication facility). I would like to express my honest feelings toward all the members of these groups for the friendship, and assistants.

Table of Contents

List of Figures

List of Tables

Nomenclature

MIS	Minimally Invasive Surgery
MIRS	Minimally Invasive Robotic Surgery
DOF	Degree Of Freedom
FA	Fast Adapting
SA	Slow Adapting
Type I	Small Receptive Fields
Type II	Wide Receptive Fields
MEMS	Micro-Electro-Mechanical Systems
PVDF	Polyvinylidene fluoride
IPMC	Ionic Polymer-Metal Composite
DFSA	Deformable Force-Stretch Array
PZT	Lead Zirconate Titanate
CCD	Charge-Coupled Device
CMOS	Complementary Metal–Oxide–Semiconductor
AHC	Artificial Hair Cell
PDMS	Polydimethylsiloxane
DC	Direct Current
DAQ	Data Acquisition Card
PC	Personal Computer
FE	Finite Element
Det	Determinant

FEA	Finite Element Analysis
V	Version
2D	Two Dimensional
N	Newton
V	Volt
mm	millimeter
kΩ	kilo Ohm
Hz	Hertz
sec	Second

List of Symbols

R_t	Tunneling resistance
R_c	Constriction resistance
R_{tot}	Total resistance
L	Number of particles assembling one conductive line
S	Total number of active conductive lines
E	Young modulus
σ	Engineering stress
ε	Engineering strain
F	Force
ΔL	Change in length
C	Constant
l_o	Initial length
A	Initial surface area
$R.H$	Relative hardness
R_{film}	Resistance of the piezoresistive film
R_{const}	Constant resistance
V_i	DC input voltage to the voltage divider circuit
V_{out}	Output voltage of the voltage divider circuit
F_{cont}	Contact force
Fls	Reaction force at the left support
Frs	Reaction force at the right support

Xls	Conductance of the piezoresistive film underneath the left support
Xrs	Conductance of the piezoresistive film underneath the right support
δ_{beam}	Deflection of the elastic beam
X_{beam}	Conductance of the middle piezoresistive film
W	Strain energy function
$I_1, I_2, and\ I_3$	Principle invariants of the left Cauchy-Green deformation tensor
$\boldsymbol{S}$	Stress tensor
$\boldsymbol{A}$	Deformation gradient tensor
μ	Initial shear modulus
κ	Initial bulk modulus
J	Ratio of the current volume to the reference volume
C_{10}	Mooney-Rivlin constants
C_{01}	Mooney-Rivlin constants
ν	Poisson's ratio
δ	Deflection

Chapter 1 : Introduction and Related Work

1.1. Introduction

Humans contact the outside world through their five senses. Most frequently used senses are the sight and hearing, and touch usually comes after them. However, the usage of touch in our life is not less important than the usage of sight and hearing, although it is not noticeable as them. For instance, handling and orientating objects would be impossible without the sense of touch, where touch works in parallel with, or a little after, sight to accomplish the task.

The sensory receptors in human skin instantly convert and transfer information about our contact with the surrounding, allowing us to differentiate between contact objects based on their size, temperature, shape, and texture. Having this information, one is able to identify the proper contact pressure needed to handle an object with a great dexterity. Therefore, the loss of this sense limits one's knowledge of the surrounding crucially [1], especially in the cases where the surrounding constraints would break down the vision sense. A practical example of such a case, where the vision sense is limited, is the heart surgery in which Minimally Invasive Surgery technique is used. Due to the importance of the tactile information transferred by the sensory receptors, many researchers have focused on improving tactile sensors and displays to help in recovering the loss of touch in different applications.

This thesis presents a novel multifunctional piezoresistive-based tactile sensor for MIS purposes. The research aims to develop a suitable tactile sensor for MIS that would provide the magnitude of contact force and the relative hardness of contact object or tissue, which can be used in handling and distinguishing the contact objects or tissues.

1.2. Minimally Invasive Surgery (MIS)

Recent developments in materials science, micro-mechanical science, and manufacturing have allowed surgeons to use special accurate surgical instruments and robotic equipments in order to perform complicated surgeries through very small cuts "ports" [2]. Such an operation is known as Minimally Invasive Surgery [3] (Figure 1.1). Depending on what part of body is under surgery, MIS is categorized as laparoscopy, pelviscopy, thoracoscopy, angioscopy, etc. The typical category of MIS that has the largest number of operations is laparoscopy field that includes belly and pelvic organs [4, 5]. MIS is performed by the use of small cameras and long-shaft tools (around 30 cm in length, and 2-7.5 mm in radius) that are inserted into body through small cuts to reach the operated organ. Figure 1.2 shows a typical endoscopic tool that is used in different fields of MIS. Medical devices companies have made various endoscopes that are suitable for specific operations, such as thoracoscope that is used for the examination of the chest area, and the laparoscope that is designed to be used in abdominal surgeries. In a laparoscopic surgery, as illustrated in Figure 1.1, the surgeon uses Carbon Dioxide to expand the patient abdomen. Metal tubes with pneumatic check valves (known as Cannulas) are placed using small incisions [6] to serve as an entrance for the MIS endoscopes and tools such as the endoscopic grasper. Then, the surgeon inserts the MIS tools through the

cannulas and handles them in the site of the operation by pushing them in and out or rotating them roughly around the small incisions. A monitor displays a view of the workspace provided by the endoscope, which helps the surgeon perform the surgery.
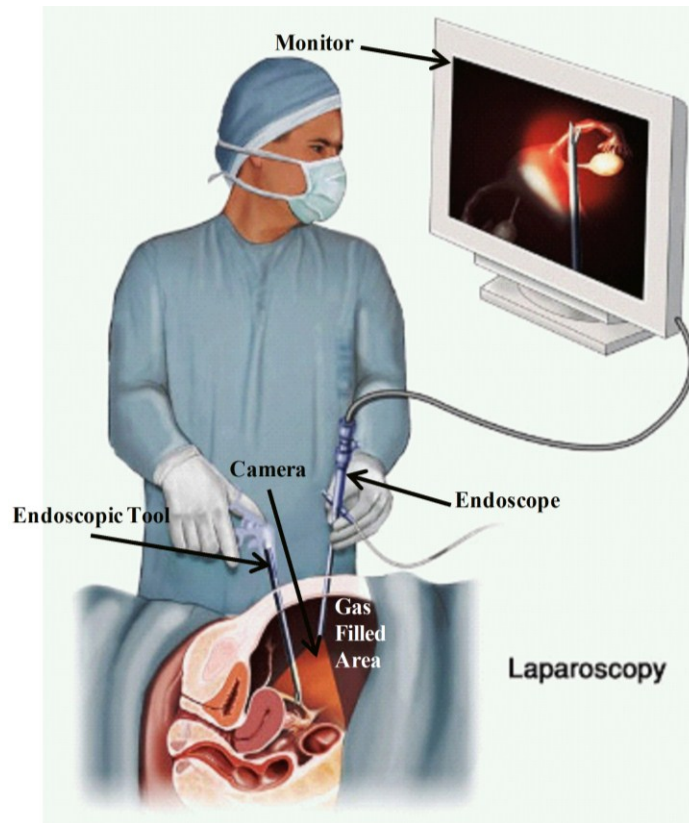
Figure 1.1: Illustration sketch for minimally invasive laparoscopy procedure[7].
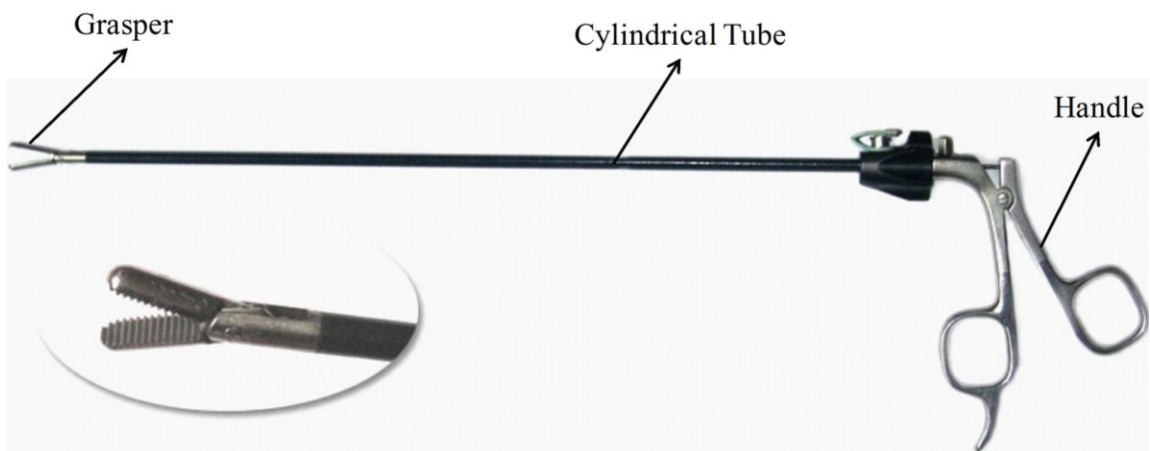
Figure 1.2: Endoscopic tool [8].

The history of MIS goes back to almost a century ago, when it was confined to some endoscopic investigations in the abdomen area due to the limitations in the available medical tools and equipments [6]. With the developments in materials science and manufacturing, it became possible to perform more complex surgeries using MIS technology. The first laparoscopic appendectomy surgery and the first laparoscopic cholecystectomy surgery were performed in 1981 and 1985, respectively [6]. These two operations represent the beginning of a new age for the MIS. The great advances of the MIS technology seen in these two operations opened the door to general surgeons to apply the MIS technique in their fields using modified tools and endoscopes. Rapidly, more and more complex operations were added to the list of MIS surgeries [9]. Partially, the rapid extension of MIS applications is attributed to the considerable incite of the medical contributors and their institutions to present MIS to other medical fields. Moreover, surgeons realized that MIS reduces both the hospital stay and hospital costs, in addition to other great benefits of MIS over the classical open surgeries [10]. For instance, the classical open surgeries need large incisions that allow the surgeon to view the site of the surgery clearly and handle the tissues and instruments freely. Most of the times, the large incisions, which could include injury of connective tissues, muscles, or bones would harm the patients much more than the operation itself. Consequently, the patients would suffer of more pain, longer stay in hospital, and larger possibility for infection, for example, eradication of a kidney via open surgery includes an incision that require 5-7 days hospital stay for recovery plus 6-12 weeks at home to return to normal activities. MIS limits all of these disadvantages of open surgeries by replacing large incisions with small ones (less than 0.5 inch) [11].

MIS offers many other benefits over open surgeries: less injury results in better cosmetic outcomes and less bleeding; MIS reduces patient's post operation pain; shorter recovery time results in a quick return to life activities; MIS reduces difficulties and possibilities of infection in post-operation stage; less stay in hospital results in reducing the costs and increases the availability of beds in hospitals; and finally it improves clinical outcomes [12, 13, 14, 15, 16]. The surgeons expert in MIS procedures usually require the same period of time to perform either MIS operations or the corresponding open operations [14].

The MIS technology in medical field has attracted many researchers over the past twenty years, since MIS has been able to replace classical open surgeries in almost all surgical disciplines [2]. Moreover, many researchers have focused on MIS because of its promising results [17]. Therefore, MIS has become the most popular method for detection and treatment of cancer, which is predicted to be the single most agent of death in the world in the near future [18]. Also, it is reported that MIS could give the same or improved results compared to the classical open surgery for heart valve replacement [19]. Additionally, there has been an effort to replace the multiple-port MIS operation with a single-port operation [20]. In Minimally Invasive Robotic Surgery (MIRS), a new branch of MIS, medical robots are used, which are controlled by the surgeon, using either a tele-manipulator or a computer, to perform the MIS operation. Main advantages of the MIRS are: increasing the dexterity of handling the instruments, performing complicated and sensitive surgeries precisely, eliminating some undesirable vibrations that could happen by surgeon's hand, and finally open the door for remote surgery or telesurgery. Telesurgery allows surgeons to perform operations on patients in other places, for

instance a surgeon can perform a transcontinental surgery on a patient who is far away from him, or even for a patient in a spaceship that in a mission on the lunar surface. Telesurgery can be improved to provide health care and support for such cases [9].

Despite the abovementioned improvements and advantages of MIS, it has some significant shortcomings. Current MIS technology suffers of [14, 16]: (1) the view of the surgical site is reduced from a three dimensional to a two dimensional view, (2) the degree of freedom available for the surgeon to orient and handle both the instruments and biological tissue is reduced from 6 DOF to 4 DOF, and (3) the loss of touch sense. Since in MIS the surgeon's hands are outside the site of operation, it is considered as a teleoperation application, where direct contact with the object is lost [21]. This main shortcoming is a limitation for expanding the MIS applications and improving the MIS performance. Essentially, surgery relies on vision and touch; so, any constrains on these senses of the surgeon must be thought about. For example, palpation is one of the routine procedures in many surgeries, where the surgeon in open surgeries passes his hand over the tissue to investigate if there is any abnormality or tumor hidden in the tissue. Palpation is a common practice since it is known that tumors are harder than surrounding healthy tissues, and tissues composition usually changes under the effect of different illnesses [22]. Unfortunately, in MIS the surgeon is not able to insert his hand through the small incisions to palpate the tissues. However, surgeons have found alternative palpation methods, such as inserting a metal rod through the incision to detect the abnormalities. Though, any deep tumors will be hardly detected with this method, and extensive training is needed to avoid mistakes and harms to the tissue [23]. Moreover, the metal rod method is not suitable for all MIS surgeries especially those near sensitive tissues such as brain.

Additionally, the loss of touch in MIS could arise in cardinal safety issues, since hidden arteries included in a tissue and soft tissues need special treatment. Extra force applied to soft tissues may lead to a serious damage in that tissue, and hurting hidden arteries could cause dangerous bleeding [21, 24, 25]. This is why surgeons nowadays need to have extensive training in performing MIS surgeries. In some cases, such as brain surgeries, additional techniques are needed, for example, MRI and CT images. Those images are taken prior to the operation to be used as a guiding map during the operation [18, 26, 27]. For instance, surgeries including the removal of cancerous tumors are considered to be a complicated mission [26]. Hence, the cancerous tumor should be completely removed in order to ensure a full recovery of patient's health, and expanding the time needed for the tumor to revert up to the maximum. Moreover, the surgeon should treat the healthy surrounding tissues very carefully to avoid any damage or extra cut. Particularly, the tumor size should accurately match the cut boundary in neurosurgery cases. Otherwise, serious disabilities could occur because brain tissue would have some shifting after opening the skull due to pressure change, and so the previously taken images of MRI or CT are no longer accurate [26, 27]. Nowadays, surgeons perform these surgeries with the help of imaging techniques before the surgery and the extensive training which are expensive, time consuming, and inaccurate solutions.

MIS apparently is the fastest growing area of research, from an engineering point of view, where the use of tactile and vision senses have critical influence [9]. Furthermore, for a safe treatment of soft biological tissues, it has been stated that the distribution of forces applied to these tissues by an MIS tool (e.g. grasper) should be measured [28]. Therefore, most of the problems associated with MIS can be greatly reduced or even

solved if a bio-comfortable, accurate, multifunctional, and in-vivo tactile sensor is used on the tips of MIS tools such as endoscopic grasper. Such a tactile sensor will replace the sense of touch in the surgeon's hand and give a precise feedback to the surgeon, while the surgery is being performed. It provides the surgeon with important information about the contacted tissue regarding its relative hardness, and contact force. If the feedback from tactile sensors is integrated with the available visual feedback, then it will improve the MIS efficiency and expand its applications. It is important to note that the features of soft tissues alter when they are detached from body; therefore, the sensor should be able to work in-vivo that also would reduce the time needed to do the operation. In summary, a tactile sensor would have a great influence on MIS efficiency. To introduce a suitable tactile sensor, tactile sensing is discussed in the following sections.

1.3. Tactile Sensing Definitions and Applications

Tactile sensing could be defined as the assessment of vertical forces distribution over a specified sensory field and the consequential understanding of this distribution [29]. A tactile sensor measures and evaluates the properties of an object by means of physical contact [30, 31]. Consequently, the job of a tactile sensor is to evaluate the physical parameters of contact between the tactile sensor and the sensed object and analyze these parameters to identify some of the physical properties of the object. Information gathered by tactile sensing includes the detection of the contact with an object, the magnitude of the applied force, determination of the hardness of an object or tissue, and the surface texture of the object or tissue [32].

A tactile sensor is ideally desired to be used in minimally invasive surgery to replace a surgeon's hand. Among many fields in which tactile sensing is used, minimally invasive surgery, minimally invasive robotic surgery, and robots for industrial and space applications are the most absorbing fields for tactile sensors [33]. Tactile sensing is a fundamental need for the improvement of many fields such as virtual systems, robotic manipulators, tele-operations and medical applications. Indeed, the use of tactile sensing extends to many fields in industry, such as food processing and agriculture [34, 35].

1.4. Human Hand Tactile Perception

Since tactile sensing is defined by the haptic functionality of a human finger and in order to develop an artificial tactile sensor with sensing facilities similar to those of the human hand, it is important to understand the structure, units of sense, principles of work, and the sensing facilities of the human hand. A human finger tip is able to sense texture, temperature, pain, softness, shape, force, vibrations, and many other physical properties [36, 37]. All of these properties are forms of tactile sensing of the human hand. Considering the various forms of tactile sensing that human finger detects, the logarithms and mechanisms that is used in the human hand would be much more complex than direct conversion of a physical property to a nerve impulse [35]. Moreover, our understanding of the human touch is not in the same level of our understanding of the human vision and hearing, and in terms of applications researchers in tactile sensing are working with the basics of tactile measurements [38, 39]. Overall, the human touch sense system is a complex system and it is not a simple mission to mimic this system into industrial devices [1, 40].

The skin of the palm of a human contains 17000 mechanoreceptors of four different types, and countless number of free nerve terminations [41, 42]. These sensors in the skin are sensitive to different physical properties. The hand's skin, specifically, is well prepared to render tactile feedback very accurately [43]. With these sensors, the human hand is capable of transferring tactile information with speeds less than 60 m/s. The fingertip can sense the deformation starting from 0.07 mm up to 5 mm [10, 44]. It can distinguish between two points of oscillation stimulation (i.e. spatial resolution), if the minimum distance between them is 1-2 mm [45, 46]. The pain stimuli are fired for a pressure of 1.3 MPa [44]. The skin can detect oscillations as long as their frequencies are less than 1000 Hz [47]. Force measuring of the skin is in the range of 0.01-10 N [34]. In summary, the human tactile sensing is very sensitive, and it includes sensors that are nonlinear, time varying, and slow, and it is able to detect various physical properties.

A tactile sensor should contain a set of small sensors with similar criteria to finger ones. Their principles should be extracted from investigating human skin. In terms of analogy, this set should achieve equivalent high sensitivity, sensibility of various physical properties, spatial resolution, force sensitivity range, deformation sensitivity range, speed of data transformation, pain recognition, and sensibility of static and dynamic stimuli with similar range of vibration. However, a hard capability to be mimicked in a tactile sensor is the skin's sensibility to vibrations [9]. The response time of the small sensors should be as fast as possible. This is a result of considering the use of an artificial complex processing unit, integrated with the tactile sensor to analyze the provided data, and the continuous need for the updated data. In addition, the tactile sensor should be prepared for harsh condition use to stay unaffected regardless of the harsh environment,

repeated impacts, or continued usage. Furthermore, the tactile sensor should be designed to attenuate cross-talking.

The haptic sensing in humans includes the use of two main classes of sensing [48]: Kinesthetic Sensing and Cutaneous Sensing. These two modes of sensing are discussed below.

1.4.1. Kinesthetic Sensing:

Kinesthetic Sensing, also called "Proprioception", is a kind of sensing that provides humans with the data related to geometric, kinetic, joints position and velocity, and acting force of the shrunken muscle. Kinesthetic along with vestibular sensing keeps tracking the body position and motion [49, 50, 51, 52]. Kinesthetic information is collected by sensory receptors located at the muscles, joints, and capsules. Examples of these receptors are the muscle spindles and Golgi organs (tendon organs) [53].

1.4.2. Cutaneous Sensing:

Sensory receptors of this form of sensing are called "Mechanoreceptors" and they are located in the skin in different layers. The function of cutaneous sensing is to recognize the contact information, such as vibration and force, in space and time, using the mechanoreceptors as the sensing elements. One of the unique properties of human skin is its spatial resolution, and human anatomy has proved that spatial resolution of the skin has different values in different parts of the human body [34], Figure 1.3.

Many researchers have studied the functions of Cutaneous sensing [1, 54]. Mechanoreceptors in the skin form a complex array that is heavy-duty but very sensitive.

The mechanoreceptors are categorized into four types [40, 55] which are linked to individual specific feelings: shear, texture, oscillation, and pressure [40]. The common feature of these four types is that their sensing elements are placed in the skin and physically packaged in a way that is particularly accommodated to their functions.

However, based on the adaptation type of the mechanoreceptors, they have been separated into two categories: fast adapting (FA) and slow adapting (SA) [56]. The FA (Meissner and Pacinian) category feels the skin indentation caused by an oscillated stimulus, but not a static one. On the other hand, the SA (Merkel and Ruffini) category feels the static indentation of a static stimulus. Piezoresistive and piezoelectric sensing elements are equivalent to SA and FA categories, respectively [56]. Another classification for mechanoreceptors is dividing them based on their receptive field properties [57, 58]: Type I (Meissner and Merkel) that has small receptive fields and is located closer to the skin surface, and Type II (Pacinian and Ruffini) that has wide receptive fields and is located in the dermis [10, 58],

Figure 1.4.

Sensing the force is one of the contact properties that is important to be measured between MIS tools and soft tissues [28]. If a force is applied to the fingertip of a human, then all the Pacinian corpuscles (FA II) (PC) in fingers and the palm will flash discrete signals announcing that a stimulation is happening somewhere. Accordingly, FA I receptors (Meissner Corpuscles) around the place of the applied stimulus will flash too. Whenever the stimulus continuously act on the same place both SA I (Merkel disks) and SA II (Ruffini endings) will respond by producing discrete signals [9]. For softness

sensing that is important for MIS and MIRS application, softness sensing is considered to be connected with the SA I, since their rate of sparking depends on the magnitude of the static indentation. Recognizing the softness will require vertical motion [37]. It is important to note that the recognition of the object's stiffness requires the combination of both cutaneous sensing and kinesthetic sensing [48].
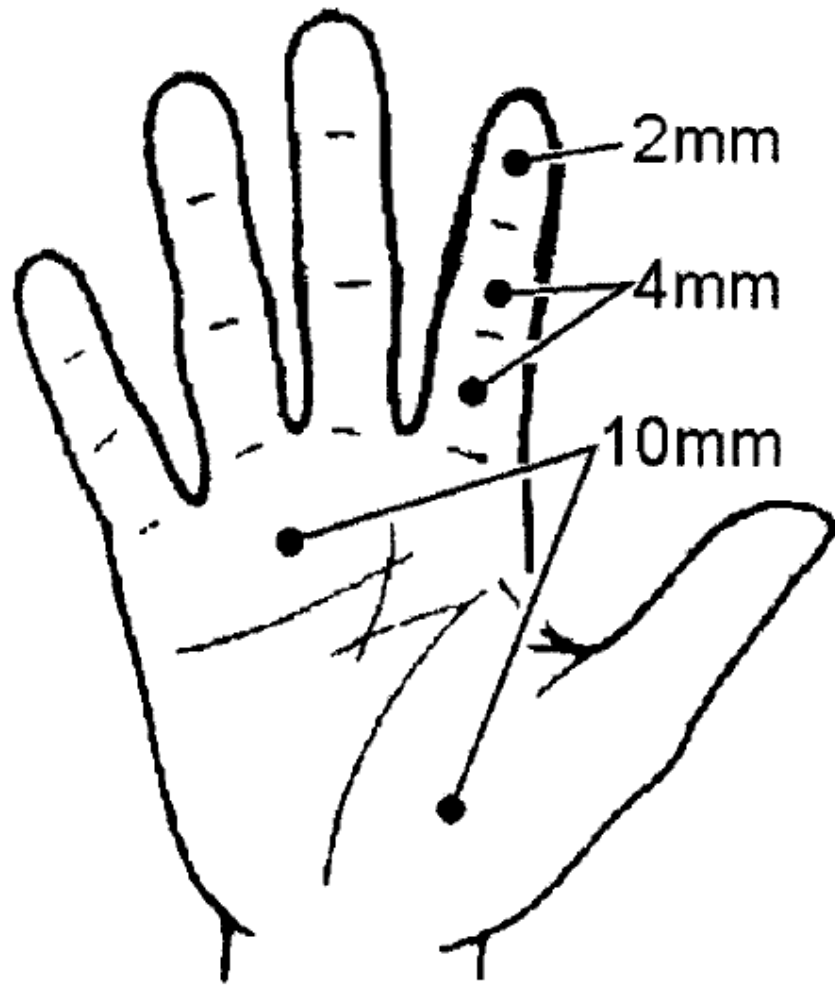
Figure 1.3: Spatial resolution in human hand [10]

In both MIS and MIRS fields, surgeons frequently deal with soft tissues that exclusively can be accurately examined and identified by their softness, elasticity properties, and viscosity [59, 60]. Furthermore, in MIS applications, some tactile sensing types are required to be measured more than others for the purpose of medical treatment. For example, tissue softness and contact force among other tactile sensing types have a great influence in improving the MIS, while temperature sensing does not have the same influence. Considering these reasons, MIS is one of the important fields where tactile sensing has an important and efficient application. Therefore, future MIS tools should be developed by adding built-in tactile sensors, which will replace the surgeon's hand's functionality. Such developed tools will increase the safety and accuracy of MIS operations. Since MIS is a critical procedure that requires accurate actions, the associated sensors in future MIS tools should be sensitive and precise [61], range in micron to few millimeters [59]. Due to the small size of the MIS tool end-effecter, these tactile sensors should be small and able for microfabications. Additionally, they are preferred to be economic and disposable. Required types of tactile sensing in MIS are presented in the following section.
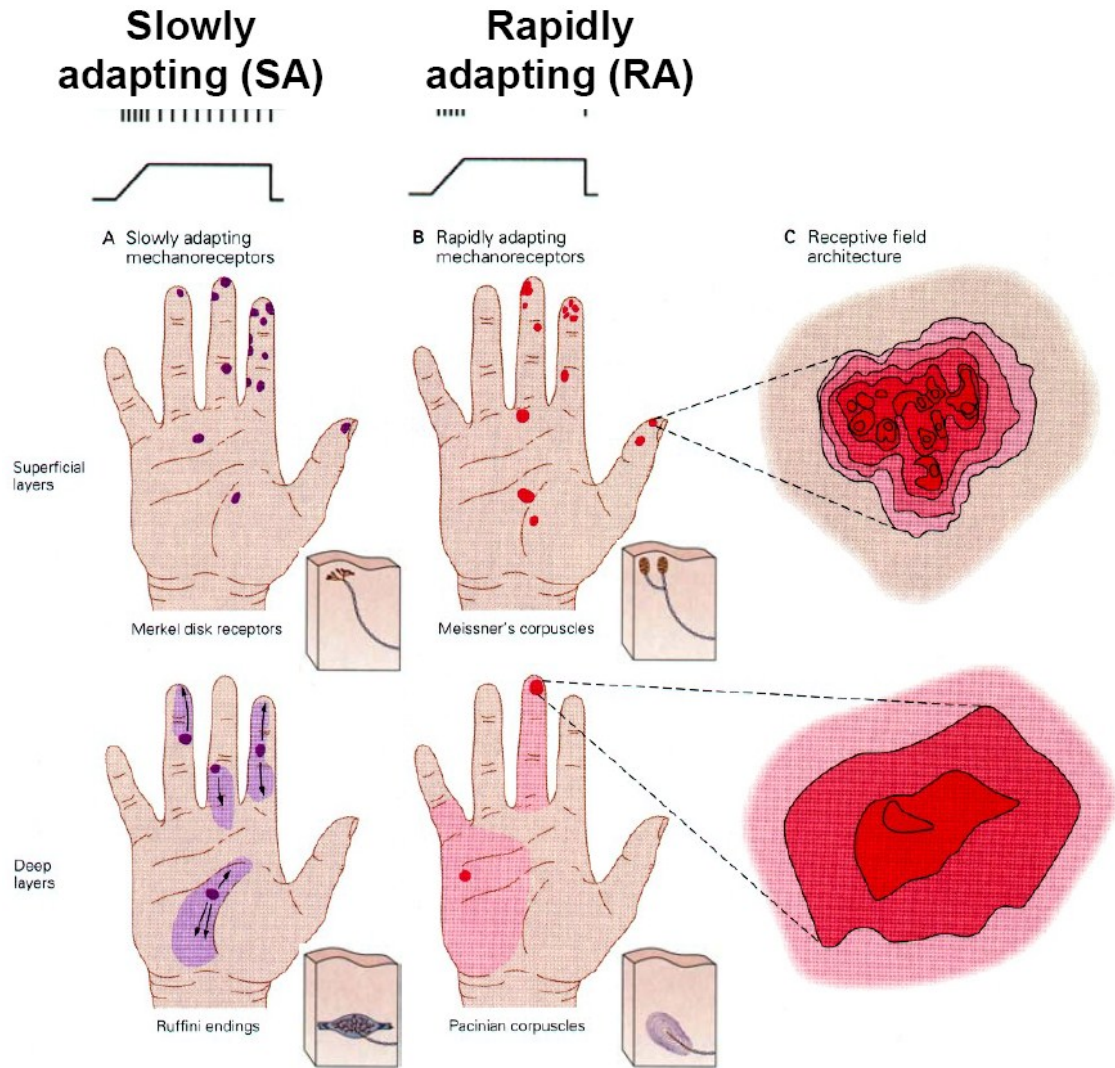
Figure 1.4: Mechanoreceptors categories and their properties [62]

1.5. Artificial Tactile Sensing in MIS

If an industrial tactile sensor is to replace the surgeon's hand in MIS, ideally, it should be able to measure all the various types of tactile perception that the hand can sense. This may include temperature, texture, force, softness, vibration, pressure, pulses, etc. Accordingly, a perfect developed MIS tool would be able to sense and measure all these various types of tactile sensing. In that case, surgeons will be able to measure and feel, if

a suitable tactile display is provided, all types of tactile sensing a human hand can detect. Practically, surgeons usually need to feel contact force, softness, palpation, and texture more than other tactile sensing types. Therefore, a practical tactile sensor included in an MIS tool should be able to sense and transfer magnitude of applied force and the softness of the tissue to the surgeon. In summary, MIS tactile sensors are preferred to be able to provide force sensing, force position, lump detection, and softness sensing.

1.5.1. Force Sensing

Force sensing has been inspected and studied in depth, since it is the main property that a tactile sensor should measure. Therefore, many well-defined and commercially available force sensors have been presented. These force sensors measure different types of forces: concentrated, distributed, static, and dynamic forces. The sensing principle of these sensors alters between piezoresistive, piezoelectric, optical, and capacitive, or a combination of these principles [1, 35, 63, 64].

1.5.2. Force Position Sensing

In a soft object/tissue, a hidden abnormality acts as a concentrated force contained in a distributed load, if this object/tissue is compressed uniformly [9, 65, 66]. However, if the uniformly compressed soft object is homogenous, it will exhibit a uniform distributed load on the surface of compression. Therefore, force position sensing is of great help in MIS, where it could be used to locate hidden lumps or abnormalities in grasped soft tissues. Many researchers have studied this type of sensing and they are discussed in the literature review section [13, 31, 65, 66].

1.5.3. Softness Sensing

Softness sensing is one of the most important required tactile sensing for MIS applications, since different types of tissue can be distinguished based on their physical properties such as their modulus of elasticity, and softness [66, 67]. In order to perform an operation safely, it is important to distinguish between soft tissues. The surgeon should be able to find out what type of tissue is being cut, if it is muscle, vessel, or fat, before making the cut. Identifying the treated tissue would avoid any dangerous consequences. For instance, if the surgeon does not identify a nerve and mistakenly cuts it, then the patient my lose control of motion, or lose the sense of that part. Furthermore, it is well-known that cancerous tumor is generally harder than the surrounding healthy tissues [17, 68, 69]. Therefore, measuring the relative hardness of a grasped tissue would extremely help identifying any abnormality in the tissue. The identification would be based on comparing its softness to other surrounding healthy tissues.

Softness of a soft object is described as the resistance of the object material for indentation [70, 71]. In order to measure the softness of soft materials such as soft tissues, their physical behavior should be considered. For the soft tissues, they are characterized as viscoelastic, nonlinear and hysterical response materials. Complication of this issue increases due to the fact that different soft tissues have different characteristics. In addition, the characterization of soft tissues alters considerably from *in vivo* to *ex vivo* conditions. This can be referred to both the essential change in the testing conditions such as temperature and water content, and to the fact that tissues inside the body normally are under tension.

Various methods have been developed to measure the softness of soft objects. The most familiar and certified method for softness testing is the Durometer test, or shore test. This method uses a pin, with a specific geometry connected to a known-stiffness spring, to apply an indentation toward the targeted object. The object's resistance to this indentation (softness) is proportional to the penetration of the pin in the object. This test provides experimental hardness value, which is not connected clearly in a mathematical relation to the other material properties. There are many different shore hardness scales for this method; they have been distinguished based on the hardness of the tested objects, the indenter geometry, or other test conditions. The most commonly used scales for soft objects are shore A, shore D, and shore OO. Shore A is used for soft rubbers, while shore D is used for harder rubbers and shore OO for the very soft ones [71]. Nevertheless, the modulus of elasticity of a material is related nonlinearly to the softness of the material. Modulus of elasticity of a soft object expresses the spring stiffness that the object would act against its indentation. Some researchers have developed different methods to measure the softness of soft objects. For example, Omata [72] implemented the piezoelectric material in its natural frequency to find the relative hardness of the tested object depending on the shift in the natural frequency. Furthermore, Bajcsy [73] implemented a tactile sensor on the tip of a robotic finger, then used the robot to apply several defined steps against the tested object. At each step the tactile sensor reading was recorded.

Major types of tactile sensing that are required for MIS applications have been discussed. However, all of these types were implemented in tactile sensors using different sensing

principles and materials. Different types of sensing principles/material that are used in tactile sensors are discussed in the following section.

1.6. Tactile Sensing Transduction Principles

Improvements in automation and micro-electro-mechanical systems (MEMS) have enabled researchers to produce various tactile sensors [31]. The design of any tactile sensor is decided by two main considerations: the field of use and the type of tested objects [63]. If the tested objects are selected to be soft object, as it is the case in this study, the design would be more complicated. Generally, tactile sensors can be classified based on their sensing principle. The most common categories are Piezoelectric Sensors, Capacitive Sensors, Optical Sensors, Magnetic Sensors, and Piezoresistive Sensors [74]. The working principle of these sensors is discussed in the following section.

1.6.1. Piezoelectric Sensors

If a piezoelectric material is exposed to an electrical input, it will experience some mechanical deformations. On the other hand, if the material is under mechanical deformation, it will accumulate an electrical charge. This material property has many industrial applications. For instance, polymeric piezoelectric materials are suitable for tactile sensing applications [75, 76, 77].

Piezoelectric sensing elements can exhibit small deformations compared to other elements due to the fact that piezoelectric materials generally have a large stiffness in comparison to steel. The rigidity of this material results in a high natural frequency, which is helpful for high speed measurements [75, 77].

Polyvinylidene fluoride (PVDF) is one of the most commonly known and used piezoelectric polymers. PVDF is commercially available in sheets with thickness ranges from 5 micron to 2 millimeters. Both sides of PVDF sheets are metalized to work as electrodes, which will cluster the produced charges that appear as voltage difference [77].

In addition to the abovementioned features of piezoelectric materials, PVDF particularly shows high sensitivity, high mechanical strength, and an active response to various frequencies [75, 77]. The main disadvantage of piezoelectric sensors is that they can only sense dynamic stimuli with high frequencies. Therefore, for a dynamic load with a low frequency piezoelectric sensors are not sensitive enough. Additionally, piezoelectric sensors require a complex electrical circuit for signal conditioning and have no DC response. In addition, they are sensitive to external noise since they have different sensitivity depending on the direction of applied stress. Moreover, they are very sensitive to temperature due to their pyroelectric effect that cannot be isolated from the piezoelectric effect [78, 79].

Although piezoelectric materials suffer from not responding to static forces, many researchers have used them in developing new tactile sensors [9, 13, 80, 81]

1.6.2. Capacitive Sensors

Similar to other capacitors, a capacitive sensor mainly consists of two thin plates separated by a dielectric media. The plates are usually made of metal or quartz coated by metal. One of the plates is subjected to a pressure, while the other plate is fixed. As a result of the pressure the corresponding plate will bend and the distance between the plates will change. Since the capacitance is inversely proportional to the distance between

the plates, the capacitance will change based on the change in this distance. The change in capacitance can be measured experimentally. Therefore, one can find the applied pressure by correlating it to the change in capacitance [75, 76]. Practical examples of recently developed capacitive tactile sensors can be found in [82, 83].

The major advantages of capacitive sensors are the simplicity of their structure, active response for static and dynamic stimuli, small sizes, little weight and low cost. Despite these advantages, capacitive sensors suffer of some disadvantages, such as sensitivity to temperature and humidity, sophisticated signal conditioning circuit, and high impedance [75].

1.6.3. Optical Sensors

The advances in optical technology resulted in producing a variety of optical tactile sensors. In general, optical sensors rely on measuring the change in the light optical properties, which are intensity, polarization, phase, wavelength, and spectral distribution. Any optical tactile sensor follows one of the two operating principles: Intrinsic, and Extrinsic. In extrinsic sensors the change in the light property due to the light interacts with the stimulus out of the light path. In other words, in extrinsic sensors the light would leave the feed fibre and change due to the interplay with the stimulus before it returns via the receiving fibre. While in intrinsic sensors, the light continuously passes through the fibre without leaving it and the interaction with the stimulus occurs within the fibre, which is connected all the way from the emitter to the receiver [84, 85]. Figure 1.5 shows a schematic explanation of the two operating principles of optical sensors. Additionally, some optical tactile sensors developed by researchers are shown in [61, 86].

Optical sensors have many advantages over other common sensors. These advantages are: electromagnetic immunity, amenable for multiplexing, great ability for miniaturizing, resistivity for rough environments, lightness, flexibility, electrical isolation, and the use of low power light [61]. Nevertheless, some major drawbacks are correlated to optical sensors such as their sensitivity to vibrations, which could be a typical noise in any application causing some inaccuracy in the measurements. Another drawback is the need to use an expensive light emitter and receiver.

(a)

Light Source

Light Detector

Feed Fibre

$\longmapsto l \longmapsto$

Return Fibre

(b)

Pressure

A

Light Source

Fibre

Light Detector

B

Pressure
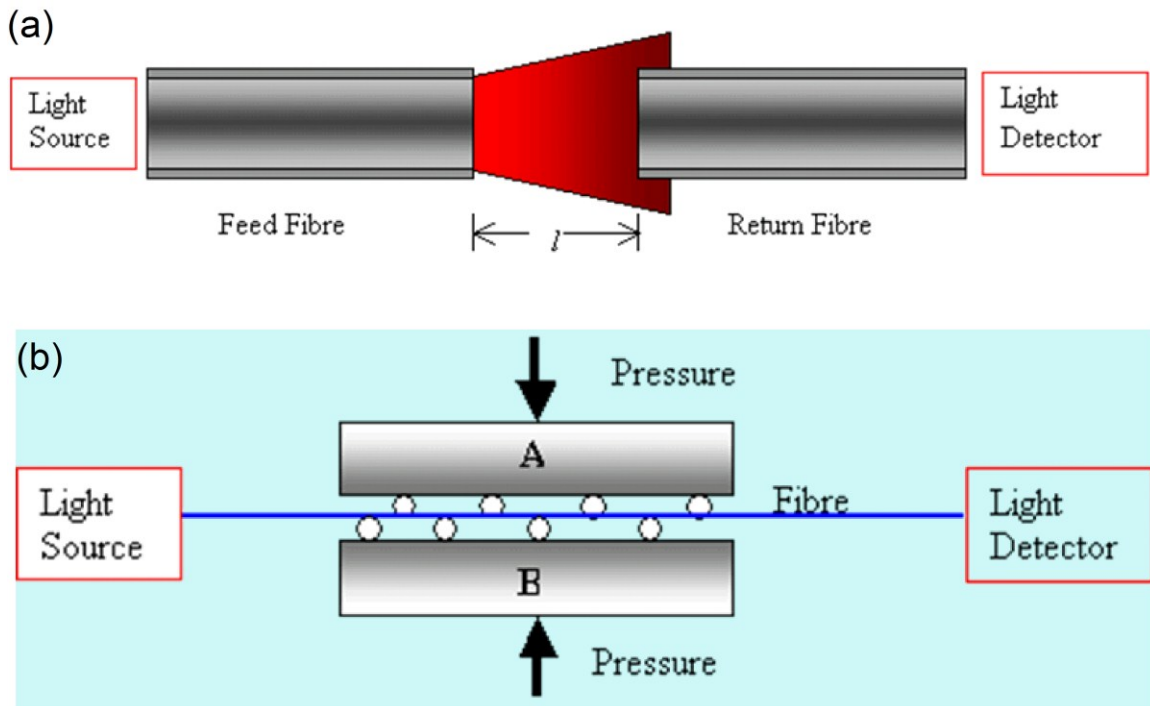
Figure 1.5: The operating principles of optical sensors (a) Extrinsic principle optical sensors. (b) Intrinsic principle optical sensors [87].

1.6.4. Magneto-Resistive Sensors

The major component of this sensor is the magneto-resistive material. If such a material is introduced to a magnetic field, it will exhibit changes in electrical resistance. Magnetic

sensors correlate the quantities required to be measured to the variation in the magnetic field. The most common principles used in magnetic sensors to measure the changes in the magnetic field are Hall-effect, and magnetoresistance. Both principles are related to current-carrying conductors [76, 79, 88].

The Hall-effect principle means that if a current-carrying conductor is subjected to a magnetic field perpendicular to the current flow, the conductor will produce a voltage proportional to the magnetic field intensity and perpendicular to both the magnetic field and the current flow; this voltage is called Hall voltage. The value of this voltage indicates the change in the magnetic field that is related to the measured physical quantity. On the other hand, the magnetoresistance principle says that a change in the resistivity of the current-carrying conductor occurs due to applying a magnetic field to the conductor perpendicular to current flow. Generally, the electrical resistivity of magnetic materials decreases when the magnetic field, perpendicular to the current flow, increases [79].

Although the magnetic sensors are characterized by their sensitivity, wide dynamic range, contactless operation (long life), and insensitivity to dust and humidity, they suffer from nonlinear response, sensitivity to temperature and external magnetic fields, mechanical pressure, and they are usually limited to small distance applications [88].

1.6.5. Piezoresistive Sensors

Piezoresistive effect is that the resistivity of a material changes due to applied pressure or mechanical stress [79]. Sensors that utilize this effect branch into different types such as conductive elastomer (semiconductive polymer), carbon fibre, and strain gauges [79, 89].

Piezoresistive sensors require the use of electrical circuits to accomplish the sensing task, in which the piezoresistive material is a variable resistance. These electrical circuits (e.g. Wheatstone bridge and voltage divider) are used to measure the change in the resistivity of the piezoresistive material [78, 79, 89]. Some examples of these types of tactile sensors are demonstrated in [90, 91, 92].

Conductive elastomers are elastic materials (e.g. polymers) infused with conductive powder or fibre (e.g. metal and carbon black). As a result, conductive elastomers undergo large deformations, and show electrical conductivity. If a compression load is applied to a conductive elastomer, its resistivity will change depending on the applied load. The change of the resistivity is referred to either the increase in the contact area between the electrodes and the conductive elastomer, or to the decrease in the thickness of the conductive elastomer. Therefore, these materials are suitable for pressure sensing. Conductive elastomers are featured by their resistivity to corrosion, high temperature, and chemicals. Additionally, they are capable of admitting heavy overloads, enduring fatigue, and can be miniaturized to micro level sizes. In addition, conductive elastomer sensors are cost effective and can be used individually or in arrays. Moreover, semiconductive polymers, in particular, show fast response to dynamic and static stimuli, and reduce the external noise effects. Despite these advantages conductive elastomers exhibit hysteresis and creep [78, 79, 93]. The relation between the applied pressure and the change in conductive elastomers resistance is not linear.

Carbon fibres are prepared by carbonizing organic fibres. The fundamental components in the structure of carbon fibres are fine cylindrical bundles of microfibrils. Figure 1.6 shows the carbon fibre structure. When a compression load is applied to carbon fibre, its

resistance would change in three stages. First the number of contact points between microfibrils in the bundle increase and cause the maximum change in the carbon fibre resistivity. In the second stage, the contact area between microfibrils increases causing another change in the resistivity. In third stage, the contact area between bundles increases resulting in the last change in the resistivity. These sensors are suitable for monitoring contacts on large surfaces. Main advantages of carbon fibres are durable, light, and formable. Moreover, they have high strength and stiffness, low hysteresis compared to conductive elastomers, and high thermal constancy. Disadvantages of carbon fibre are generating noise when they come in contact with metal or together, abrasive decay, and low shear strength [78, 79].
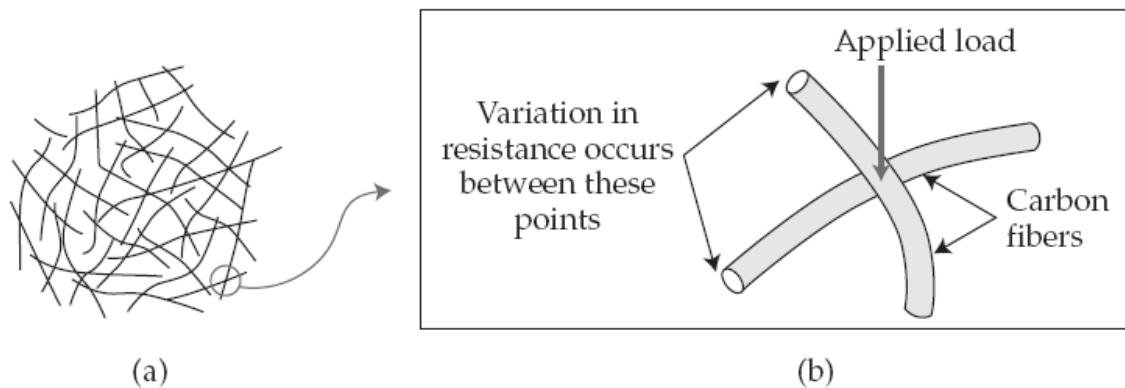
Figure 1.6: Carbon fiber structure (a) Internal structure of carbon fiber containing microfibrils. (b) The variation in resistance occurs by the points of contact between the microfibrils in carbon fibers [79].

Strain gauges are the most common and the oldest type of piezoresistive sensors. The operating principle of a strain gauge is that if it is subjected to an engineering stress, an engineering strain will occur, and its resistance will change according to this strain. Two classes of strain gauges are widely used that are metal strain gauges and semiconductor strain gauges. Metal strain gauges are mostly fabricated as a very thin foil of metal that is

fixed to a backing material. On the other hand, semiconductor strain gauges are fabricated from a thin wafer of semiconductive material, most commonly Silicon, on which a selected impurity is diffused. The selected impurity has a higher resistance than the semiconductive material or an opposite conductivity to it. Semiconductor strain gauges are usually manufactured by micro-fabrication procedures, and are commonly smaller than metal strain gauges. All strain gauges are characterized by a term known as the gauge factor. The gauge factor is defined as the ratio of the relative rate of change in the gauge resistance to the relative change in the gauge length (i.e. sensitivity of the gauge). Therefore, the higher the gauge factor the better material for fabricating the strain gauge. Semiconductor strain gauges have gauge factors (sensitivities) much higher than metal strain gauges. Moreover, semiconductor strain gauges in comparison to metal strain gauges, show higher fatigue life, higher linearity of stress-strain, insignificant hysteresis, less noise, less drift, more stable resistivity, more bendable, higher sensitivity to temperature, and a nonlinear relationship between their resistance and strain. In general, the advantages of strain gauges are their high accuracy, response to both static and dynamic stimuli, reliability, and ability to resist shock and vibration if occurred. However, their disadvantages are the limited range, the low stability, and the sensitivity to environment temperature [78, 79, 88, 89, 93].

In summary, the main advantage of piezoresistive sensors over piezoelectric sensors is their response to static and dynamic stimuli with reasonable range of frequencies. In addition, piezoresistive sensors are cheaper, and easy to be micro-fabricated, and show fast responses. Moreover, the nonlinearity response can be compensated with different methods as it will be shown later.

Additionally, one should note that it is possible to use two or more of the abovementioned principles together in one sensor in order to benefit from the advantages of different types of material. Some researchers have presented such sensors. For instance, Ahmadi [94] proposed a new hybrid catheter-tip tactile sensor for use in catheter-based heart surgery. The sensor is able to measure the relative hardness and the contact force. The principle of sensing combines both optical and piezoresistive principles. A piezoresistive film is used to measure the contact force while an optical fibre is utilized to measure the deflection of an elastic membrane. By combining both measurements, the relative hardness was calculated. The next section presents a review of the developed tactile sensors based on these principles.

1.6. 6. Comparison between Tactile Sensing Transduction Principles

The piezoelectric principle offers high speed measurements, high sensitivity and active response to various frequencies. Nevertheless, the piezoelectric principle suffers from sensitivity to temperature change due to its pyroelectric properties, sensitivity to noise and internal forces in different directions, insensitivity to static loads or loads with low frequencies. Therefore, piezoelectric is not the ideal candidate for tactile sensing that mimics the human hand in MIS [75, 77, 78, 79].

The capacitive transduction principle offers a solution for some of the disadvantages of piezoelectric in tactile sensing. For instance, it shows active response to both static and dynamic loadings, in addition to the other advantages including the simple structure, small size, little weight and low cost. However, it is still sensitive to both temperature and humidity, and requires sophisticated signal conditioning [75].

Optical principles present most of the requirements for tactile sensing that mimic hand sensing. They offer ideal solutions for the disadvantages of both piezoelectric and capacitive principles, in addition to the electromagnetic immunity, amenable for multiplexing, flexibility, electrical isolation and resistivity for rough environments. However, optical sensors are very sensitive to vibration and impact, and usually they require expensive equipments [61, 88].

The advantages of the magnetic principle include long life, sensitivity, wide dynamic range and resistance to humidity and dust. Despite these advantages they are not good candidates for tactile sensing. The primary reasons are their complicated structure, nonlinear response and sensitivity to external magnetic fields and temperature [88].

Carbon fibres are durable, light and formable, and they show high stiffness and thermal constancy. However, they generate noise when they come in contact with metal or with each other and exhibit low shear strength. Therefore, they are more suitable for monitoring contact on large surfaces than being used in tactile sensing with its various forms [78, 79].

On the one hand piezoresistive strain gauges exhibit high accuracy, active response for static and dynamic loads, reliable results and resistance to shocks. However, they show a limited range of measurements, sensitivity to temperature, low stability and exhibit a nonlinear relationship between the resistance and the strain [75, 76].

Conductive elastomers, including the Semiconductive polymer composites, seem to offer a key solution for the disadvantages of the other transduction principles that are limited in their use in tactile sensing. Conductive elastomers are the most suitable transduction

principle for tactile sensing to mimic the human hand. They are able to detect static and dynamic loads, are cost effective, can be used individually or in arrays and are very suitable for sensing pressure. Furthermore, they exhibit good resistance to corrosion, high temperature and chemicals. Moreover, they can admit heavy overloads, endure fatigue and can be miniaturized to micro level. Particularly, semiconductive polymers, in addition to the other properties, show fast response and reduce the external noise effect. Additionally, although the relation between the resistance of those elastomers and applied load is nonlinear, the relation between the conductance and the load is linear. Finally, the creep issue can be overcome by different methods as will be discussed later in the section 2.1. For these reasons, semiconductive polymer composites were selected to be the tactile sensing transduction principle for the tactile sensor in this thesis.

1.7. Literature Review

Numerous tactile sensors with different principles and designs have been presented for MIS use, many of which concentrate on contact force measurements [82, 83, 90, 95, 96, 97, 98]. For instance, Wisitsoraat *et al*. [90] proposed a piezoresistive-based micro-machined tactile sensor that can measure the contact force only. Silva *et al*. [96] presented a strain gauge-based tactile sensor for finger-mounted application, which is able to measure the finger force. The sensor was built using metallic strain gauge. It has a linear response, repeatable measurements, low hysteresis, and is rugged, and sensitive to static and dynamic loads. However, the size cannot be reduced to the micro-level due to the use of metallic strain gauge. Mehta *et al*. [97] proposed a capacitive-based micro-machined tooth-like pressure sensor for endoscopic surgery application that measures

force only. Despite the reliable results of the sensor, it can measure only few grams of contact force. Obana *et al*. [98] introduced a strain gauge-based tactile transducer for finger force measurements. It is constructed from a semiconductor strain gauge and aimed not to reduce hand dexterity. Semiconductor strain gauges offer many advantages such as the ability to manufacture micro-level sizes, high sensitivity, response to static and dynamic loads, negligible hysteresis, and linearity. However, the sensor is highly sensitive to temperature by virtue of semiconductor strain gauges.

On the other hand, some researchers have worked on evaluating different features of the contact object. For example, Bonomo *et al*. [27] presented a multifunctional tactile sensor that employs the ionic polymer-metal composite (IPMC) cantilever beams as the sensing element to measure the relative hardness of the contact object. An IPMC beam deflects in an electric field and produces electricity. Although the use of IPMC technology offers many advantages, the range of measurements of the sensor is limited to less than 1 kPa. This constrain refers to the IPMC's properties and the maximum force it can create. Furthermore, its complex structure for micro-fabrication makes it hard to be integrated into MIS tools.

Engel *et al.* [91, 92] have presented a polyimide-based multimodal and micro-machined tactile sensory skin that measures several mechanical properties of the contact object including the relative hardness. Although their sensor shows reliable results, it cannot measure any hardness higher than the hardness of polyimide material, and a rough contact surface (object) causes inaccurate measurements of relative hardness.

Dargahi *et al.* [13] have presented a Polyvinylidene Fluoride (PVDF) piezoelectric-based micro-machined tactile sensor for endoscopic grasper, which is able to measure the magnitude and position of the contact force. Despite the acceptable results of their sensor, it is complex to evaluate shear force from the sensor output. In addition, the sensor measures only dynamic loads by virtue of the PVDF properties.

Sokhanvar *et al.* [31, 67] designed a Polyvinylidene Fluoride (PVDF) piezoelectric-based micro-machined multifunctional tactile sensor for endoscopic grasper, which is able to measure the contact force, relative hardness of the contact object, and the position of any hidden lump inside the object. The sensor suffers from inaccuracy in evaluating the contact force because of the PVDF sensitivity to external noise. Furthermore, the sensor measures dynamic forces only. Moreover, the sensor assembling makes it not ideal for mass production and commercial use. In addition, the sensing range was limited to Newton's that makes detecting the low forces, such as blood vessels pulses, impossible. Additionally, the sensor is active at the teeth area only; other areas are inactive from measuring point of view.

Qasaimeh *et al.* [65] proposed another multi-purpose PVDF piezoelectric-based tactile sensor for endoscopic grasper, in which the functionality of Sokhanvar's [31] sensor is improved by modifying the endoscopic grasper so that the sensor will be able to cover the entire grasped surface. Regardless of the reliable results of the sensor of Qasaimeh *et al.* [65], due to the PVDF properties, it measures dynamic forces only. Furthermore, the new proposed structure for the endoscopic grasper is brittle.

Barmana *et al*. [99] presented a deformable force-stretch array (DFSA) tactile sensor that is able to detect nodules in palpation. The DFSA sensor consists of two main sensing elements: (i) the strain gauges attached to a piston-cylinder system harder than the palpated tissue; and, (ii) the stretch sensor elements that give an output proportional to their length. Despite the novel design of the DFSA sensor and its acceptable results, there is no proof that its complex structure is appropriate for micro-fabrication or MIS applications.

Shikida *et al*. [100] proposed a pneumatically actuated piezoresistive-based micro-fabricated and multifunctional tactile sensor that is able to measure the contact force and relative hardness of the contact object. Even though the sensor is micro-fabricated and shows promising results, building and controlling an accurate pneumatic system for an array of this sensor is costly.

Kalantari *et al*. [101] have presented a piezoresistive-based tactile sensor to be used on a catheter tip, which is able to measure contact force and relative hardness of the contact object. Regardless of the promising results of their sensor in differentiating between material hardness and its robustness, it has a main shortcoming, which is in order to measure the hardness of a material, a surgeon needs to progressively apply force to the material until it is deformed enough to touch the smaller sensor. This condition could cause damage to some tissues. In addition, the sensor covers the whole tip of the catheter, which will block the way for other catheter functions.

Lindahl *et. al*. [80] presented a Lead zirconate titanate (PZT) piezoelectric-based tactile sensor that evaluates the physical properties, stiffness and elasticity of human skin *in*

vivo. The sensor utilizes the PZT in an oscillation mode integrated with a vibration pick up electronic circuit and computer software that measures the variation in the frequency of PZT when it comes in contact with an object. When an object comes into contact with the PZT its frequency will vary depending on object stiffness. Essentially, the sensor was proposed as a hand-held device. Despite the reliable results of the sensor, there is no report on micro-fabrication of the sensor. Furthermore, the sensor's ability to detect the softness of contacted object in MIS applications was not examined since no experiments were performed in association with MIS tools.

Dargahi [102] presented a PVDF piezoelectric-based prototype with only three piezoelectric elements for tactile sensing system, which is able to measure the magnitude and position of the applied force. The tactile sensing system utilizes the triangulation technique integrated with membrane stress to obtain the measurements. However, the concurrence between experimental and theoretical results is very weak due to, as expected, both the experimental errors and theoretical analysis assumptions.

 Gray *et al*. [103] proposed a capacitive-based micro-machined micro-tactile surface of sensor array that detects the features and objects of sub-millimeter size. In other words, it can detect the contact force as long as the textures include small sizes features. The array is 8 x 8 with a total size less than 1 mm that is the normal human spatial resolution. The array is developed to sense organic tissues on small scales, which could be useful in applications such as endoscopic surgery, tele-manipulators used in surgery, and small un-medical manipulators. The array was able to detect milli-Newton forces with a good interpolation, spatial uniformity and high spatial resolution. Although the array was disposable and inexpensive, it suffers from hystereses that make the results unreliable.

Reston *et al.* [104] proposed another PVDF piezoelectric-based robotic tactile sensor array that detects the sub-millimeter tactile features, i.e. texture and contact force. The array consists of 5 x 5 sensors which are combined with integrated circuit (IC) developed to be used on the finger of a manipulator. Despite the linear response of the array and the high spatial resolution, its range of measurements is limited and by the virtue of PVDF the array does not stand static loading.

Narayanan *et al.* [105] presented a PVDF piezoelectric-based micro-machined endoscopic tactile sensor for MIS applications, which is able to measure the viscoelastic properties of tissues. The sensor contains rigid and compliant coaxial cylinders that are placed on top of two piezoelectric sensing elements. The sensor is mounted on an endoscopic grasper forming a tooth in the grasper. The sensor was able to measure the contact object compliance, softness, and the equivalent viscous damping. However, the active region of the sensor is just the cylindrical teeth, and other regions of the contact object cannot be examined. In addition, the sensor is not a suitable candidate for mass production and commercial use due to its multi parts and hard assembling and alignment. Furthermore, the sensor failed to detect small magnitudes of loading and static loading.

Ohka *et al.* [106] developed an optical-based tactile sensor that is able to detect the distribution of three-axis forces. The optical sensor is equipped with a special optical waveguide plate and fixed to a robot arm. The sensor structure includes a CCD camera, light source, the optical waveguide plate (acrylic sheet), and a silicon rubber sheet. Although the experimental and calculated results of the sensor are well agreed, the structure of the sensor reduces the ability for micro-fabrication and providing a light source with the endoscope would be a problem to solve.

Qasaimeh *et al*. [61] developed an optical-based tactile sensor that measures the contact force magnitude, pressure distribution, and the softness of the contact object. The sensor consists of thin membrane deflects due to the interaction with contact object; the deflection is measured by means of optical fiber. Since optical fiber is utilized in the sensor, it needs an optical source, optical receiver, multiplexer, and complicated computer processing.

Clark [107], proposed a magnetic field tactile sensor that renders the texture of the contact object. The sensor is developed to be used on robotic hand at the fingertip. Basically, the sensor consists of two arrays matched with each other. The first array includes magnetized material that patterned on the flexible membrane of the fingertip. The second array includes hall-effect magnetic sensors which fixed on a rigid substrate and fabricated by CMOS technology. Due to the use of CMOS technology the sensor is miniaturized to the micro level. Although the sensor is able to successfully render the texture of the contact object, it is not able to measure other important tactile information for MIS application such as the contact force. Additionally, the sensor suffers from noise due to the sensitivity of each Hall-effect sensor to other magnetized material around it.

1.8. Motivation

As it was discussed in the section 1.2, MIS offers many advantages that attract the medical media to prefer MIS over classical open surgeries in various operations. However, MIS suffers of some major drawbacks that limit its expansion and development to replace many other operations that are currently performed by means of open surgery methods. Consequently, the benefits of MIS procedure are also limited by these major

drawbacks. The loss of touch is the main drawback in MIS since surgeons rely on some tactile information in medical treatments such as the softness of the tissues and the contact force. Therefore, development of a suitable tactile sensor that provides the surgeon or the tactile display, if applicable, with this tactile information would be of a great help for the expansion and development of MIS. Accordingly, this research aims to develop a novel tactile sensor for use in MIS and MIRS applications. Finally, although many tactile sensors have been presented, most of them suffer from some weak points that limit their usage as a practical solution for MIS tools.

1.9. Research Objectives

The literature review shows that the majority of tactile sensors are force sensors, and the other tactile sensors that measure several features of the contact object have some disadvantages. For instance, some of them have constraints in measurements by virtue of the properties of the sensing materials used in the sensor or fabricating the sensor. Moreover, some sensors have a complicated structure that makes the micro-fabrication of the sensors a formidable task. Furthermore, to the best knowledge of the author, none of the previously proposed tactile sensors has been tested with real tissues or with materials that can represent the real tissues. In other words, the sensors have not been examined using realistic materials that represent the practical conditions in MIS applications.

The main objective of this thesis is to develop a piezoresistive-based multifunctional tactile sensor for MIS applications that will enable the following:

- Detection both dynamic and static loadings by virtue of a new piezoresistive tactile sensor.

- Measurement of both the contact force and the relative hardness of the contact object.

- To design a less fragile tactile sensor compared to other sensors [65, 67].

- The structure of the sensor to be simple to ensure the ability for micro-fabrication [108, 109, 110].

- The sensor should be able to be integrated with a commercial MIS endoscopic grasper.

1.10. Thesis Outline

Following the introduction in the first chapter, the second chapter of this thesis describes the design of the proposed sensor and its working principle. Then, a brief background theory about the sensing element used in the sensor is presented. Next, the fabrication process is described.

The third chapter is the experiments section. It describes the tests that were carried out to model the silicone rubber samples, calibrate the piezoresistive sensing elements, and verify the functionality of the sensor.

Chapter four is the modeling section. The sensor as well as the tissue-like materials (Silicone rubbers) is numerically modeled using a finite element modeling (FEM) software.

Finally, chapter five discusses and compares the results of both numerical analysis and experiments on different silicone rubber samples. Furthermore, the overall sensor functionality and features are discussed.

Chapter 2 : Design and Fabrication of the Tactile Sensor

The proposed sensor utilizes piezoresistive films as the sensing element. Among all types of sensing principles discussed in the introduction, the semi-conductive polymer composite piezoresistive film is used in this work because of its (1) quick response to both dynamic and static loading, (2) reduced sensitivity to external noise, (3) compliance with micro-fabrication techniques [108, 109], (4) cost effectiveness for mass production. In this section, the composition, mechanical properties, and working principle of this sensing material are presented.

2.1. Semiconductive Polymer Composite Film

Semiconductive polymer composites are commonly used in compressive force and pressure measurements in different applications [111]. Mainly, a semiconductive polymer consists of two parts: the nanoscale conductor particles and a nonconductive matrix. The nanoscale conductor particles are distributed inside the nonconductive matrix structure randomly (Figure 2.1). Due to random distribution of conductor particles, these composites are considered as random whisker composites [112]. However, when a distributed load is applied to a semiconductive polymer composite film, the filler conductor particles show micro-Brownian motion. Therefore, the distance between the nanoscale particles inside the nonconductive matrix will change. This, in turn, appears as a change in the electrical resistivity of the polymer. Semiconductive polymer sensing elements exhibit a creep behavior, i.e. a permanent deformation in the material structure, under a constant load, and so they are treated as a viscoelastic material. The creep behavior appears as drift in the sensing elements outputs [113]. Various researchers had

worked on eliminating the drift in the resistance of the semi-conductive polymers under constant loads, such as Hall *et al*. [114] who compensate the drift of the semi-conductive polymer output by means of signal conditioning, and Kalantari *et al*. [115] who developed a mathematical model that could be used for compensating the drift in the semi-conductive polymer exhibiting viscoelastic behavior. Additionally, it has been shown that the semi-conductive polymer can be manufactured as a biocompatible material using special manufacturing approach. Laukhin *et al*. [116] proposed approach to engineering biocompatible and highly piezoresistive membrane for flexible weightless pressure and force sensors. Furthermore, semi-conductive polymer is comfortable with microfabrication techniques. Engel et al. [108] used micro molding technique to micro fabricate the semiconductive polymer as a part of an artificial hair cell (AHC) sensor. Therefore, Engel used a combination of elastomer patterning techniques, basically designed for Polydimethylsiloxane (PDMS), and composite materials processing methods. Moreover, semi-conductive polymers are commercially available as wide sheets with thickness values vary within the Micron level. Therefore, accurate laser-cutting devices can be used to cut out the semi-conductive polymer into small parts, then micromanipulators can be used to assemble them to the sensor structure [109].

The semiconductive polymer that is used to fabricate the sensing elements in this work is Linqstat, which consists of carbon black for the filler nanoscale conductive particles and polyethylene as the matrix. A Linqstat film structure includes 80.11% polyethylene and 19.89% of carbon black particles [115].

An electrical current passes through two types of resistance in a film of Linqstat as a semiconductive polymer: the tunneling resistance (Rt) and constriction resistance (Rc).

Tunneling resistance is the electrical resistivity between two adjacent conductive particles where the electrical current would flow via the vacuum of matrix between abutting particles. Therefore, The R_t varies depending on the distance between the adjacent filler particles and the surface area of contact between two particles [113]. The constriction resistance is the resistance of the carbon black, which is independent of the compressive loading and remains constant. The total resistance (R_{tot}), of a semi-conductive polymer composites is given by [117]:

$$R_{tot} = \frac{(L-1)R_t + LR_c}{S}$$
(2-1)

where R_{tot} is the total resistance of the semi-conductive polymer composites, L is the number of particles assembling one conductive line, and S is the total number of active conductive lines. Since Linqstat contain carbon as the conductive particles which are extremely conductive comparing to the matrix that is made of polyethylene, Rc can be neglected. Assuming that $L-1 \simeq L$ [115], then the Equation (2-1) can be written as:

$$R_{tot} = \frac{L}{S} R_t$$
(2-2)

The fabricated piezoresistive sensing elements using Linqstat contains two layers of the semiconductive polymer in between two electrodes all hold together by two pieces of an adhesive nonconductive silicone tape. The pressure built by the adhesive silicone tape on the piezoresistive sensing element is enough only to assemble its layers together. Therefore, some air will stay inside the sensing element in-between its different layers during manual fabrication of the sensing element. Consequently, the area of contact between the electrodes and the semi-conductive polymer will decrease, and the contact resistance between them will increase. As a distributed pressure is applied to the

piezoresistive sensing element, the air inside the element will blow off, through the small open in the tail of the sensing element, and the resistivity of the sensing element will drop markedly as a result of both: the change in the semi-conductive polymer, and the increase in the contact area, that is a decrease in the contact resistance.

Also, one has to mention that due to the roughness of the contact surfaces of both the electrodes and the semi-conductive polymer layers, the active contact area in the microscopic level is a small fraction of the contact area. The active contact area is a group of asperities, i.e. sharp protrusions, and it would increase when a compressive load is applied to the contact surfaces, Figure 2.2. Therefore, the current will face higher contact resistance without loading and the resistance of the contact will reduce as the load applied due to the increase in the contact area. The sudden increase in the area of the contact after loading is another reason for the drop in the sensing element resistance as the load applied [115, 118].
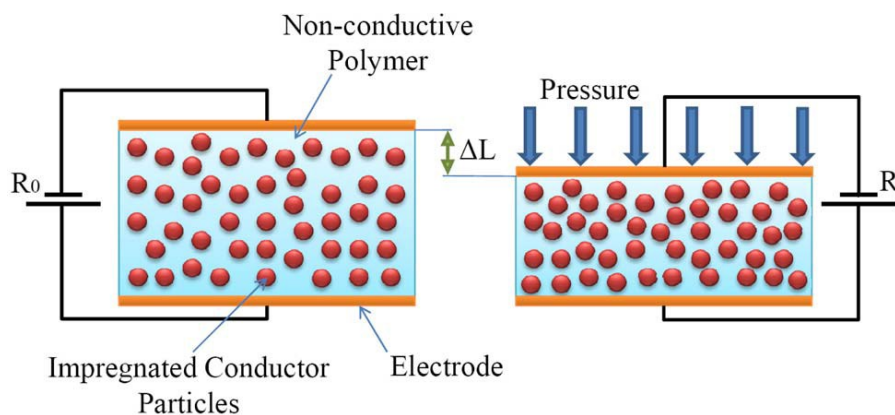
Figure 2.1: Semiconductive polymer composite structure and its working principle [115]
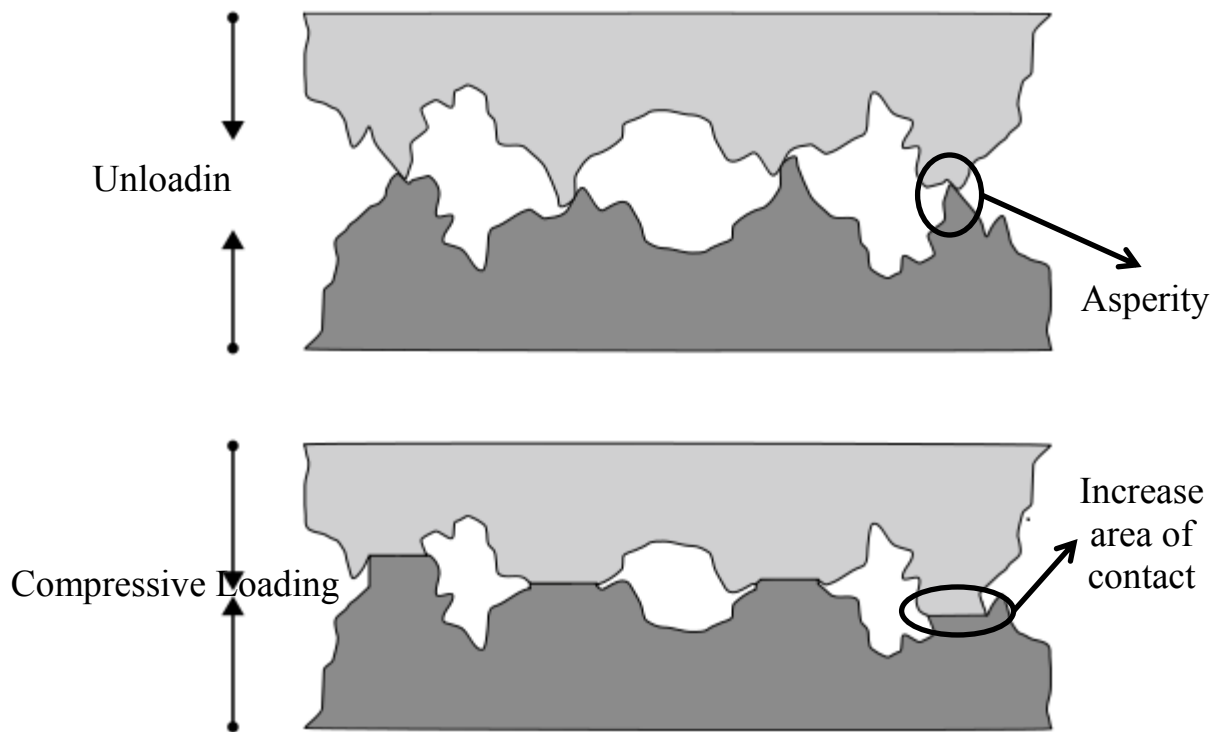
Figure 2.2: The effect of the asperities on the contact area [119]

2.2. Tactile Sensor Design

The mechanical structure of the sensor consists of an elastic beam sitting on two supports placed at each end of the beam. The gap between the elastic beam and the substrate is filled with a soft hyperelastic filler material, i.e. a soft silicone rubber, as it is shown in Figure 2.3. The piezoresistive semiconductive polymer sensing elements are placed at three positions in the sensor. As illustrated in Figure 2.3, two of the piezoresistive films are placed under the beam supports, one at the left side and one at the right side. The third film is in the middle attached to the beam at the lower surface in between the beam and the silicone rubber.

Using this configuration of the sensor structure and piezoresistive films, it would be possible to measure the contact force and the relative hardness of the contact object. The piezoresistive films underneath the supports of the sensor will measure the total contact force applied to the top of the sensor. Whilst, the piezoresistive film attached to the beam will measure the beam deflection resulted from the deformation of the contact object. Since piezoresistive films work with compressive forces only, the silicone rubber is used under the middle film to transfer enough pressure to the middle film. The presence of the silicone rubber will increase the sensor's capability to stand larger forces without breakage. However, the hardness of the silicone rubber is an important factor in the design, since it will define the range of hardness values that the sensor can measure. Experiments showed that for a wider range of measurements the filler material should be softer. In other words, the filler material should be softer than the softest material to be tested by the sensor, in order to ensure that the beam is able to deflect under the deformation of the softest material. In addition, choosing the filler material to be very soft will decrease the part of the applied force transferred through filler material to the base. As a result, the contact force can be measured from the summation of the output of the piezoresistive films on both sides, since the supports are rigid and will transfer almost all the force to the piezoresistive films underneath. This has been also proved by FEM analysis in this work.
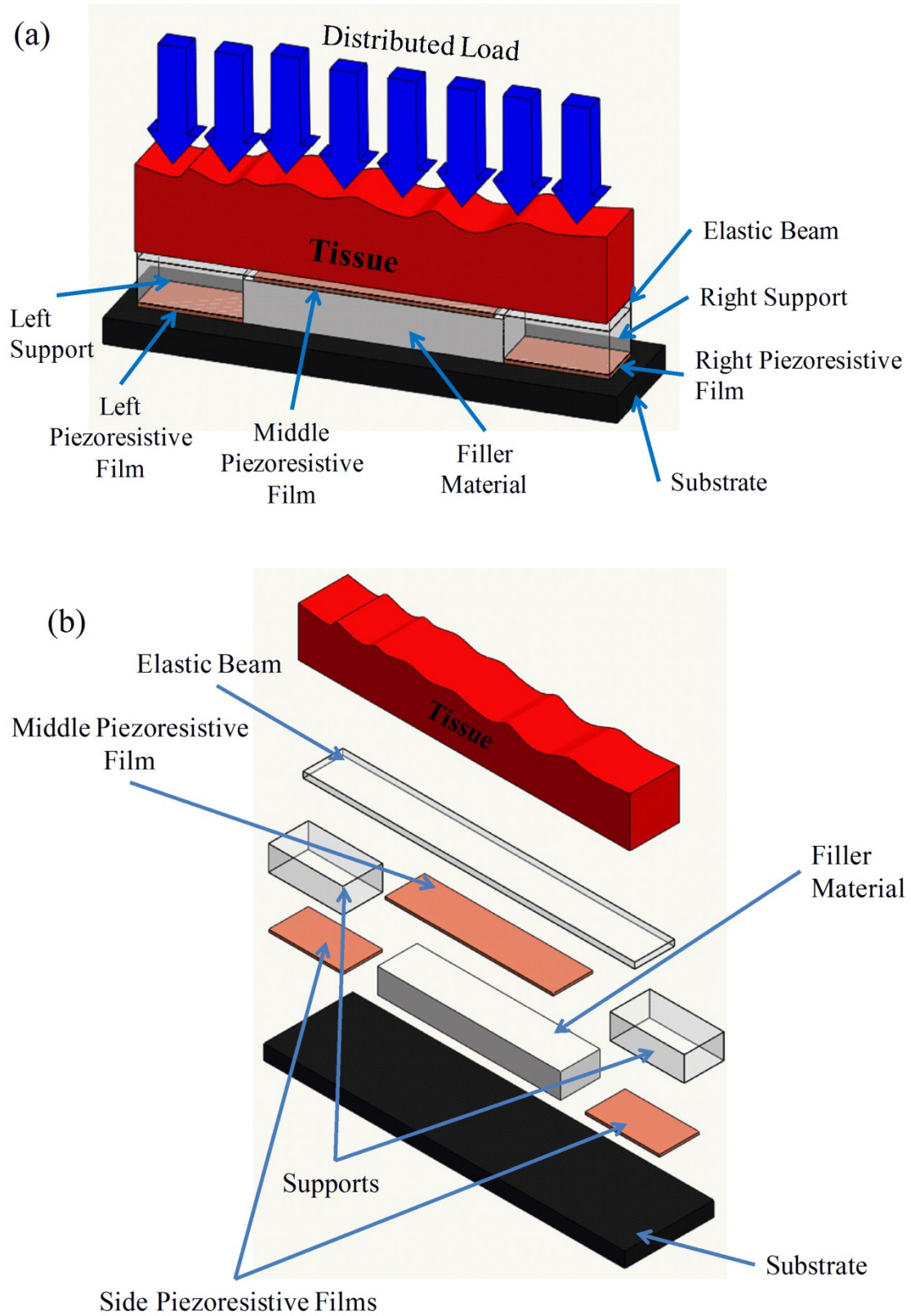
Figure 2.3: (a) Sensor design in contact with the tissue. (b) 3D exploded view of the sensor and the tissue.

2.3. Relative Hardness Measurement

The hardness of a material is directly related to its Young's modulus (E), which is a function of the engineering stress (σ) and strain (ε). Equation (2-3) shows that the modulus of elasticity of a material, which is the slope of the engineering stress-strain curve, can be estimated with the slope of the force-deformation curve of a sample of that material.

$$E = \frac{\sigma}{\varepsilon} = \frac{F * L_o}{A * \Delta L} = C \frac{F}{\Delta L} \qquad (2\text{-}3)$$

where C is a constant, and L_o and A are the initial length and cross sectional surface area of the given sample of material, respectively.

Consequently, the relative hardness ($R.H$) of the material can be written as

$$R.H \approx \frac{F}{\Delta L} \qquad (2\text{-}4)$$

Similar to the modulus of elasticity, as the $R.H$ value increases, the hardness of the material increases. So, in order to differentiate between contact objects, force and deformation should be measured simultaneously to give an indication of the relative hardness of the materials.

2.4. Working Principle of the Sensor

The sensor is aiming to measure the relative hardness of the contact object depending on its behavior under different loadings. Materials deform under the same loading based on their hardness. An ideal hard material will have zero deformation, but as the material

hardness decrease the deformation of the material would increase under the same loading. Hence, for a specific material, the deformation is proportional to the loading magnitude. Evaluating the relative hardness of a material will require measuring the contact force and the material deformation simultaneously. In the proposed sensor, it is assumed that the contact object is in full contact with the beam, the applied load to the material by the MIS tool is distributed, and the material or the tissue is homogenous unless there is a hidden lump. So, a softer contact object will have more deformation under the same loading, and generate more deflection of the beam as well as more output of the middle piezoresistive film. Regardless of the hardness of the contact object, the piezoresistive films underneath the supports will measure the contact force transferred to them through the sensor structure. Therefore, the relative hardness of the material can be evaluated. Figure 2.4 illustrates the measurement principle.

It is important to note that measuring only the relative hardness does not need more than two piezoresistive films. One measures the contact force, which could be placed either on the base along with the sensor structure, or under one of the supports. The second piezoresistive film should be placed in the same place as the current middle piezoresistive film. However, three piezoresistive films have been used in the proposed sensor in order to find the contact force and the relative hardness of the contact object.

The range of hardness measurements can be tuned to fit the required application, depending on many factors such as the filler material hardness. In addition, the elastic beam dimensions and its modulus of elasticity play a crucial role in the sensor sensitivity, range of measurements, and the maximum applicable force before the sensor fails. For instance, a thinner beam will increase the sensor sensitivity, and reduce the maximum

applicable force. Same results will be obtained if the beam gets longer, narrower, or more elastic (lower modulus of elasticity).
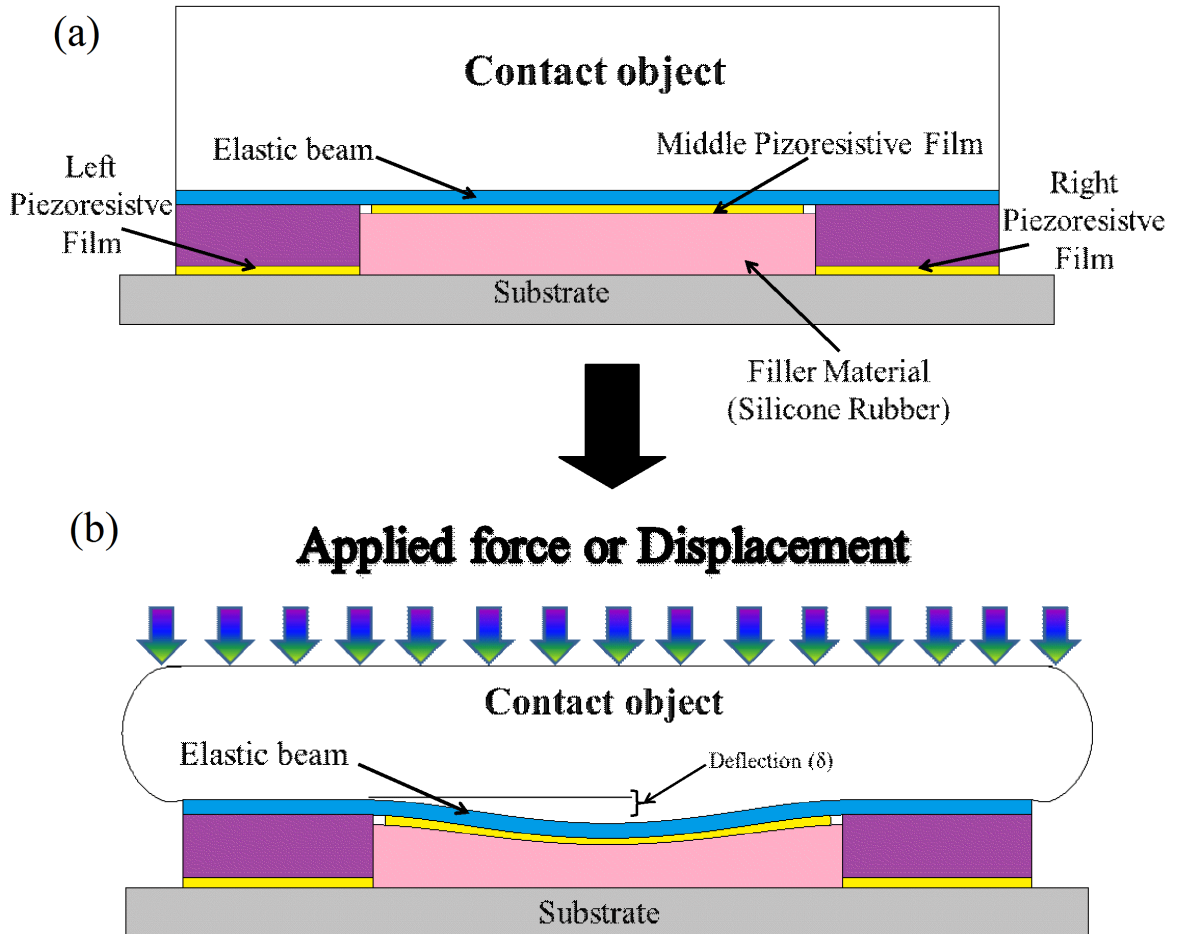
Figure 2.4: Working principle of the sensor (relative hardness measurements) (a) before applying force or displacement, (b) after applying force or displacement.

In MIS applications, usually the end-effecters of the tools are of small size compared to the total size of the treated tissues. Therefore, it is assumed that the grasped tissue is longer than the length of the sensor.

The proposed design can be used in an array to be implemented in the endoscopic grasper jaws. In an endoscopic grasper, the number of sensors used will depend on the grasper

dimensions. In order to cover the entire grasper jaw surface, each tooth and spacer will include two sensors, one in the tooth, and the other in the spacer. Each sensor contains the beam, the supports, three piezoresistive films, and the filler material. In order to give the toothed shape to the grasper and for staple grasping, the support of the tooth is higher than the support of the spacer. Figure 2.5 presents the proposed design for the grasper's Jaw. Due to the simple structure of the sensor, micro-fabrication is possible.

2.5. Sensor Fabrication

Fabrication of the proposed prototype was carried out manually. Figure 2.6 shows the dimensions of the prototype. The elastic beam and the supports were cut out from an elastic Polystyrene sheet (Plaskolite Inc.) and an Acrylic sheet (Plaskolite Inc.), respectively. Then, the elastic beam and the supports were glued together. Next, the soft filler material was molded from a silicone liquid rubber called "Ecoflex 00-10", produced by SMOOTH-ON Inc. This type of silicone rubber was used since it is the softest material among the five silicone rubber types, as shown in the experiment, section 3.3. Therefore, a wider range of measurements and testing can be performed to investigate the functionality of the prototype. Table 2.1 shows the components of the mechanical structure of the prototype.
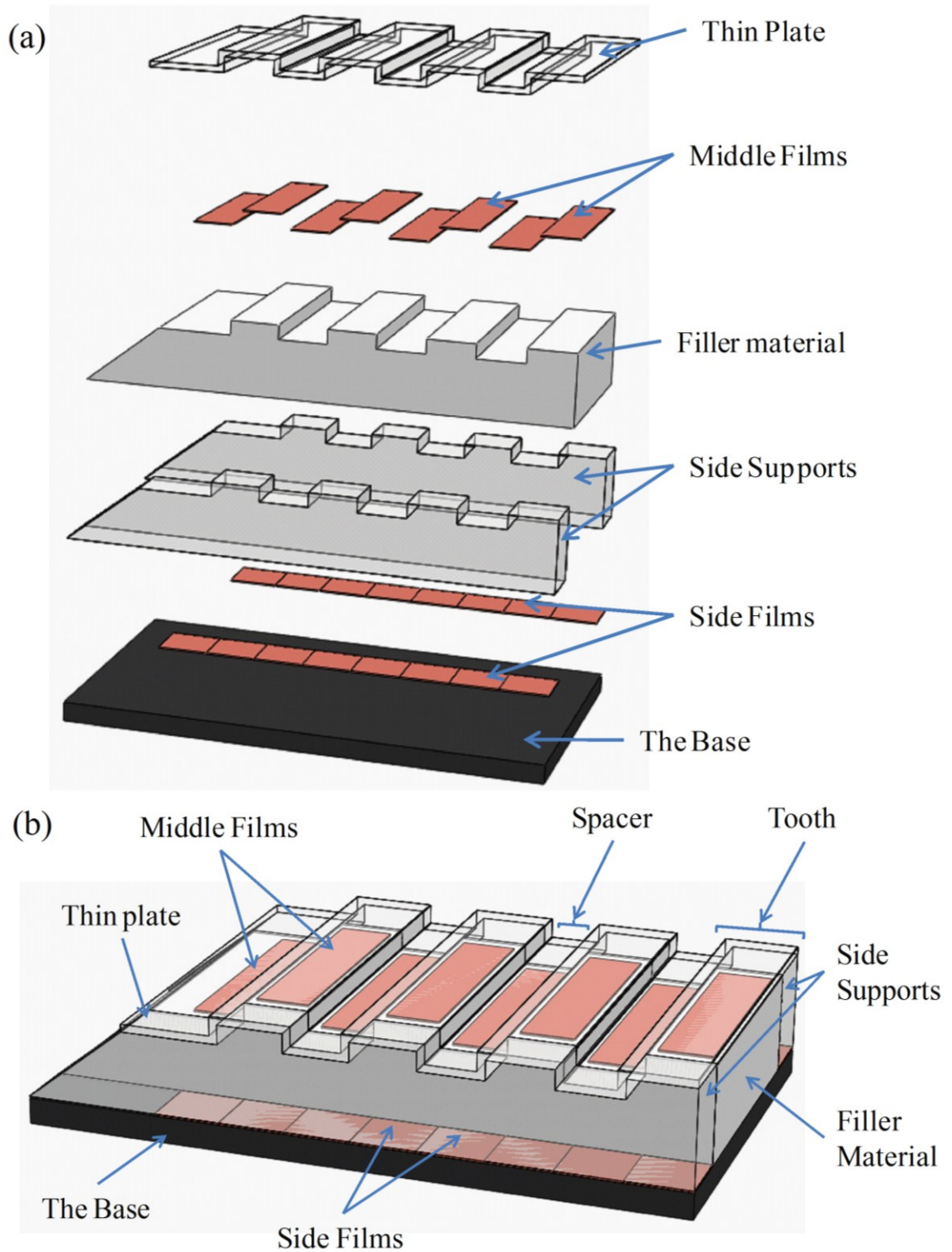
Figure 2.5: The proposed sensor integrated with an endoscopic grasper jaw, (a) 3D exploded view of the jaw components. (b) 3D isometric view of the jaw.
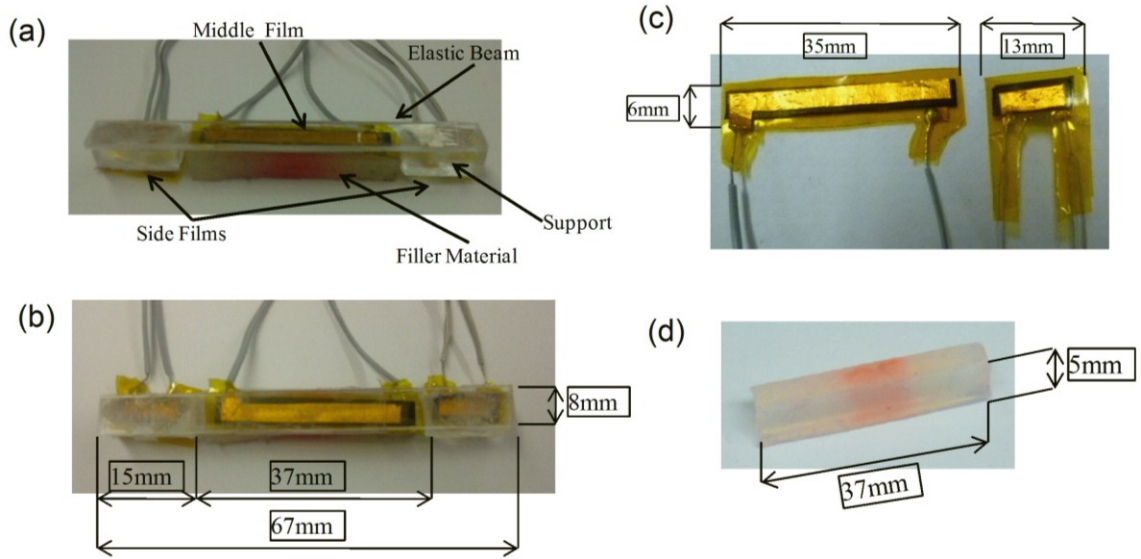
Figure 2.6: The fabricated prototype, its parts and dimensions: (a) Isometric view of the prototype. (b) Top view of the prototype. (c) Piezoresistive films used in the prototype. (d) The hyperelastic filler material.

Figure 2.7 shows a sensing element. The piezoresistive films (sensing elements) were fabricated in the lab from a semiconductive polymer composite sheet. A double layer of semiconductive sheet was inserted freely between two copper electrodes that were soldered to electrical wires. Then, two layers of nonconductive silicone sheets were used to cover the electrode and create the initial pressure that was enough to hold all the sheets together.
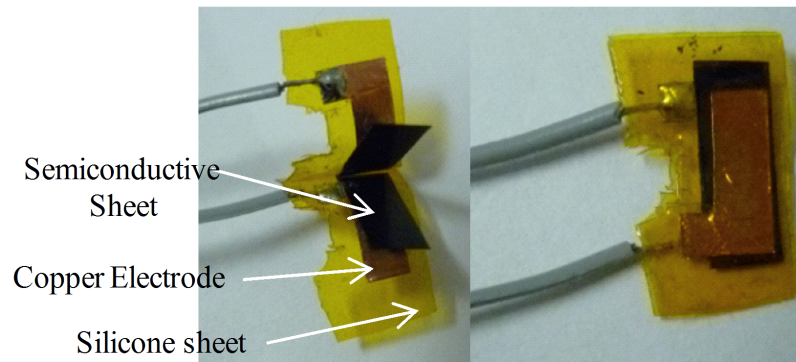
Figure 2.7: A fabricated sensing element and its components

The proposed design, shown in Figure 2.3 and Figure 2.6, needs three piezoresistive elements: two of the same size under the supports, and one in the middle under the beam. The resolution of those fabricated sensing elements is 0.1 N.

Table 2.1: The components and materials of the sensor's mechanical structure

Structure component	Material	Dimensions (mm)
Supports	Plexiglas	$15 \times 8 \times 5$
Filler Material	Silicone rubber (Ecoflex 00-10)	$37 \times 8 \times 5$
Elastic Beam	Polystyrene	$67 \times 8 \times 1.2$

Chapter 3 : Experiments

Several experiments were carried out to initially test the measuring principle of the sensors, calibrate and test the proposed prototype, and validate its output for measuring the relative hardness of the contact object and contact force.

3.1. Initial Tests on the Sensor Using Elastomeric Materials

Since the work presented in this thesis is experimental-based, after building a prototype of the sensor, the measuring principle of the sensor was initially tested experimentally. A series of experiments were conducted to study the behavior of the sensor in contact with soft material.

The soft materials needed for this investigation were chosen to be elastomers. Elastomers can undergo large deformations when stress is applied to them. Therefore, they show hyperelastic behavior and can be used to estimate the response of the sensor. However, unlike silicone rubbers or biological tissues, elastomers show compressible behavior. Consequently, elastomers cannot be used to simulate biological tissues in the experiments of validating the sensor. Nevertheless, their hyperelastic behavior makes them an appropriate candidate for the initial tests.

3.1.1. Testing Principle

Figure 3.1 shows a sketch that illustrates the sensor structure. Figure 3.2 presents a photo that illustrates the fabricated sensor under the initial tests. Using a Bose Electroforce device, a distributed force is applied on top of the tested contact object. In this case, the

objects are two elastomeric materials named EVA, and B3. EVA is the softer one. Due to the applied force, these materials will deform accordingly. For the same applied force, the harder the test object, the less deflection of the sensor beam. This deflection is measured by the top middle piezoresistive film. In the meantime, the total load, which transfers through the sensor structure to the sensor bottom part, can be measured by the bottom piezoresistive films of the sensor. Using such a combination, both contact force and resulted deformation of the test objects is obtained. Consequently, the relative hardness of soft contact objects can be measured. For initial test purposes, it is enough to measure the deflection of the beam to confirm the sensor ability in differentiating materials based on their hardness.
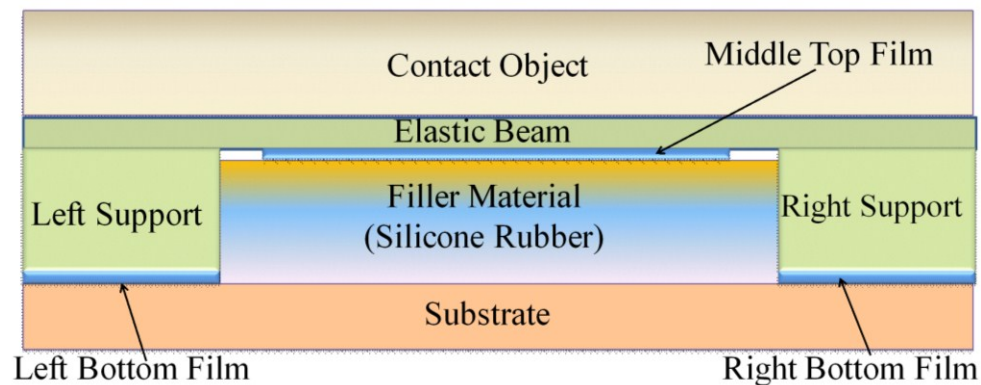
Figure 3.1: Illustration sketch of the sensor structure.

3.1.2. Testing Protocol

In order to obtain the final results for the beam deflection, the top middle piezoresistive film should be calibrated. In order to obtain a measurable output from the sensor, the sensing elements should be integrated with a special electrical circuit. Since they are resistive sensing elements, as in normal resistance measuring tools, a DC voltage is required to measure the change in their resistivity. A combination of a voltage divider

circuit, buffer circuit, and a LabView program with the use of a data acquisition card (DAQ) was used to read the change in the sensing elements resistivity.
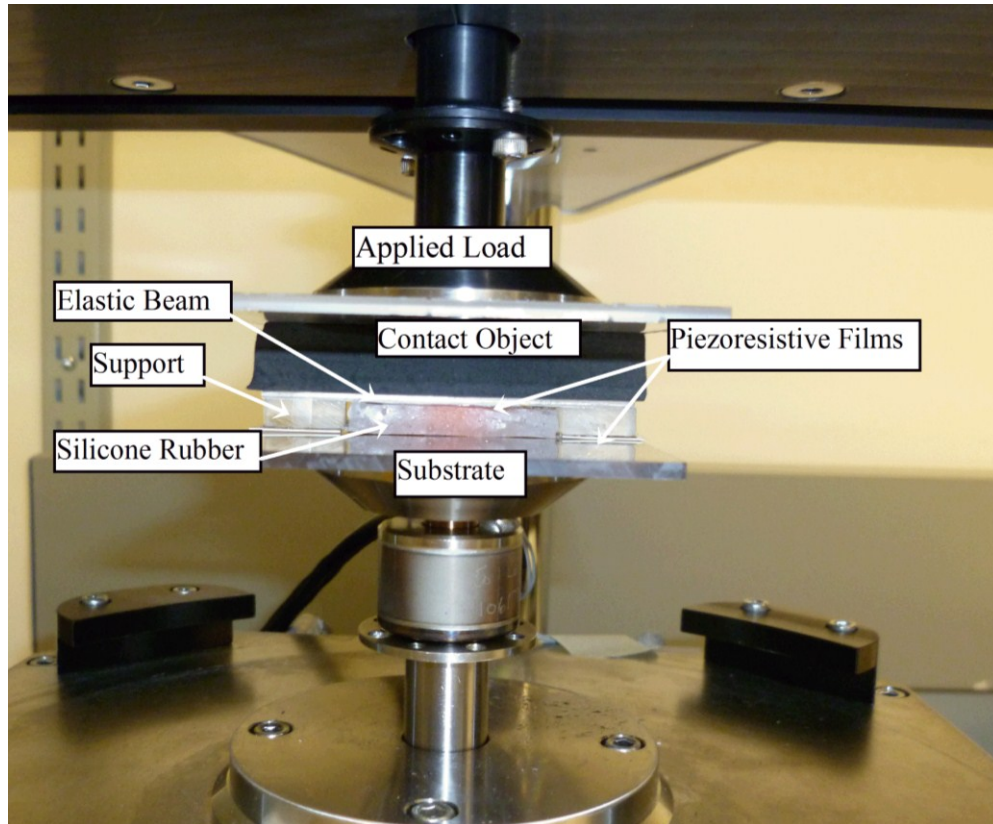
Figure 3.2: Photo of the prototype under test.

As illustrated in Figure 3.3.a., a DC voltage was applied to one terminal of the sensing element, and the other terminal was connected in series to a grounded constant resistance. The constant resistance (9.4 kΩ) was chosen to be in the range of the resistance of the piezoresistive films; this will avoid any cross talking between different sensing elements. The output voltage was taken to the DAQ, through a buffer circuit, from in between the two resistances, i.e. the sensing element resistance and the constant resistance. Then, the output voltage of the sensing element is recorded to a computer. The buffer circuit protects the DAQ from cross talk between the channels. Using the LabVIEW software,

the output voltage is processed to calculate the deflection of the sensor beam. It is important to note that the contact between electrodes and the composite polymer shows a large resistivity, since it contains some air. When a compressive force is applied to the sensing element, the air inside the contact surface will be pushed out and, therefore, the contact area will increase. That would result in a sudden decrease in the resistance of the piezoresistive films. Figure 3.3.b. shows the resistances of the sensing element (piezoresistive film).
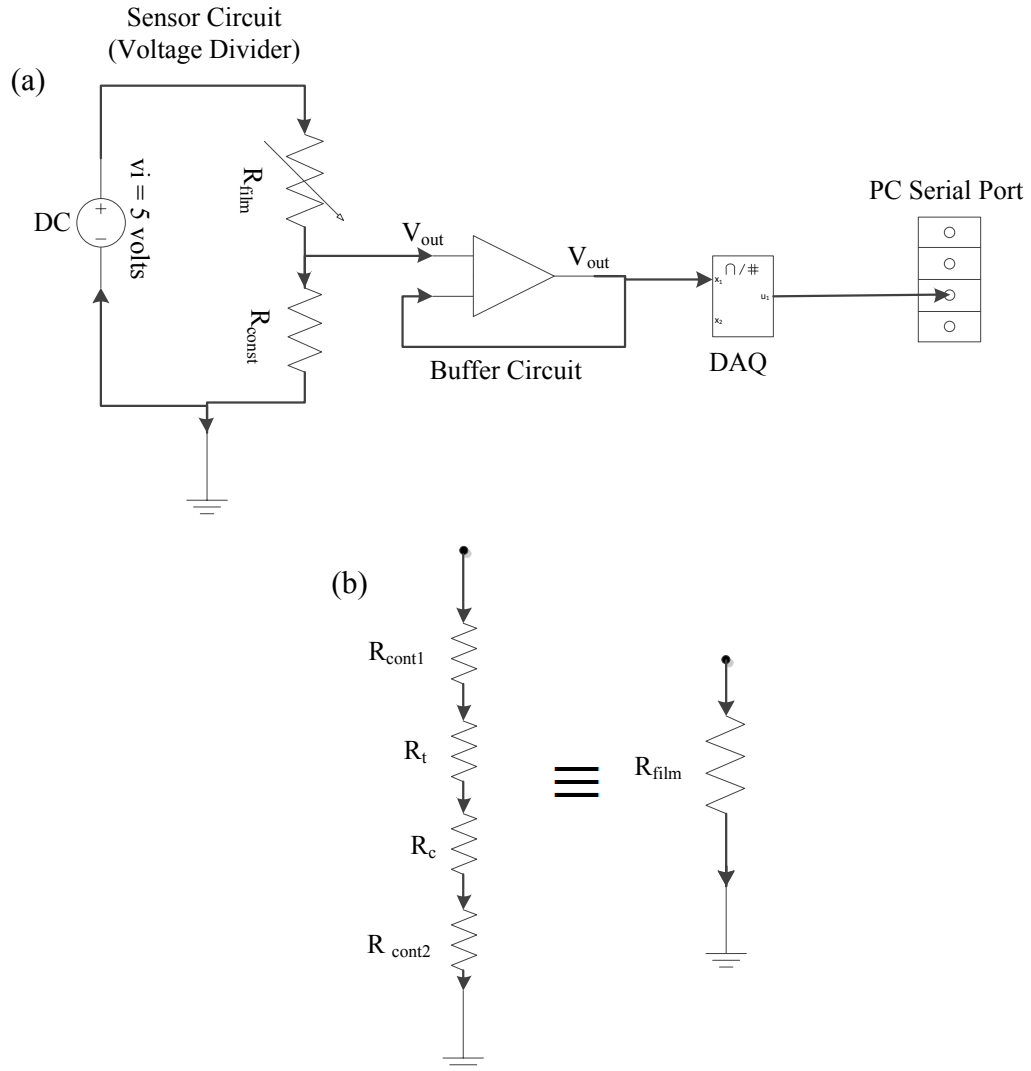
Figure 3.3: (a) The electrical circuit used to connect one sensing element of the proposed sensor (signal processing). (b) The resistances included in the fabricated piezoresistive film.

3.1.3. Initial Tests Results and Discussion

The same procedure and setup was used in calibrating the sensor, which will be explained in section 3.2, were used to initially calibrate the middle piezoresistive film of the prototype. The results of initial calibration were used in the initial tests. Figure 3.4 illustrates the output of the middle piezoresistive film for two different test scenarios. In the first scenario, the contact material is EVA whereas in the second scenario a harder material, B3, is used. As shown in the figure, for the same contact force, the deflection of the sensor beam for the softer material (EVA) is greater than the deflection for the harder material (B3). In order to validate the sensor output, the hardness of the two elastomeric materials was tested using the typical Durometer. Durometer results show that B3 is the harder material with a hardness of 64 shore 00, while EVA is the softer material with a hardness of 42 shore 00. Furthermore, the stress-strain curve obtained experimentally for both B3 and EVA confirms that EVA is the softer material. Figure 3.5 shows the stress-strain curve of the two elastomeric materials; for simplicity, only the linear part of the curve is shown in this figure. In both tests, the Durometer and the stress-strain confirm the sensor results. In fact, the sensor is able to distinguish between the hardness of these two elastomeric materials. This output is obtained when a reference square force function is applied. The range of the force function varies between 0 to 5.0 N with the frequency of 0.05 Hz.

Figure 3.4: The output of the middle piezoresistive film for two different elastomeric materials under constant square load.
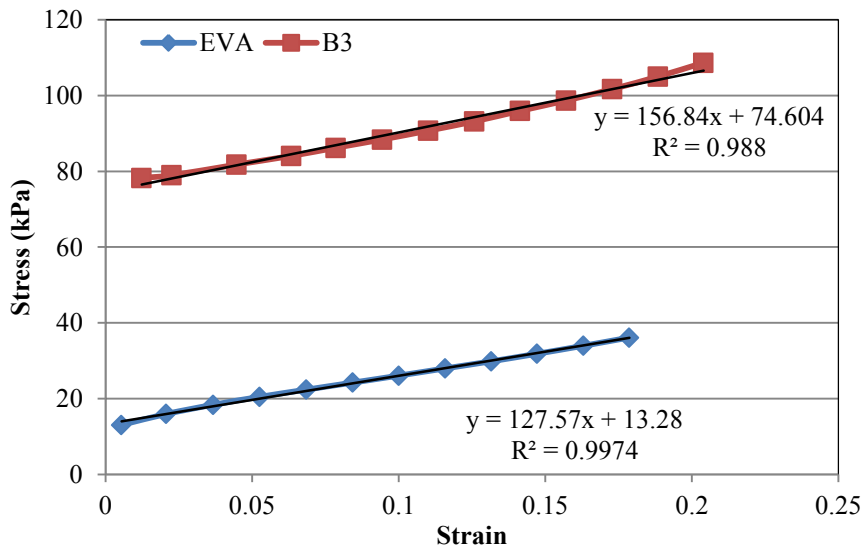
Figure 3.5: Experimental stress-strain obtained for B3 and EVA
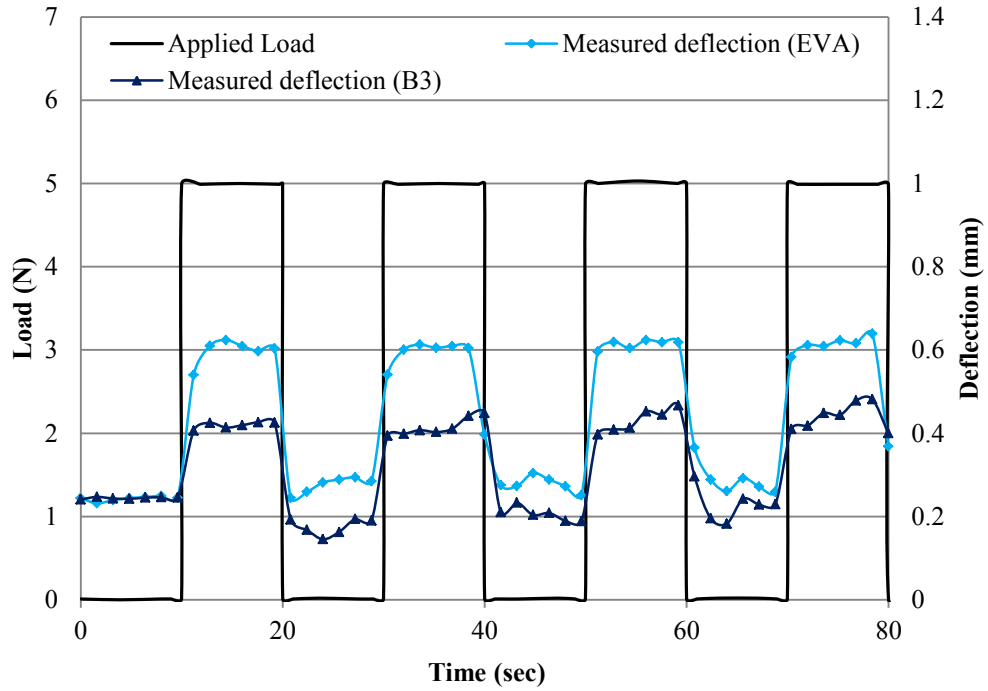
The experimental results confirm the validity of the sensor measuring principle, which used to measure the relative hardness of two different elastomeric materials. These two

materials, at this stage of experiments, are used to resemble two biological tissues with two different mechanical properties. The range and the resolution of the sensor can be fine-tuned by changing the design parameters of the sensor. As a future development for the next stage of experiments, the sensor should be calibrated in a way that it can measure the total contact force as well as the relative hardness of contact objects.

3.2. Sensor Calibration

In order to use the proposed prototype in measuring the relative hardness and contact force, all the sensing elements (piezoresistive films) should be calibrated experimentally. The objective of calibration is to identify the relationship between the resistivity change in piezoresistive films on both sides and the applied force to the top of the sensor. For the middle film, however, the relationship is obtained between the film resistivity and the beam deflection.

The experimental setup contains the piezoresistive film that is integrated into a voltage divider electrical circuit provided with a DC voltage of 5 V from a voltage supplier. As was illustrated in section 3.1.2, Figure 3.3.b., the piezoresistive film is fed with a DC voltage and is considered as a variable resistance connected in series to a grounded constant resistance (9.4 kΩ). An output voltage signal is taken out after the variable resistance film to a buffer circuit that is connected to the DAQ. The buffer circuit will minimize the loading effect of the piezoresistive film on the DAQ amplifiers as well as the crosstalk between the DAQ channels. Then, the DAQ is connected to a PC with LabView software. Via this combination of the DAQ, voltage divider circuit, buffer circuit and the LabView software, the output voltage signal can be read.

With a simple analysis of the electrical voltage divider circuit, shown in Figure 3.3.b, the following Equation (3-1) can be obtained

$$R_{film} = R_{const} \times \left[\frac{V_i - V_{out}}{V_{out}} \right] \qquad (3\text{-}1)$$

where R_{film} is the resistance of the piezoresistive film, R_{const} is the constant resistance (9.4 kΩ), V_i is the DC input voltage to the voltage divider circuit, and V_{out} is the output voltage taken from the voltage divider circuit.

Once Equation (3-1) is implemented in LabView, the readings of the output voltage can be processed to calculate the resistance of the piezoresistive film corresponding to each output voltage value. The output voltage entered in LabView was filtered with a third-order Butterworth low-pass filter with a cut off frequency of 6 Hz to eliminate the noise from the voltage signal. An Electroforce 3200 Bose device (BOSE Co.) was used in order to calibrate the sensing elements. The accuracy of this device in measuring displacement and force is 0.01 mm and 0.01 N, respectively.

The Electroforce 3200 Bose was used to apply different distributed forces discretely on each of the side piezoresistive films. The resistance of the film was recorded from LabView one second after applying the force. The applied force was increased each time with a step of 1 N up to a maximum force of 9 N and the resistance of the film was recorded. Figure 3.6.a. and b. show the obtained results for this calibration. The experiments showed a linear relationship between the film conductance, which is the inverse of resistance, and the applied compressive force.

In another calibration process, the same setup and Electroforce device were used; this time, with a sharp head to apply a load to the center of the elastic beam. As presented in Figure 3.7, the experiment was done on the mechanical structure of the prototype including the filler material and the middle piezoresistive film. For each deflection value, the resistance of the middle film was recorded from LabView. The maximum deflection applied to the beam was 1.3 mm with an increment of 0.2 mm. Figure 3.6.c. shows the calibration results for the middle film. Experiments showed that the relation between the conductance of the middle film and the square of the beam deflection is linear.

Using interpolation for the collected data from the calibration tests, the following Equations can be obtained to calculate the contact force and the beam deflection:

$$F_{cont} = F_{ls} + F_{rs} \qquad (3\text{-}2)$$

$$F_{ls} = 34.806\, X_{ls} \qquad (3\text{-}3)$$

$$F_{rs} = 71.423\, X_{rs} \qquad (3\text{-}4)$$

$$\delta_{beam} = \sqrt{(35.15\, X_{beam} - 0.0432)} \qquad (3\text{-}5)$$

where, F_{cont} is the contact force (N), F_{ls} and F_{rs} are the reaction force at the left and right support (N), respectively, X_{ls} and X_{rs} are the conductance of the piezoresistive film underneath the left and right support $(k\Omega^{-1})$, respectively, δ_{beam} is the deflection of the elastic beam (mm), and X_{beam} is the conductance of the middle piezoresistive film $(k\Omega^{-1})$

.
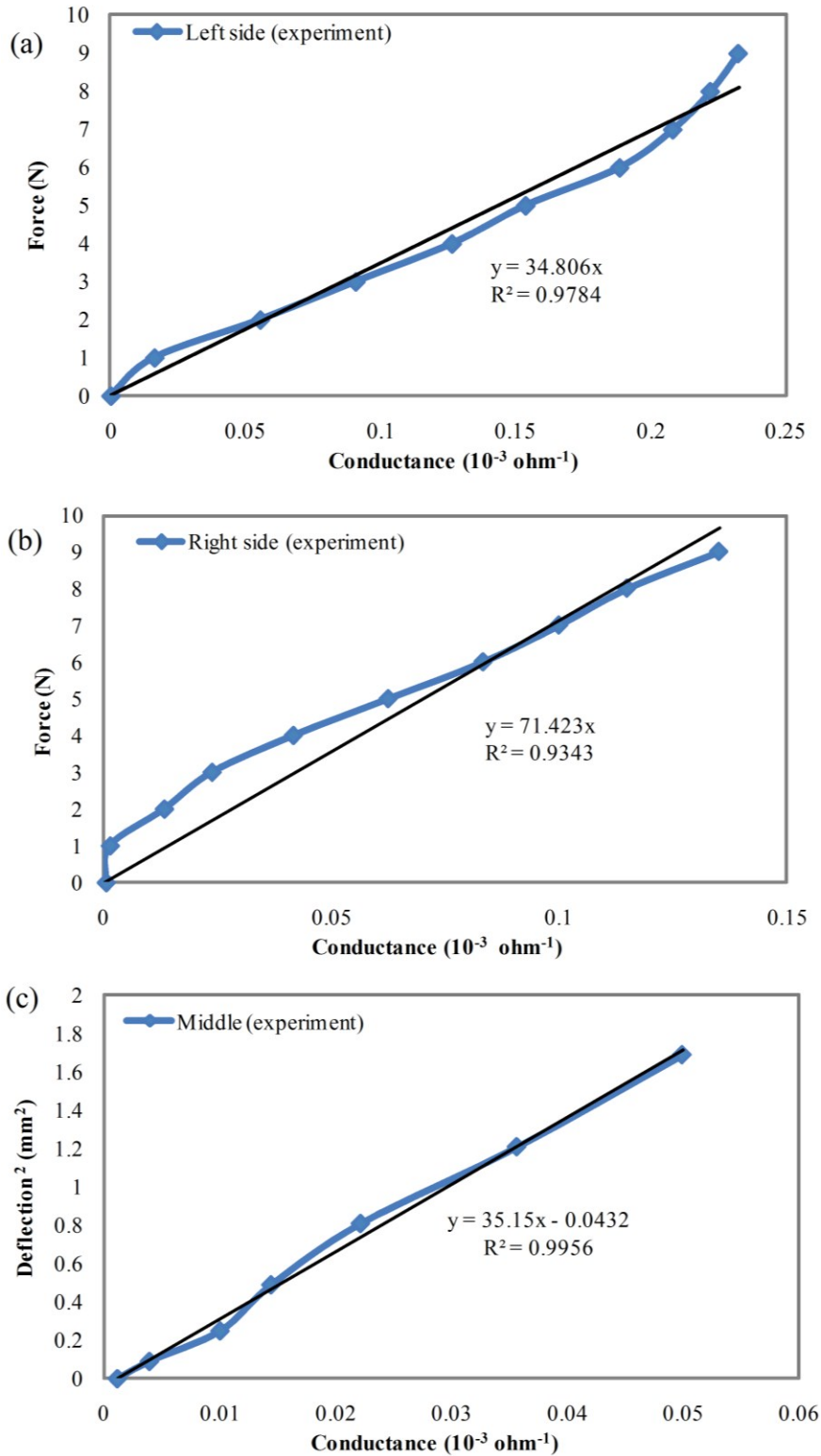
Figure 3.6: Calibration results used to obtain the mathematical relationships between the piezoresistive films conductance and either force or deflection. (a) Calibration of the left side piezoresistive film. (b) Calibration of the right side piezoresistive film. (c) Calibration of the middle piezoresistive film.
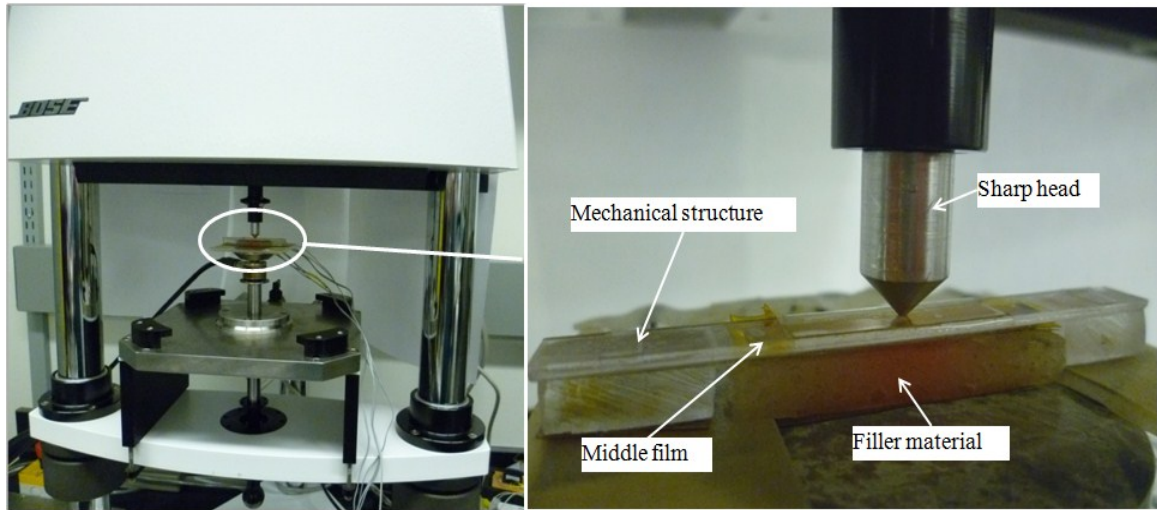
Figure 3.7: The calibration test for the middle top piezoresistive film.

3.3. Silicone Rubbers Stress-Strain Test

Different hyperelastic silicone rubber materials with different hardness values were molded and cured to be used in the experiments, instead of using elastomeric materials that, unlike the real tissues, are compressible and have different mechanical properties than the real tissues. The silicone rubber materials, which are incompressible, were used in the experiments in order to have a realistic simulation for the real tissues. Five different silicone rubber specimens were chosen to be used in this work: Ecoflex 00-10, Ecoflex 00-30, Ecoflex 00-50, Dragon Skin F/X PRO, and Dragon Skin 20, all from SMOOTH-ON Inc.

In order to find the hardness of the silicone rubbers and to simulate them in a finite element (FE) environment, their stress-strain curve should be obtained experimentally. For this purpose, five specimens of five different silicone rubbers were molded and used in a compression test. Their dimensions are shown in Table 3.1. The compression test

was performed using the Electroforce device by applying a 1.5 mm displacement to the specimens with a feed rate of 0.05 mm/sec and sampling rate of 0.83 point/sec. The device has built-in sensors to measure and record both the displacement and force. The feed rate of the displacement was chosen based on various experimental results, which ensured that for higher feed rates the silicone rubber exhibits relaxation behavior, i.e. while the displacement on the silicone rubber is fixed, the internal force of the silicone rubber (stress) changes. The feed rate was set to be slow enough to prevent the viscoelastic relaxation effect. Figure 3.8 illustrates the relaxation behavior under a higher feed rate.

Figure 3.9 shows the recorded force-displacement curves converted into stress-strain curves. These curves were used to differentiate between the silicone rubbers based on their hardness, and for the FE simulation purposes. The experiments showed the order of the hardness values of the silicone rubber samples: Ecoflex 00-10 < Ecoflex 00-30 < Ecoflex 00-50 < Dragon Skin F/X PRO < Dragon Skin 20. The experiments results in Figure 3.9 show the nonlinear elastic behavior of silicone rubbers. Due to hyperelasticity of silicone rubbers one can notice that the Dragon Skin F/X PRO hardness, which is clearly harder than both Ecoflex 00-30 and Ecoflex 00-50 in the range of strain higher than 0.11, is slightly less than them at strain values less than 0.11. However, this would not negatively affect the results of the final experiments in calculating the relative hardness since the applied force (5 N) is enough to accomplish a compression strain in Dragon Skin F/X PRO sample higher than 0.11.
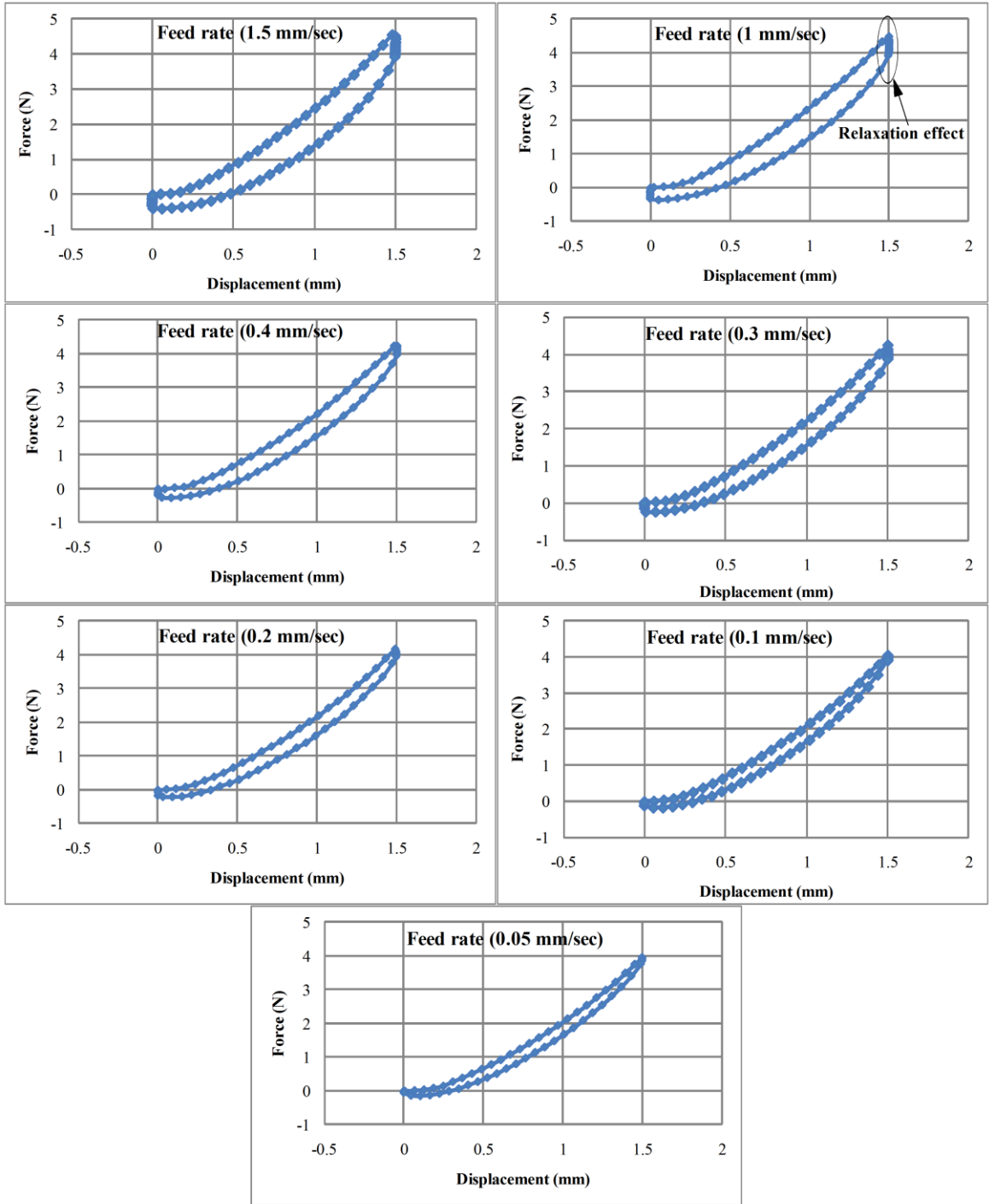
Figure 3.8: The relaxation behavior of silicone rubber in the compression tests with different feed rates of the applied displacement.

Using a Durometer, further tests were carried out to verify the order of the silicone rubber hardness values. Table 3.1 shows the results of these tests. The values of hardness presented in Table 3.1 are the average values of ten repeated readings carried out for each silicone rubber. As mentioned earlier, Durometer method for measuring the hardness or the shore has different scales. In Table 3.1 two types of these scales are mentioned, they are shore 00 and shore A. It is important to mention that shore A is expressing higher values of hardness than shore 00. Hence shore A is used for soft rubbers while shore 00 is used for very soft rubbers. Ecoflex 00-10 specimen was used in the structure of the prototype as the filler material, since it is the softest silicone rubber specimen. The other four silicone rubbers were used to mold and cure a new four larger samples that resemble four different biological tissues in the experiments.

Table 3.1: The Durometer results for the hardness of the silicone rubbers and their dimensions in both the compression test and sensor test.

Silicone rubber Name	Shore hardness Value/ type	Dimensions of compression test specimen (mm)	Dimensions of the silicone rubber specimen used in the sensor test (mm)
Ecoflex 00-10	9.5 / (shore 00)	$37.11 \times 7.92 \times 5$	$37.11 \times 7.92 \times 5$
Ecoflex 00-30	27.025 / (shore 00)	$37.47 \times 8.12 \times 5.3$	$75.08 \times 10.99 \times 7.84$
Ecoflex 00-50	41.79 / (shore 00)	$36.75 \times 7.5 \times 5.48$	$78.72 \times 11.66 \times 8.44$
Dragon Skin F/X PRO	2.69 / (shore A)	$37.14 \times 7.05 \times 5.73$	$82.96 \times 11.49 \times 8.07$
Dragon Skin 20	19.25 / (shore A)	$37.49 \times 7.98 \times 5.4$	$80.57 \times 10.24 \times 8.49$
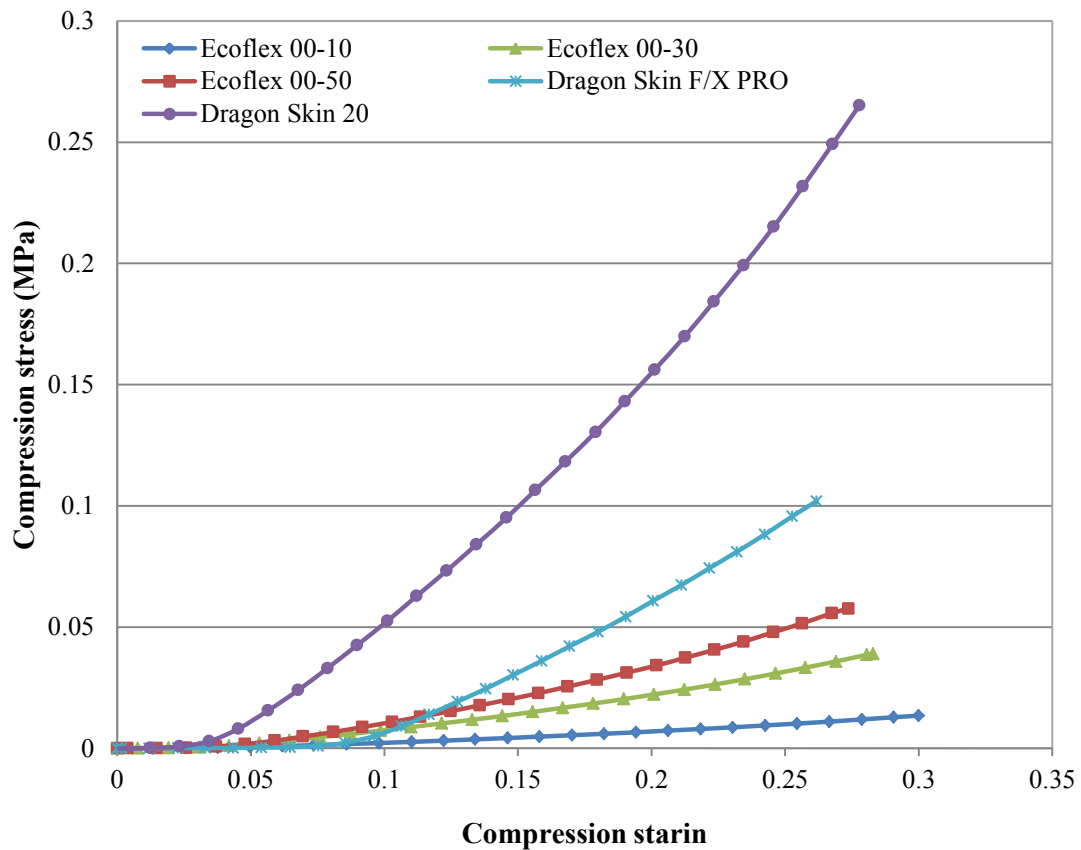
Figure 3.9: The obtained stress strain curves from compression tests

3.4. Experimental Test on the Sensor

The calibration process provides the mathematical relations between the films resistances and both the compressive force and the beam deflection. These relations (Equations (2-4), and (3-1)-(3-5)) can be implemented in a LabView program that will calculate and record, simultaneously, the contact force and the relative hardness of the contact object directly from the change in the resistance of the piezoresistive films in the sensor.

The same experimental setup as the one used in the calibration test is employed to test and validate the functionality of the proposed prototype. The prototype was fixed to a base on the stationary jaw of the Electroforce device. The four different specimens of silicone rubbers, which resemble biological tissues, were individually placed on the top of the prototype. Then, using the movable jaw of the Electroforce, a distributed compressive load was applied to the specimen as a reference square force function to simulate the grasping process in MIS. The reference square force function was repeated five times with a frequency of 0.2 Hz and a magnitude of 0 to 5 N. The applied force function tests the repeatability of the sensor and its ability to work with both dynamic and static forces, and shows the quick response of the sensor. Figure 3.10 shows the experimental setup used for testing the prototype.

3.4.1 Force Sensing

Figure 3.11 shows the contact force measurement when different types of silicone rubber are placed on top of the sensor. It is clear in the figure that the sensor is able to evaluate the contact force with acceptable accuracy no matter what is the hardness value of the contact object.   One could also see from Figure 3.11 that the sensor is able to perform under both static and dynamic conditions. The variation in static response with time in Figure 3.11 could be attributed to the drift in the response of the piezoresistive sensing film.
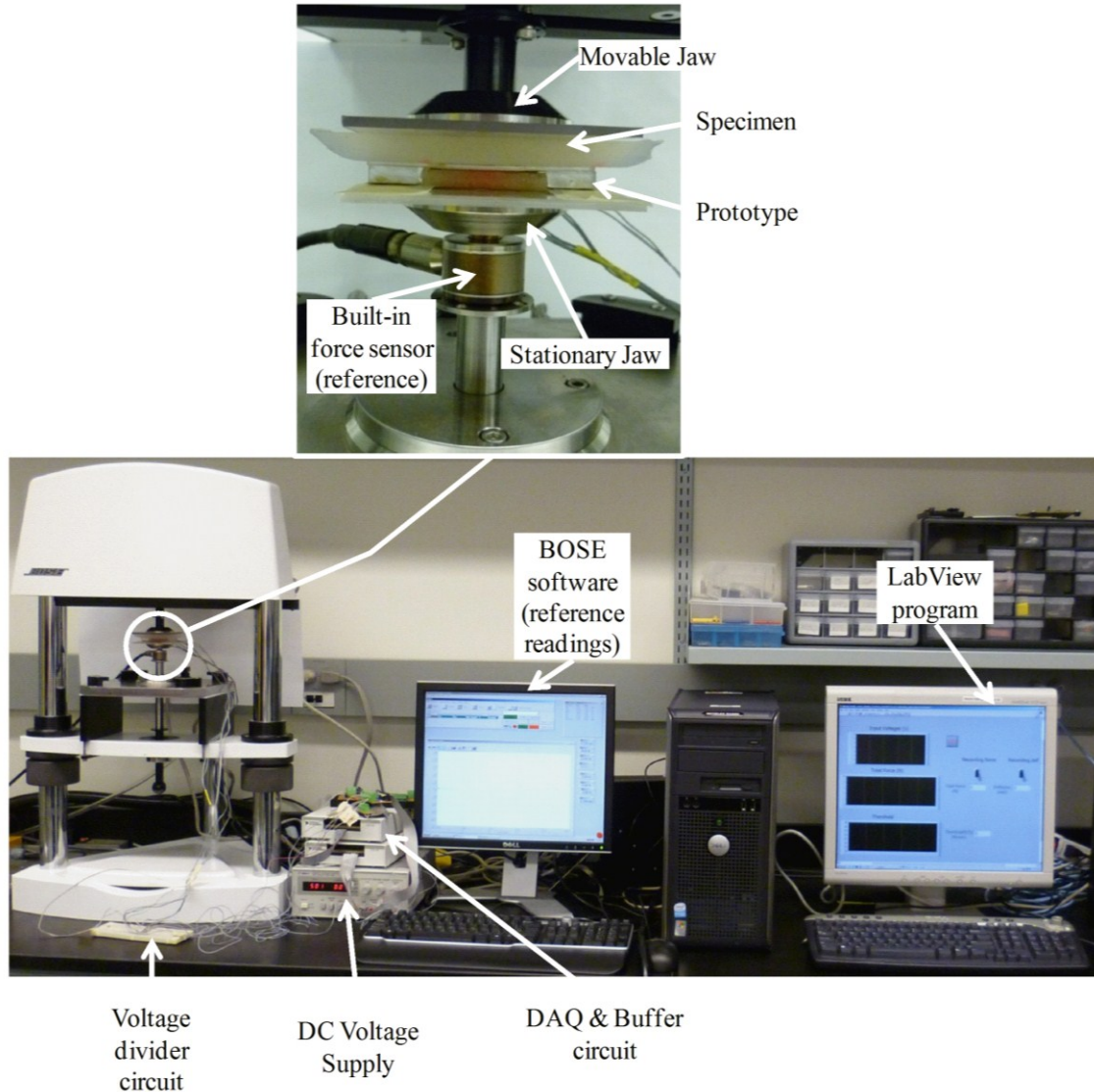
Figure 3.10: The experimental setup

3.4.2. Relative Hardness Testing

Figure 3.12 shows the beam deflection for different types of silicone rubber. The four tested samples are Ecoflex 00-30, Ecoflex 00-50, Dragon Skin F/X PRO, and Dragon Skin 20.
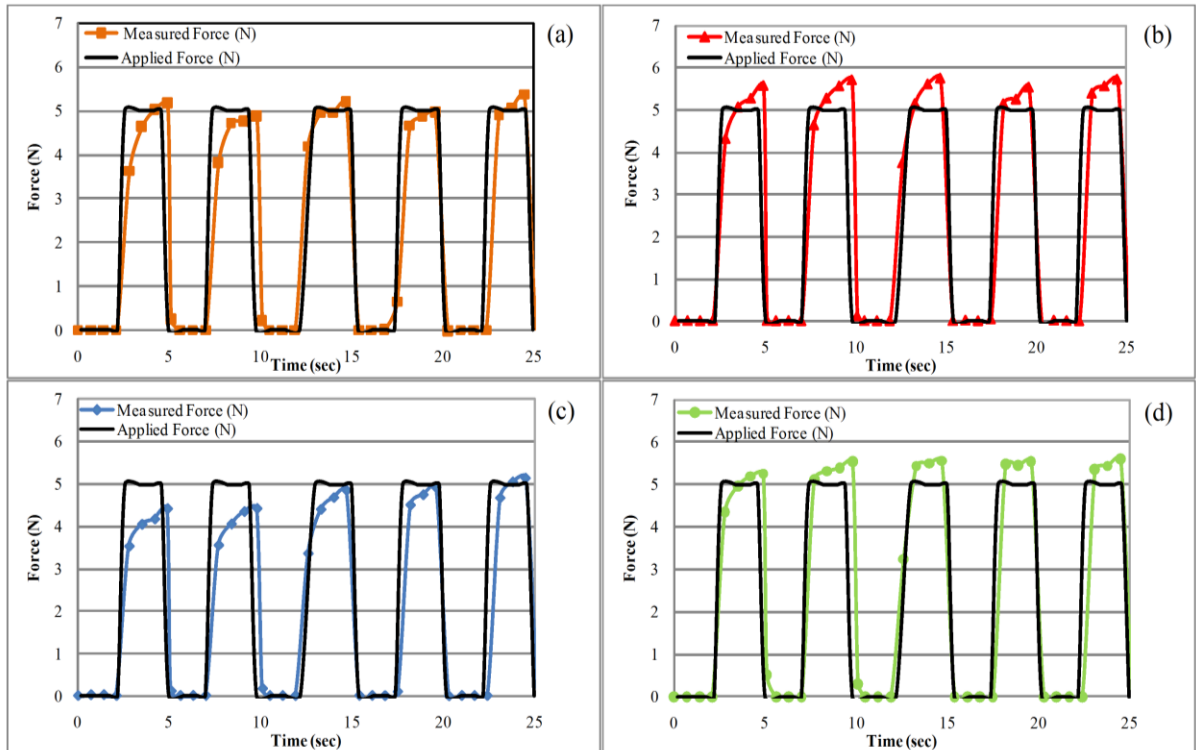
Figure 3.11: The measured contact force by the prototype using different silicone rubbers. (a) Measured contact force when Ecoflex 00-30 is tested. (b) Measured contact force when Ecoflex 00-50 is tested. (c) Measured contact force when Dragon Skin F/X PRO is tested. (d) Measured contact force when Dragon Skin 20 is tested

As Figure 3.12 illustrates, the Dragon Skin 20 (the hardest) has the minimum deflection, and the Ecoflex 00-30 (the softest) has the maximum deflection. Moreover, Dragon Skin F/X PRO that is softer than Dragon Skin 20 has a higher deflection than Dragon Skin 20. Same principle is applied for Ecoflex 00-50 when it is compared to Dragon Skin F/X PRO. Therefore, Figure 3.12 shows that as the material hardness increases, its deformation and the corresponding beam deflection decrease. Consequently, the sensor is able to distinguish between different materials based on their hardness.
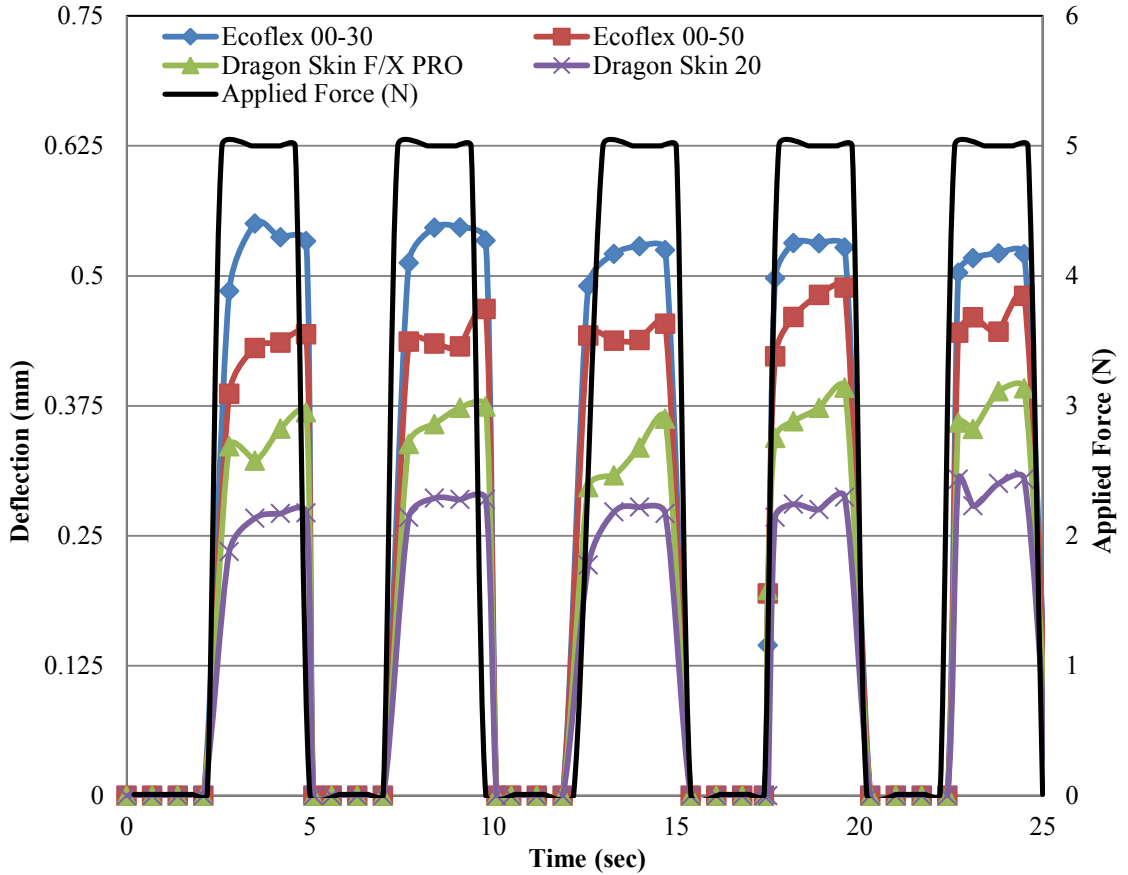
Figure 3.12: The deflection of the elastic beam measured by the middle piezoresistive film for four different silicone rubbers under a square force function. Ecoflex 00-30 is the softest material, while Dragon Skin 20 is the hardest material.

The stress-strain curves obtained in section 3.3, Figure 3.9, were used to calculate the Young's modulus of elasticity for each silicone rubber used in the experimental test of the sensor as a contact tissue. Since the silicone rubber shows a nonlinear stress-strain relationships, therefore the linear part of each stress-strain curve were used to estimate the Young's modulus of elasticity of that silicone rubber, Figure 3.13. The calculated Young's modulus of silicone rubbers are shown in Table 3.2.

Figure 3.14 shows the deflection of the beam of the proposed sensor at the center of the beam versus different values of stiffness, expressed in terms of Young's modulus of

elasticity, of different silicone rubbers that resemble different biological tissues at 5 N grasping force.

Table 3.2: Derived Young's modulus of elasticity for silicone rubbers.

Silicon Rubber	Ecoflex 00-30	Ecoflex 00-50	Dragon Skin F/X PRO	Dragon Skin 20
Young's modulus of elasticity (MPa)	0.1694	0.2642	0.5604	1.1143
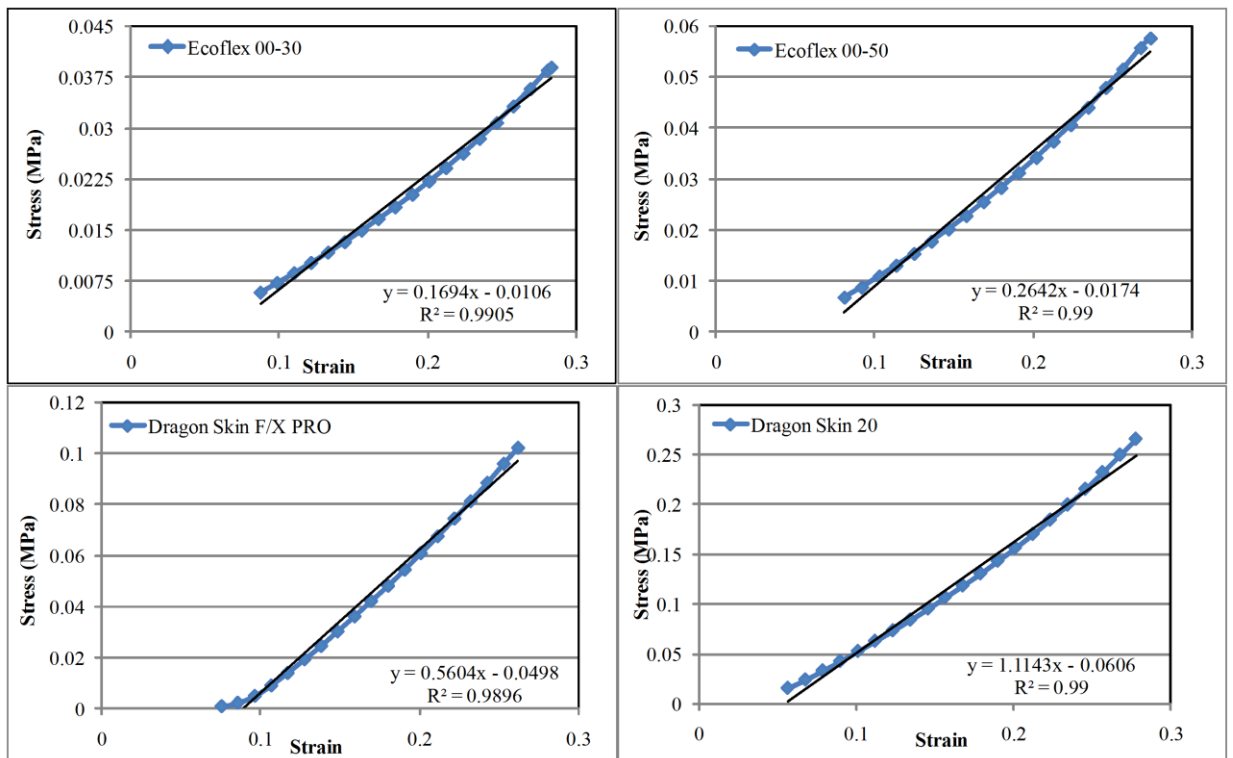
Figure 3.13: Deriving the Young's modulus of elasticity for the silicone rubbers.
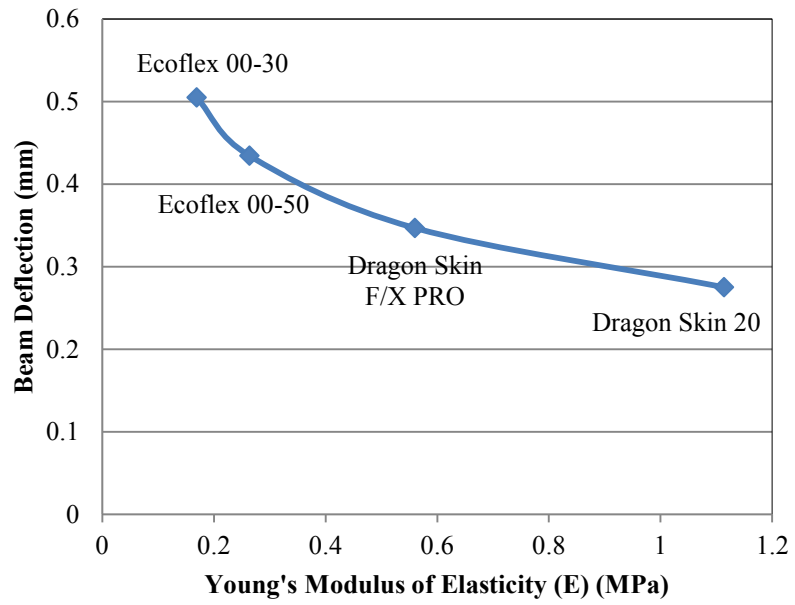
Figure 3.14: Measured beam deflection at the center of the beam versus different silicone rubbers (biological tissues) stiffness at 5 N grasping force.

Chapter 4 : Finite Element Analysis (Modeling, Simulation and Verification)

A finite element (FE) model for the proposed prototype is built to investigate and validate the sensor response and functionality regarding the measurement of the contact force and relative hardness of the contact object. The purpose of the FE model, from one side, is to verify, and test the proposed design when it comes in contact with biological tissues. And from the other side, the FE model is aiming to verify the results obtained experimentally in order to confirm that the FE model can be used to predict the sensor output. The silicone rubbers, which are hyperelastic materials, were used in the sensor structure. They were also used as testing samples that interact with the proposed sensor in the experiments, since the biological tissues can be simulated as silicone rubbers [120]. Therefore, accurate models for these silicone rubbers should be developed. In the following sections the mathematical modeling of hyperelastic materials is briefly discussed. Then, the FE models for different silicone rubbers and the interaction between the sensor and the biological tissues are presented.

4.1. Hyperelastic Material Modeling

Rubberlike materials, including silicone rubbers, are incompressible isotropic materials which endure large elastic deformations [121, 122, 123]. Therefore, they can be modeled using the non-linear elastic theory that is often used for modeling isotropic incompressible hyperelastic materials. A green elastic (hyperelastic) material is a specific type of Cauchy materials which is defined by its strain energy function (W) [122, 123].

The strain energy function (W) for isotropic green elastic materials can be identified by the principle invariants (I_1, I_2, and I_3) of the left Cauchy-Green deformation tensor [123]:

$$W = W(I_1, I_2, I_3) \qquad (3\text{-}6)$$

When the material is incompressible, I_3 is equal to one since there is no change in the volume of the material. In consequence, W in Equation (3-6) becomes [123]:

$$W = W(I_1, I_2) \qquad (3\text{-}7)$$

The stress tensor ($\boldsymbol{S}$) of an incompressible isotropic hyperelastic material is obtained by [123]:

$$\boldsymbol{S} = \frac{\partial W(\boldsymbol{A})}{\partial \boldsymbol{A}} \qquad (3\text{-}8)$$

where $\boldsymbol{A}$ is the deformation gradient tensor.

Several mathematical models have been proposed for representing hyperelastic materials. A commonly used mathematical model that is appropriate for modeling an isotropic incompressible hyperelastic material is the Neo-Hookean model [122, 123] which uses the following Equation for the strain energy function [124]:

$$W(I_1, I_2) = \frac{\mu}{2}(I_1 - 3) + \frac{\kappa}{2}(J - 1)^2 \qquad (3\text{-}9)$$

where μ is the initial shear modulus of the material, κ is the initial bulk modulus of the material, and J is the ratio of the current volume to the reference volume ($J = \det(\boldsymbol{A})$). The initial bulk modulus and the initial shear modulus are given by [124]:

$$\kappa = \frac{2(c_{10} + c_{01})}{1 - (2v)} \qquad (3\text{-}10)$$

$$\mu = 2(c_{10} + c_{01})$$
(3-11)

where c_{10}, and c_{01} are Mooney-Rivlin constants of the material, and ν is the Poisson's ratio of the material, which is approximately equal to 0.5 for incompressible materials.

At this stage, for modeling purposes, the Mooney-Rivlin constants for a hyperelastic material should be determined; they can be evaluated from the data collected in any stress-strain test of the material [121, 122].

4.2. Finite Element Analysis

This section presents the finite element models that developed to simulate the silicone rubbers and the interaction between the sensor and the silicone rubbers.

4.2.1 Silicone Rubber Modeling

In order to simulate the interaction between the prototype and the silicone rubbers, accurate FE models for the silicone rubbers should be created. Three different silicone rubber specimens from the five molded silicone rubbers were chosen to be used in FEA: Ecoflex 00-10, Ecoflex 00-50, and Dragon Skin 20. In order to obtain their stress-strain data, the compression test is carried out as presented in the section 3.3. The stress-strain data were, then, used in a Matlab code [122] to obtain the Mooney-Rivlin constants for each specimen. Finally, the mechanical properties of each silicone rubber were calculated using Equations (3-10) and (3-11) to be employed in finite element analysis (FEA). Table 4.1 shows the calculated mechanical properties of each specimen.

Table 4.1: The calculated mechanical properties of silicone rubbers

Silicone rubber	Initial shear modulus (μ) (MPa)	Initial bulk modulus (κ) (MPa)
Ecoflex 00-10	0.002743	0.030477
Ecoflex 00-50	0.007439	0.165302
Dragon Skin 20	0.063297	0.703228

Separate FE models for the selected tested silicone rubber specimens were built using COMSOL Multiphysics software (v 3.4). The dimensions of the specimens in the compression test, Table 3.1, and the calculated mechanical properties of the material, Table 4.1, were used in the FE models. The FE models were built in 2D space using the structural mechanics module in a plane strain application. The structural mechanics module was selected since it is appropriate for hyperelastic modeling as the module allows a large deformation [122]. The analysis was performed using Lagrangian-quadratic triangular elements, large deformation, parametric analysis, and the ideal constrains. The Lagrangian-quadratic triangular element reduces the error in comparison with the linear Lagrangian element. Additionally, Lagrangian-quadratic triangular elements are characterized with hyperelasticity, large strain facilities, and large deformation. All of these properties of this element are required in our models. The FE models were prepared to simulate the compression test that was carried out on the silicone rubber samples. The models include three layers (sub-domains): top and bottom sub-domains represent the upper (free) and lower (fixed) jaws of the testing device

(Electroforce 3200), respectively, while the middle sub-domain represents the tested specimen. In order to simulate the compression test, the free jaw was set to move in steps of 0.05 mm, with a total displacement of 1.5 mm. The stress-strain curve for each model was obtained and compared to the experimental stress-strain curve. The comparison ensured acceptable accuracy of the FE models to be used in modeling the interaction between the sensor and the silicone rubbers. However, the negligible differences between stress-strain curves obtained via both experiments and FEA can be attributed to either experimental error by human or equipment, or to the inaccuracy of the FEA software. Figure 4.1 shows the comparison between both the experimental and FEA results of the compression test of each silicone rubber.
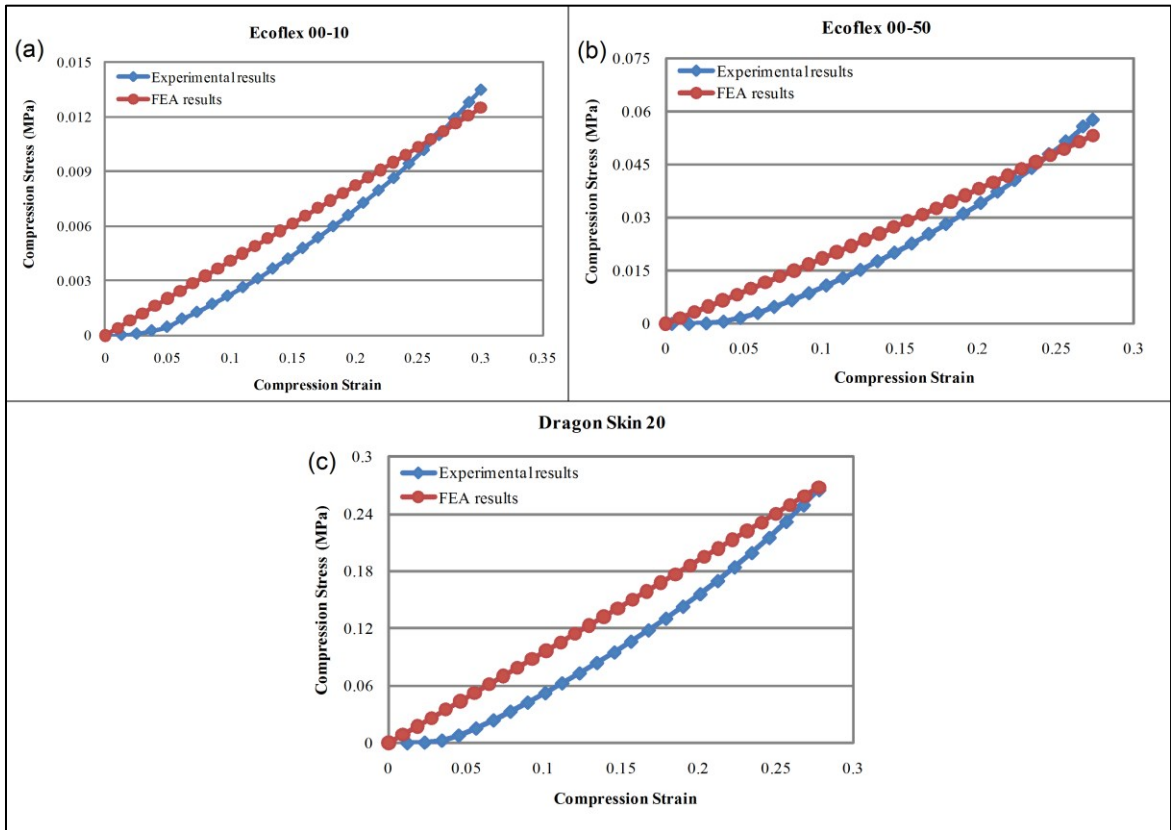

Figure 4.1: Experimental and FEA results of the compression test (a) for Ecoflex 00-10, (b) for Ecoflex 00-50, and (c) for Dragon Skin 20.

4.2.2. Testing of the Sensor Using FEA

Once the silicone rubber models were obtained accurately, an FE model for the proposed sensor and its contact with the simulated biological tissues was built to analyze the sensor's mechanical behavior during the contact and to validate the sensor response obtained in experiments. As illustrated in Figure 4.2, the last FE model includes the jaws of the testing device, filler material, supports, elastic beam, and the tested silicone rubber. The new FE model has specifications and analysis settings similar to previous silicone rubber models. The materials of the parts of the new FE model were given mechanical properties similar to the actual mechanical properties of the materials used to build the prototype (Table 2.1). Table 4.1 presents the calculated mechanical properties of the silicone rubbers in the new FE model. The dimensions of the silicone rubbers in the new FE model are presented in Table 3.1. The silicone rubbers resembling the biological tissues had the same dimensions as those used in the experimental test of the sensor (Table 3.1).

To investigate the interaction between the prototype on the MIS tool's tip and the biological tissues, it was assumed that the grasped tissue is given either displacement or distributed load by the MIS tool, i.e. the endoscopic grasper. The new FE model is able to simulate both the displacement and distributed load.

In the distribution load scenario, the parametric analysis in COMSOL is used to apply an incremental distributed load to the upper jaw in the negative direction of the y-axis. While, the Displacement scenario is simulated by applying an incremental negative displacement to the upper jaw along the y-axis, using the parametric analysis.
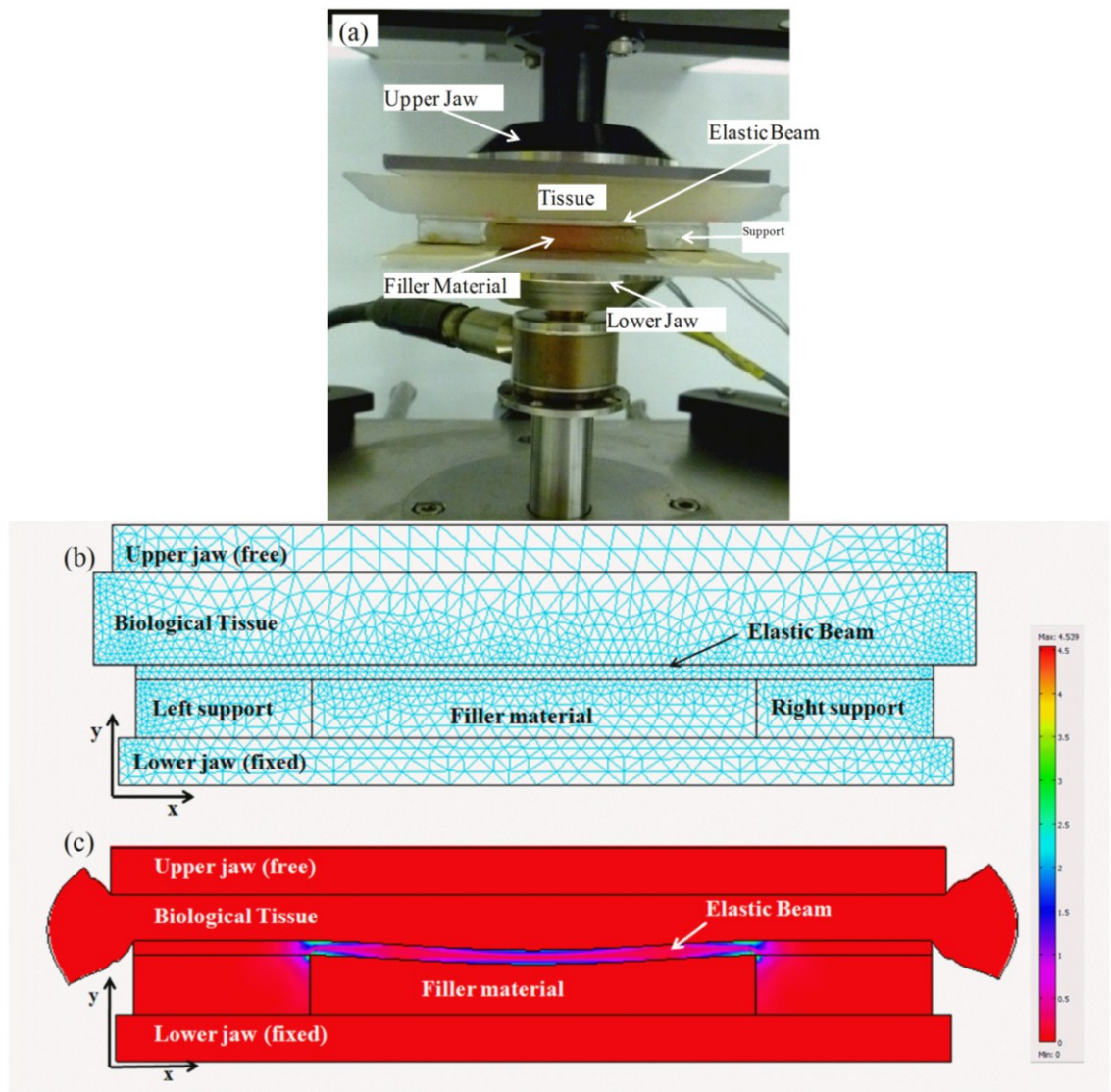
Figure 4.2: The FEM of the tactile sensor and its interaction with Silicone rubber. The model is simulating a practical test of this interaction using the Electroforce 3200 device. (a) The experimental test of interaction between sensor and Silicone rubber. (b) Meshed structure of the sensor and silicone rubber. (c) The silicone rubber and sensor structure after applying displacement to the upper jaw.

Table 4.2 shows the measured force at the supports at different values of the applied distribution load to the upper jaw. The results show that the summation of the forces at the supports is almost equal to the total applied load. Therefore, the supports transfer almost all the applied force on the contact object to the substrate underneath the supports.

Table 4.2: Measured contact force at the supports in FE model of the interaction between the sensor and silicone rubber

Applied distributed load to the upper jaw (N)	Total measured force at the supports, Dragon Skin 20 in contact (N)	Total measured force at the supports, Ecoflex 00-50 in contact (N)
1	0.9737505	0.96075886
3	2.9212947	2.8829231
5	4.8690457	4.8065963

Figure 4.3 presents the results of applying the distribution load scenario on the tested silicon rubbers. The load increases from 0 to 5 N, with 0.25 N steps. The figure shows the selected tested silicone rubbers had different beam deflections under the same load, depending on the silicone rubber hardness. The hardest material (Dragon Skin 20) always had the smallest beam deflection; while, the softest material (Ecoflex 00-50) had the highest beam deflection for all loading values. Simulation results, of load scenario, show that Dragon Skin 20 is the hardest material. Furthermore, the curves show that as the applied load increases the difference between the beam deflections for the silicone rubbers increases. In other words, the sensor's sensitivity will increase with increasing the applied load since the contact object will undergo a larger deformation and, consequently, a larger corresponding beam deflection.

Figure 4.4 illustrates the output of applying the displacement scenario on the tested silicone rubbers. The displacement varies from 0 to 3 mm with 0.1 mm increments. The

figure shows the curves of the measured beam deflection (δ) (mm) versus the measured contact force on the supports (N) obtained from the FEA solution. The slope of each curve is equal to F/δ, which can be used to estimate the relative hardness of the material, Equation(2-4). An estimated slope, or average of the slope, can be determined from the derivative of the Equation of the linear trend line for each curve. It is found that this slope of Ecoflex 00-50 and Dragon Skin 20 is 37.927 and 74.633 N/mm, respectively. The simulation shows that Ecoflex 00-50 is the softest material. Furthermore, the figure shows the non-linear behavior of the silicone rubbers modeled in FE.
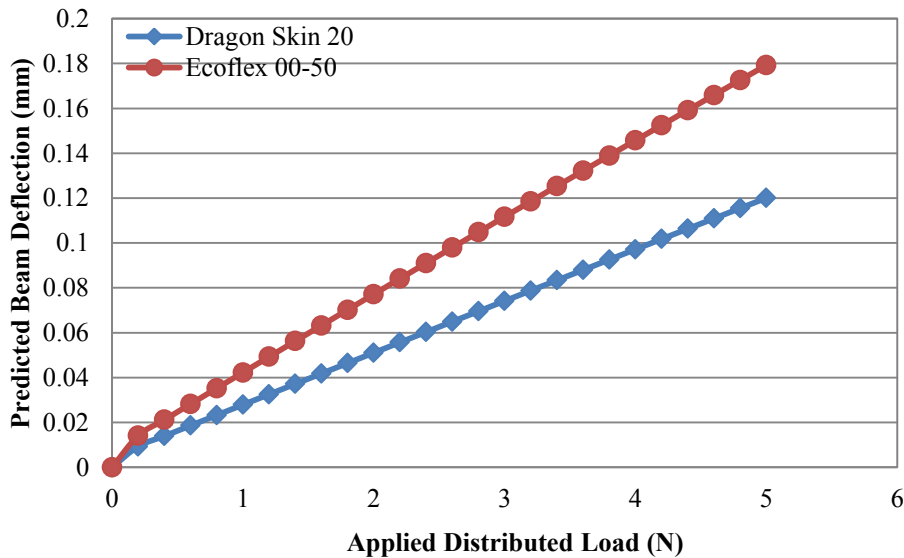
Figure 4.3: FE results of applying the distribution load scenario on two different silicone rubbers: Dragon Skin 20 (hard) and Ecoflex 00-50 (soft).
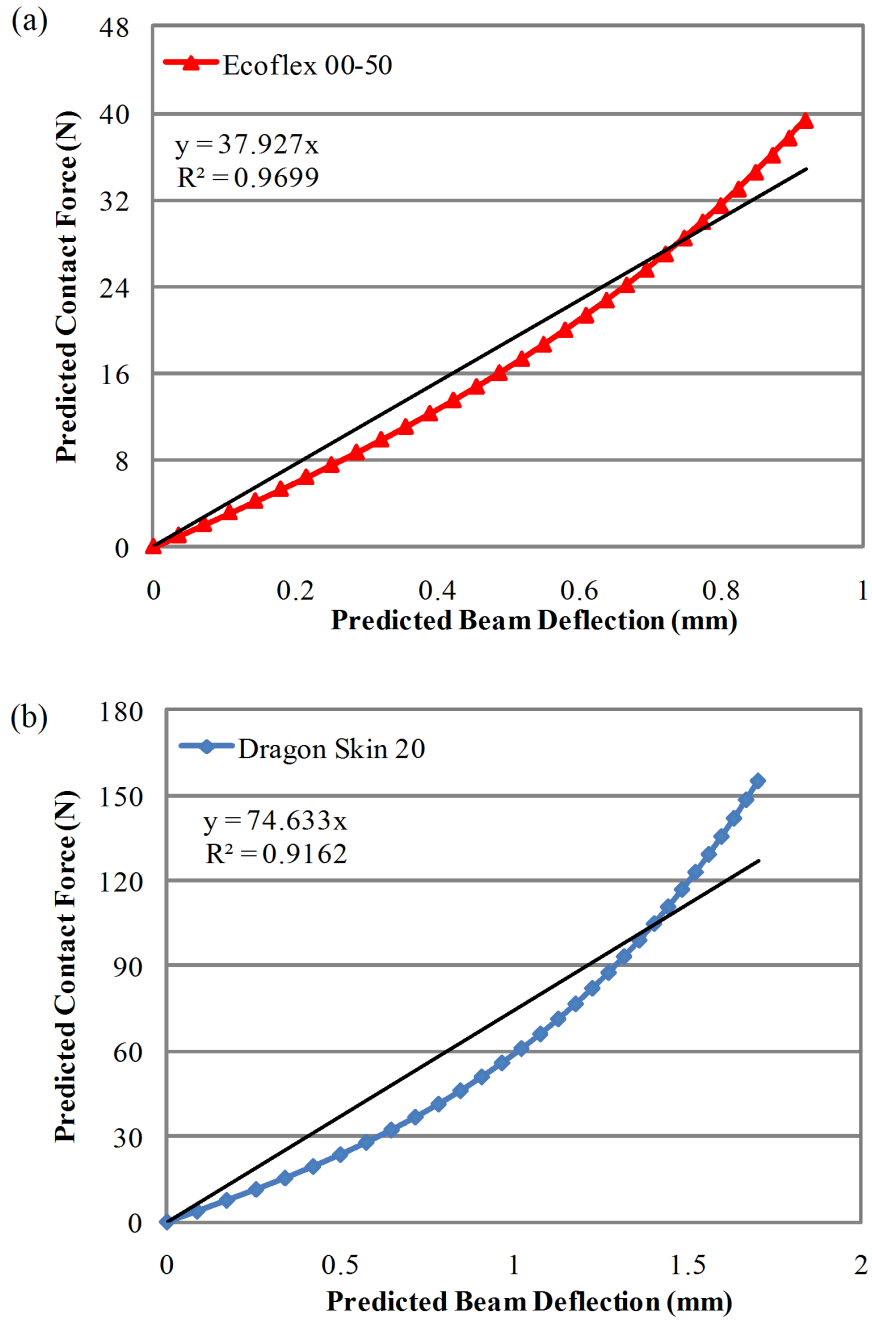
Figure 4.4: FE results of applying the displacement scenario on two different silicone rubbers: (a) Ecoflex 00-50 (soft) and (b) Dragon Skin 20 (hard).

4.3. Discussion

Figure 4.5 shows a Comparison between the beam deflections obtained for two different silicone rubbers (contact tissues) by FEA and experimental analysis when a 5 N load is applied to the contact tissue. The figure shows the error, i.e. difference between experimental and FEA results.
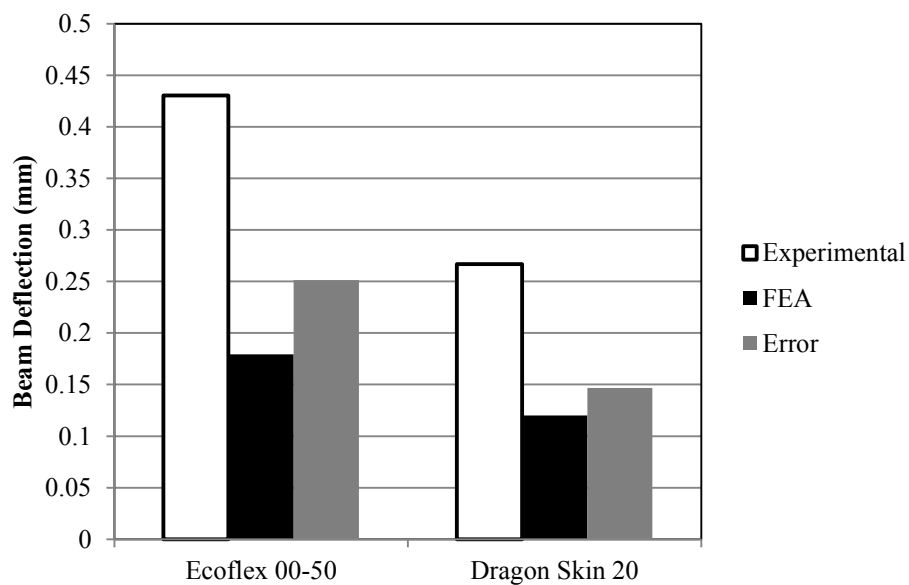
Figure 4.5: Comparison between the beam deflections obtained for two different silicone rubbers (contact tissues) by FEA and experimental analysis when a 5 N load is applied to the contact tissue.

Both simulation and experimental results ensure the validity of the sensor principle. The results show the same order of hardness for the three closed silicone rubbers, i.e. Ecoflex 00-10 < Ecoflex 00-50 < Dragon Skin 20. In the interaction between the proposed sensor and the silicone rubber, both experimental and simulation results show that Dragon Skin 20 is harder than the Ecoflex 00-50. Nevertheless, the obtained experimental values for the contact force and beam deflection are greater than those obtained in the FE

simulations. This difference is caused by several factors. For instance, the inaccuracy in calibrating the sensing elements could be one of the main factors. Other reasons may be (i) the drift issue in the piezoresistive sensing element that can be eliminated using special signal conditioning, (ii) the inaccuracy of manual fabrication for both the sensor structure and the molded silicone rubbers, and (iii) the inaccuracy of the FEA solutions. Overall, the FE simulations and experimental results show general agreement regarding measuring the contact force and the relative hardness of the contact object.

The ratio of deflections for Ecoflex 00-50 to Dragon Skin 20 is 0.6 experimentally and 0.64 predicted which are found to be in agreement. Here, the difference between model and experiments could be attributed to non-linearity in material properties, omitting of glue and sensor's films in modeling, contact properties including roughness, pre-stressing, etc.

Chapter 5 : Summary, Conclusion and Future Work

The main objective of this thesis is to design and fabricate a prototype of a novel tactile sensor that can be integrated to minimally invasive surgery endoscopic grasper and restore the important missing tactile information to the surgeon *in vivo*. The thesis presents a sensor that is aimed to serve and develop the rapidly growing MIS field, since the main constraint faced by the MIS surgeon is the loss of touch with the biological tissues. The main function of the sensor, as aimed by the author, is to feedback the contact force and the relative hardness of the contacted tissue when a static or dynamic loading is applied to the object. Grasping in MIS is a static loading process, and most of the tactile sensors for MIS use presented in the literature review suffer from their disability to work under constant loadings.

A novel multifunctional piezoresistive-based tactile sensor for MIS applications is developed in this work. In order to conduct a realistic test using the proposed sensor, silicone rubber samples were chosen to represent different samples of biological tissues with different hardness values in both the FE models and experiments. Since silicone rubbers have similar mechanical properties to the real tissues, the results of the numerical and experimental tests provide investigations of the sensor response in realistic conditions similar to the real surgical operations.

5.1. Summary

A miniaturized prototype of the proposed sensor was built manually and tested experimentally to characterize the sensor. Initially, the prototype was tested with

elastomers. At the second stage: (1) further calibration was carried out; (2) silicone rubbers were molded and their mechanical behavior was studied experimentally; and (3) the prototype was experimentally tested with the molded silicone rubbers. The experiments tested the ability of the sensor to measure the contact force as well as the relative hardness of the contact object, and consequently the sensor's ability to differentiate the relative hardness of materials. The results of the contact force measurements, Figure 3.11, ensure the sensor's capability to measure the contact force regardless of the hardness of the material that is used as a contact object. The results of measuring the relative hardness of the contact object, Figure 3.12, show that the sensor is capable of differentiating four different silicone rubbers, which potentially simulate four biological tissues, based on their hardness and the corresponding beam deflection. The sensor detects smallest beam deflection, i.e. about 0.28 mm, for the hardest silicone rubber sample, which is the Dragon skin 20. While for the softest silicone rubber, i.e. Ecoflex 00-30, the sensor has the highest beam deflection, which is around 0.53 mm. The difference in beam deflection measured for both materials is around 0.25 mm, which is a considerable difference at only a 5 N loading. This difference will increase as the loading is increased. The square force function applied in the experiments shows the fast response of the sensor, the output stability, and repeatability. The experimental results show some small variation in the output values that can be eliminated by using a suitable filter to attenuate the noise, or by using the precisely calibrated commercial pressure sensors.

In order to validate the experimental results, confirm the ability of the FEA to predict the sensor response, and the suitability of FEA to be used to investigate the proposed sensor, three silicone rubbers were chosen to be modeled in FE. Two were used as biological

tissues in the models, and the third was implemented in the sensor structure in the FE models. The FE models for the silicone rubbers were built in COMSOL Multiphysics software. The mechanical behavior of the silicone rubbers models were compared to the mechanical behavior of the prepared silicone rubber samples to ensure acceptable accuracy of the models. Furthermore, the proposed sensor was modeled in COMSOL to investigate its interaction with silicone rubber samples. The analysis of the FE model of the sensor ensures the validity of the experimental results, and the ability of the FEA to expect the sensor output for both contact force and relative hardness of the silicone rubber samples. The FE model of the sensor simulates the grasping process in different scenarios.

5.2. Conclusions

As mentioned in the objective section in Chapter 1 and the literature review, a good candidate for restoring tactile sensing in MIS application is a sensor with the following properties: dynamic and static response, firm grasping, biocompatible, softness sensing, force sensing, ability for microfabrication, cost effective, good working range, simple structure, and durable. The work done in this thesis takes a step forward on the way to address these properties by presenting a novel design of a piezoresistive tactile sensor that satisfies most of these requirements. The experiments show the sensor's ability to sustain both static and dynamic loads and also to measure both contact force and relative hardness. It is important to note that the loading in MIS applications is not dynamic all the time. In fact, grasping in MIS is often considered as a static loading process. This feature makes the proposed sensor an appropriate candidate for MIS applications. The

sensing element is made up of semiconductive polymer composite films that could be produced in biocompatible forms with high piezoresistive properties.

The simple structure of the sensor ensures the ability for micro-fabrication and, consequently, the costs can be significantly reduced since the sensor can be mass-produced. The sensor's structure includes semiconductive polymer composite films and silicone rubbers that are cost effective and compatible with MEMS. It is possible to integrate arrays of the sensor in a commercial endoscopic grasper, which will allow the measurement of the tissues mechanical properties in situ. The proposed design for the endoscopic grasper integrated with the proposed sensor ensures that the entire surface area of the grasper jaw will be active in the grasping process. The array of the sensor will form tooth-like shape that will ensure a firm grasping of the slippery soft tissues. The ability of the sensor to measure in situ is of great importance since the mechanical properties of the tissue alter dramatically when they move from *in vivo* to *ex vivo*.

Although, in this study, the range and sensitivity of the sensor are reliable, the range of the hardness values considered in MIS applications is wide depending on the targeted tissues in the surgery. However, the range of hardness measurements and the sensor sensitivity can be tuned by changing the design parameters such as the hardness of the filler material that should be softer than the hardness of the softest targeted tissue, or by changing other design parameters such as the dimensions and mechanical properties of the elastic beam. For instance, by increasing the hardness of the filler material, the maximum measured hardness would be increased while sacrificing the sensitivity of the sensor. The composite structure of the sensor, or of its deformable part, by means of using the silicone rubber under the beam ensure the ability of the sensor to stand with

some mechanical collision and to be less fragile than those presented in [31, 65, 66, 67] because of the capability of the silicone rubber as an incompressible hyperelastic material in absorbing the applied energy.

5.3. Contributions

This thesis proposes a piezoresistive-based tactile sensor for Minimally Invasive Surgery applications. For the best knowledge of the author, the following are the novel and original contributions of this thesis:

1. A novel multifunctional piezoresistive-based tactile sensor is designed and fabricated.

2. The sensor ability to measure the static and dynamic loadings.

3. The sensor measures the contact force as well as the relative hardness of the contact object/tissue.

4. The sensor is experimentally tested with silicone rubber materials, which simulate real tissues.

5. A nonlinear hyperelastic finite element model for tissue-like materials (Silicone rubbers) is developed in COMSOL Multiphysics.

6. The sensor has a potential to be micromachined, and to be integrated with a commercial endoscopic grasper.

7. The FEA of the sensor with silicone rubber is presented.

5.4. Future Work

The presented thesis includes a novel design for a tactile sensor that has been tested and validated by both FEA and experiments. However, by the end of this research, there are still several improvements that can be carried out in a future work:

1. Using accurate and precise machinery to fabricate the macro level prototype of the sensor.

2. Micro-fabrication of a single sensor including its sensing elements and the mechanical structure, and then micro-fabrication of an array of them. This should include the optimization process on the micro level.

3. Designing the suitable packaging method to protect the sensor from harsh environmental conditions including the leakage of organic liquids to the sensor. In addition, in future work, one can include the electrical chip that would be connected to the sensor in the packaging.

4. Integration of the sensor with a commercial endoscopic grasper.

5. Testing the sensor's ability in finding the position of a concentrated force applied to the sensor.

6. Since the range of hardness values in MIS applications varies dramatically, it would be of great help to optimize the sensor for a specific range of hardness related to one of the MIS operations.

7. The experimental and FEA results were based on the assumption that the applied loads on the tissue and on the presented sensor are vertical. While, in reality, in the contact between the bulky tissue and the commercial grasper, there are a lot of

pressure points where the force is applied to the grasper in different angles. Therefore, studying these contacts would make the experiments more realistic.

Bibliography

[1]   J. Dargahi and S. Najarian, "Human tactile perception as a standard for artificial tactile sensing—a review," *The International Journal of Medical Robotics and Computer Assisted Surgery,* vol. 1, pp. 23-35, 2004.

[2]   S. Awtar, T. T. Trutna, J. M. Nielsen, R. Abani, and J. Geiger, "FlexDex: A Minimally Invasive Surgical Tool With Enhanced Dexterity and Intuitive Control," *Journal of Medical Devices,* vol. 4, pp. 035003(1-8), 2010.

[3]   A. L. Trejos, R. V. Patel, M. D. Naish, A. C. Lyle, and C. M. Schlachta, "A sensorized instrument for skills assessment and training in minimally invasive surgery," *Journal of Medical Devices,* vol. 3, pp. 041002(1-12), 2009.

[4]   F. E. Silverstein and G. N. J. Tytgat, *Atlas of Gastrointestinal Endoscopy*. New York: Gower Medical, 1991.

[5]   L. W. Way, S. Bhoyrul, and T. Mori, *Fundamentals of Laparoscopic Surgery*. London, U.K: Churchill Livingstone, 1995.

[6]   W. Wayand, "The History of Minimally Invasive Surgery," Touch Briefings PLC, LondonOctober-2004 2004.

[7]   http://www.gynaemd.com.sg, "laparoscopy," ed.

[8]   http://gammaendo.com/catalog/popup_image.php?pID=50, "Endoscopic Tool," ed.

[9]   S. Sokhanvar, "Micromachined multifunctional polyvinylidene fluoride tactile sensor for minimally invasive surgery graspers," 68, CONCORDIA UNIVERSITY, 2007.

[10]   M. Ramezanifard, "Design and development of new tactile softness displays for minimally invasive surgery," CONCORDIA UNIVERSITY, 2009.

[11]   *Minimally Invasive Surgery Within The Genitourinary System*. Available: https://www.cornellurology.com/clinical-conditions/minimally-invasive-surgery/

[12]   M. Doria and L. Birglen, "Design of an Underactuated Compliant Gripper for Surgery Using Nitinol," *Journal of Medical Devices,* vol. 3, pp. 011007 (1-7), 2009.

[13]   J. Dargahi, M. Parameswaran, and S. Payandeh, "A Micromachined Piezoelectric Tactile Sensor for an Endoscopic Grasper-Theory, Fabrication and Experiments," *Microelectromechanical Systems, Journal of,* vol. 9, pp. 329-335, 2000.

[14]   F. Tendick, S. S. Sastry, R. S. Fearing, and M. Cohn, "Applications of micromechatronics in minimally invasive surgery," *Mechatronics, IEEE/ASME Transactions on,* vol. 3, pp. 34-42, 1998.

[15]   M. C. Carrozza, P. Dario, and L. P. S. Jay, "Micromechatronics in surgery," *Transactions of the Institute of Measurement and Control,* vol. 25, pp. 309-327, 2003.

[16]   V. R. C. Kode, M. C. Cavusoglu, and M. T. Azar, "Design and characterization of a novel hybrid actuator using shape memory alloy and DC motor for minimally invasive surgery applications," 2006, pp. 416-420.

[17]   S. Sokhanvar, M. Ramezanifard, J. Dargahi, and M. Packirisamy, "Graphical rendering of localized lumps for MIS applications," *Journal of Medical Devices,* vol. 1, pp. 217- 224, 2007.

[18] M. Kalantari, M. Ramezanifard, J. Dargahi, and J. Kövecses, "3D Graphical Rendering of Localized Lumps and Arteries for Robotic Assisted MIS," *Journal of Medical Devices,* vol. 5, pp. 021002 (1-10), 2011.

[19] Q. Wang, F. Jaramillo, Y. Kato, L. Pinchuk, and R. T. Schoephoerster, "Hydrodynamic Evaluation of a Minimally Invasive Heart Valve in an Isolated Aortic Root Using a Modified In Vitro Model," *Journal of Medical Devices,* vol. 3, pp. 011002 (1-6), 2009.

[20] F. L. Hammond Iii, K. Shimada, and M. A. Zenati, "Measurement and Optimization of Minimally Invasive Intervention Device Design Fitness Using a Multiobjective Weighted Isotropy Index," *Journal of Medical Devices,* vol. 4, pp. 011002 (1-9), 2010.

[21] J. Dargahi, S. Najarian, R. Ramezanifard, and F. T. Ghomshe, "Fabrication and Testing of a Medical Surgical Instrument Capable of Detecting Simulated Embedded Lumps," *American Journal of Applied Sciences,* vol. 4, pp. 957-964, 2007.

[22] K. Miyaji, A. Furuse, J. Nakajima, T. Kohno, T. Ohtsuka, K. Yagyu, T. Oka, and S. Omata, "The Stiffness of Lymph Nodes Containing Lung Carcinoma Metastases," *Cancer,* vol. 80, pp. 1920-1925, 1997.

[23] A. P. Miller, W. J. Peine, J. S. Son, and Z. T. Hammoud, "Tactile Imaging System for Localizing Lung Nodules During Video Assisted Thoracoscopic Surgery," in *2007 IEEE International Conference on Robotics and Automation*, Roma, Italy, 2007, pp. 2996-3001.

[24] B. Kuebler, R. Gruber, C. Joppek, J. Port, G. Passig, J. H. Nagel, and G. Hirzinger, "Tactile feedback for artery detection in minimally invasive robotic surgery–preliminary results of a new approach," 2009, pp. 299-302.

[25] A. Bonakdar, J. Dargahi, and R. Bhat, "Investigations on the grasping contact analysis of biological tissues with applications in minimally invasive surgery," *American Journal of Applied Sciences,* vol. 4, pp. 1016-1023, 2007.

[26] T. Hemsel, R. Stroop, D. Oliva Uribe, and J. Wallaschek, "Resonant vibrating sensors for tactile tissue differentiation," *Journal of Sound and Vibration,* vol. 308, pp. 441-446, 2007.

[27] C. Bonomo, P. Brunetto, L. Fortuna, P. Giannone, S. Graziani, and S. Strazzeri, "A Tactile Sensor for Biomedical Applications Based on IPMCs," *Sensors Journal, IEEE,* vol. 8, pp. 1486-1493, 2008.

[28] P. Dario, M. Carrozza, L. Lencioni, B. Magnani, and S. D'attanasio, "A microrobotic system for colonoscopy," in *Proceeding of the IEEE International Conference on Robotic and Automation*, 1997, pp. 1567-1572 vol. 2.

[29] A. Golpaygani, S. Najarian, and G. Emamieh, "Design and modeling of a new tactile sensor based on membrane deflection," *Amer. J. Appl. Sci,* vol. 4, pp. 813-819, 2007.

[30] H. B. Muhammad, C. M. Oddo, L. Beccai, M. J. Adams, M. C. Carrozza, D. W. Hukins, and M. C. Ward, "Development of a Biomimetic Mems Based Capacitive Tactile Sensor," *Procedia Chemistry,* vol. 1, pp. 124-127, 2009.

[31] S. Sokhanvar, M. Packirisamy, and J. Dargahi, "A Multifunctional PVDF-Based Tactile Sensor for Minimally Invasive Surgery," *Smart materials and structures,* vol. 16, pp. 989-998, 2007.

[32] J. Dargahi, "An endoscopic and robotic tooth-like compliance and roughness tactile sensor," *Journal of mechanical design,* vol. 124, pp. 576-582, 2002.

[33] K. Miyaji, S. Sugiura, H. Inaba, S. Takamoto, and S. Omata, "Myocardial tactile stiffness during acute reduction of coronary blood flow," *The Annals of thoracic surgery,* vol. 69, pp. 151-155, 2000.

[34] M. H. Lee and H. R. Nicholls, "Review Article Tactile sensing for mechatronics—a state of the art survey," *Mechatronics,* vol. 9, pp. 1-31, 1999.

[35] P. Dario, "Tactile sensing: Technology and applications," *Sensors and Actuators A: Physical,* vol. 26, pp. 251-256, 1991.

[36] M. H. Lee, "Tactile sensing: new directions, new challenges," *International Journal of Robotics Research,* vol. 19, pp. 636-643, 2000.

[37] W. Schiff and E. Foulke, *Tactual perception: a sourcebook*: Cambridge University Press, 1982.

[38] R. Fearing, G. Moy, and E. Tan, "Some basic issues in teletaction," 1997, pp. 3093-3099 vol. 4.

[39] Y. Bar-Cohen and C. L. Breazeal, *Biologically inspired intelligent robots*: SPIE Press, 2003.

[40] R. S. Johansson and A. B. Vallbo, "Tactile sensibility in the human hand: relative and absolute densities of four types of mechanoreceptive units in glabrous skin," *The Journal of physiology,* vol. 286, pp. 283-300, 1979.

[41] E. R. Kandel, J. H. Schwartz, and T. M. Jessell, *Principles of neural science*: McGraw-Hill, Health Professions Division, 2000.

[42] P. Elsner, *Bioengineering of the skin: skin biomechanics*: CRC Press, 2002.

[43] M. Gentilucci, I. Toni, E. Daprati, and M. Gangitano, "Tactile input of the hand and the control of reaching to grasp movements," *Experimental brain research,* vol. 114, pp. 130-137, 1997.

[44] D. G. Caldwell, N. Tsagarakis, and C. Giesler, "An integrated tactile/shear feedback array for stimulation of finger mechanoreceptor," 1999, pp. 287-292 vol. 1.

[45] G. Moy, U. Singh, E. Tan, and R. S. Fearing, "Human psychophysics for teletaction system design," *Haptics-e,* vol. 1, pp. 1-20, 2000.

[46] K. A. Kaczmarek, J. G. Webster, P. Bach-y-Rita, and W. J. Tompkins, "Electrotactile and vibrotactile displays for sensory substitution systems," *Biomedical Engineering, IEEE Transactions on,* vol. 38, pp. 1-16, 1991.

[47] H. Z. Tan, M. A. Srinivasan, B. Eberman, and B. Cheng, "Human factors for the design of force-reflecting haptic interfaces," *Dynamic Systems and Control,* vol. 55, pp. 353-359, 1994.

[48] A. Bicchi, E. P. Scilingo, and D. De Rossi, "Haptic discrimination of softness in teleoperation: the role of the contact area spread rate," *Robotics and Automation, IEEE Transactions on,* vol. 16, pp. 496-504, 2000.

[49] B. B. Edin and A. Vallbo, "Stretch sensitization of human muscle spindles," *The Journal of physiology,* vol. 400, p. 101, 1988.

[50] B. B. Edin and Å. B. VALLBO, "Twitch contraction for identification of human muscle afferents," *Acta physiologica scandinavica,* vol. 131, pp. 129-138, 1987.

[51] B. B. Edin and J. H. Abbs, "Finger movement responses of cutaneous mechanoreceptors in the dorsal skin of the human hand," *Journal of Neurophysiology,* vol. 65, pp. 657-670, 1991.

[52] B. B. Edin, *Classification of muscle stretch receptor afferents in humans*: Univ., 1988.

[53] K. R. Boff, L. Kaufman, and J. P. Thomas, *Handbook of Perception and Human Performance: Sensory processes and perception*: Wiley, 1986.

[54] Å. B. Vallbo and R. Johansson, "Properties of cutaneous mechanoreceptors in the human hand related to touch sensation," *Human Neurobiology,* vol. 3, pp. 3-14, 1984.

[55] R. S. Johansson and A. Vallbo, "Skin mechanoreceptors in the human hand: an inference of some population properties," *Sensory functions of the skin in primates,* vol. 171, p. 185, 1976.

[56] R. S. Johansson and A. B. Vallbo, "Tactile sensory coding in the glabrous skin of the human hand," *Trends in Neurosciences,* vol. 6, pp. 27-32, 1983.

[57] A. B. Vallbo and R. Johansson, "The tactile sensory innervation of the glabrous skin of the human hand," *Active touch,* vol. 2954, pp. 29-54, 1978.

[58] R. S. Johansson, *Tactile sensibility in man: a quantitative study of the population of mechanoreceptive units in the glabrous skin area of the hand*, 1978.

[59] K. J. Rebello, "Applications of MEMS in surgery," *Proceedings of the IEEE,* vol. 92, pp. 43-55, 2004.

[60] A. Cuschieri, G. Buess, and J. Périssat, *Operative manual of endoscopic surgery* vol. 2: Springer-Verlag, 1994.

[61] M. Qasaimeh, J. Dargahi, M. Kahrizi, and M. Packirisamy, "Design and analysis of tactile optical sensor for endovascular surgery," in *Photonics North 2007 conference*, Ottawa, Canada, 2007, p. 67960J.

[62] X. Wang, "Biosystem II: Neuroscience, Sensory Systems, Lecture 2," ed, 2007, p. Mechanoreceptors vary in the receptive field (RF) size and their distributions.

[63] J. S. Son, M. R. Cutkosky, and R. D. Howe, "Comparison of contact sensor localization abilities during manipulation," *Robotics and autonomous systems,* vol. 17, pp. 217-233, 1996.

[64] J. Dargahi, N. P. Rao, and S. Sokhanvar, "Design and microfabrication of a hybrid piezoelectric-capacitive tactile sensor," *Sensor Review,* vol. 26, pp. 186-192, 2006.

[65] M. A. Qasaimeh, S. Sokhanvar, J. Dargahi, and M. Kahrizi, "A Micro-Tactile Sensor for In Situ Tissue Characterization in Minimally Invasive Surgery," *Biomedical Microdevices,* vol. 10, pp. 823-837, 2008.

[66] M. A. Qasaimeh, S. Sokhanvar, J. Dargahi, and M. Kahrizi, "PVDF-Based Microfabricated Tactile Sensor for Minimally Invasive Surgery," *Microelectromechanical Systems, Journal of,* vol. 18, pp. 195-207, 2009.

[67] S. Sokhanvar, M. Packirisamy, and J. Dargahi, "MEMS Endoscopic Tactile Sensor: Toward In-Situ and In-Vivo Tissue Softness Characterization," *Sensors Journal, IEEE,* vol. 9, pp. 1679-1687, 2009.

[68] A. Atieh, M. Kalantari, R. Ahmadi, J. Dargahi, M. Packirisamy, and M. H. Zadeh, "FEM Analysis of the Interaction Between a Piezoresistive Tactile Sensor and Biological Tissues," in *International Conference on Bioinformatics,*

Computational Biology and Biomedical Engineering, Amsterdam, Netherlands, 2011, pp. 106-110.

[69] A. Atieh, R. Ahmadi, M. Kalantari, J. Dargahi, and M. Packirisamy, "A Piezoresistive Based Tactile Sensor for Use in Minimally Invasive Surgery," in *IEEE 37th Annual Northeast Bioengineering Conference (NEBEC) 2011*, Troy, NY, 2011, pp. 1-2.

[70] H. Qi, K. Joyce, and M. Boyce, "Durometer hardness and the stress-strain behavior of elastomeric materials," *Rubber chemistry and technology,* vol. 76, pp. 419-435, 2003.

[71] D. Hertz and A. Fairnella, "Shore A Durometer and Engineering Properties," in *Fall Technical Meeting of The New York Rubber Group*, 1998, pp. 1-13.

[72] S. Omata and Y. Terunuma, "Development of new type tactile sensor for detecting hardness and/or softness of an object like the human hand," in *Solid-State Sensors and Actuators*, 1991, pp. 868-871.

[73] R. Bajcsy, "Shape from touch," *Advances in automation and robotics,* vol. 1, pp. 209-258, 1985.

[74] P. T. Moseley and A. J. Crocker, *Sensor materials*: Institute of Physics Pub., 1996.

[75] A. S. Morris, *Measurement and instrumentation principles*: A Butterworth-Heinemann Title, 2001.

[76] R. B. Northrop, *Introduction to instrumentation and measurements*: CRC Press, 1997.

[77] K. Uchino and J. R. Giniewicz, *Micromechatronics* vol. 1: Marcel Dekker, CRC Press, 2003.

[78] J. G. Webster, *Tactile sensors for robotics and medicine*: Wiley, 1988.

[79] S. Najarian, J. Dargahi, and A. A. Mehrizi, *Artificial tactile sensing in biomedical engineering*: McGraw-Hill, 2009.

[80] O. Lindahl, S. Omata, and K. Ängquist, "A tactile sensor for detection of physical properties of human skin in vivo," *Journal of medical engineering & technology,* vol. 22, pp. 147-153, 1998.

[81] S. Omata and Y. Terunuma, "New tactile sensor like the human hand and its applications," *Sensors and Actuators A: Physical,* vol. 35, pp. 9-15, 1992.

[82] T. Salo, K. U. Kirstein, T. Vancura, and H. Baltes, "CMOS-based tactile sensor for coronary artery identification," in *The 13th International Conference on Solid-State Sensors, Actuators and Microsystems*, Seoul, Korea, 2005, pp. 239-242

[83] A. T. Golpaygani, S. Najarian, and M. Movahedi, "Tactile Sensor for Robotic Applications," in *IFMBE Proceedings World Congress on Medical Physics and Biomedical Engineering*, Munich, Germany, 2009, pp. 2299-2302.

[84] R. M. Crowder, "Sensors: Touch, force, and torque," *Handbook of Industrial Automation, RL Shell and EL Hall, Editors,* pp. 377-392, 2000.

[85] W. Hyper-Librarian. (1996). *OPTICAL SENSOR TECHNOLOGIES*. Available: http://www.wtec.org/loyola/opto/c6_s3.htm

[86] R. Ahmadi, J. Dargahi, M. Packirisamy, and R. Cecere, "A new MRI-compatible optical fiber tactile sensor for use in minimally invasive robotic surgery systems," in *Fourth European Workshop on Optical Fibre Sensors*, Porto, Portugal 2010, p. 76532Z.

[87] www.ee.buffalo.edu/faculty/paololiu/566/sensors.ppt, ed.

[88] M. A. Y. Qasaimeh, "Polyvinylidene fluoride-based MEMS tactile sensor for minimally invasive surgery," M.A.Sc. MR40920, Concordia University (Canada), Canada, 2008.

[89] J. S. Wilson, *Sensor technology handbook*: Elsevier, 2005.

[90] A. Wisitsoraat, V. Patthanasetakul, T. Lomas, and A. Tuantranont, "Low Cost Thin Film Based Piezoresistive MEMS Tactile Sensor," *Sensors and Actuators A: Physical,* vol. 139, pp. 17-22, 2007.

[91] J. Engel, J. Chen, and C. Liu, "Development of polyimide flexible tactile sensor skin," *Journal of Micromechanics and Microengineering,* vol. 13, pp. 359-366, 2003.

[92] J. Engel, J. Chen, Z. Fan, and C. Liu, "Polymer micromachined multimodal tactile sensors," *Sensors and Actuators A: Physical,* vol. 117, pp. 50-61, 2005.

[93] J. Fraden, *Handbook of modern sensors: physics, designs, and applications*, 2nd ed.: American Institute of Physics, 1997.

[94] R. Ahmadi, J. Dargahi, M. Packirisamy, and R. Cecere, "A new hybrid catheter-tip tactile sensor with relative hardness measuring capability for use in catheter-based heart surgery," in *Sensors IEEE*, Kona, HI, 2010, pp. 1592-1595.

[95] T. Lomas, A. Tuantranont, and F. Cheevasuvit, "Micromachined Piezoresistive Tactile Sensor Array Fabricated by Bulk-Etched MUMPs Process," in *2003 International Symposium on Circuits and Systems (ISCAS '03)*, 2003, pp. IV-856-IV-859.

[96] J. G. da Silva, A. A. de Carvalho, and D. D. da Silva, "A strain gauge tactile sensor for finger-mounted applications," *IEEE Transactions on Instrumentation and Measurement,* vol. 51, pp. 18-22, 2002.

[97] M. Mehta, "A micromachined capacitive pressure sensor for use in endoscopic surgery," M.A.S.c, School of Engineering Science, Simon Fraser. University, 1996.

[98] F. Y. Obana, A. A. Carvalho, R. Gualda, and J. G. Da Silva, "A semiconductor strain gage tactile transducer," in *Proceedings of the 18th IEEE Instrumentation and Measurement Technology Conference (IMTC)*, Budapest , Hungary 2001, pp. 429-432

[99] I. Barman and S. K. Guha, "Analysis of a New Combined Stretch and Pressure Sensor for Internal Nodule Palpation," *Sensors and Actuators A: Physical,* vol. 125, pp. 210-216, 2006.

[100] M. Shikida, T. Shimizu, K. Sato, and K. Itoigawa, "Active Tactile Sensor for Detecting Contact Force and Hardness of an Object," *Sensors and Actuators A: Physical,* vol. 103, pp. 213-218, 2003.

[101] M. Kalantari, M. Ramezanifard, R. Ahmadi, J. Dargahi, and J. Kovecses, "Design, fabrication, and testing of a piezoresistive hardness sensor in minimally invasive surgery," in *IEEE Haptics Symposium*, Waltham, MA 2010, pp. 431-437.

[102] J. Dargahi, "A piezoelectric tactile sensor with three sensing elements for robotic, endoscopic and prosthetic applications," *Sensors and Actuators A: Physical,* vol. 80, pp. 23-30, 2000.

[103] B. L. Gray and R. S. Fearing, "A surface micromachined microtactile sensor array," in *Proceedings IEEE International Conference on Robotics and Automation*, Minneapolis, MN , USA 1996, pp. 1-6.

[104] R. R. Reston and E. S. Kolesar, "Robotic tactile sensor array fabricated from a piezoelectric polyvinylidene fluoride film," in *Proceedings of the IEEE National Aerospace and Electronics Conference (NAECON)*, Dayton, OH , USA, 1990, pp. 1139-1144.

[105] N. Narayanan, A. Bonakdar, J. Dargahi, M. Packirisamy, and R. Bhat, "Design and analysis of a micromachined piezoelectric sensor for measuring the viscoelastic properties of tissues in minimally invasive surgery," *Smart materials and structures,* vol. 15, pp. 1684-1690, 2006.

[106] M. Ohka, Y. Mitsuya, S. Takeuchi, H. Ishihara, and O. Kamekawa, "A three-axis optical tactile sensor (fem contact analyses and sensing experiments using a large-sized tactile sensor)," in *Proceedings IEEE International Conference on Robotics and Automation*, Nagoya , Japan 1995, pp. 817-824.

[107] J. J. Clark, "A magnetic field based compliance matching sensor for high resolution, high compliance tactile sensing," 1988, pp. 772-777 vol. 2.

[108] J. M. Engel, J. Chen, C. Liu, and D. Bullen, "Polyurethane rubber all-polymer artificial hair cell sensor," *Microelectromechanical Systems, Journal of,* vol. 15, pp. 729-736, 2006.

[109] M. Kalantari, M. Ramezanifard, R. Ahmadi, J. Dargahi, and J. Kövecses, "A piezoresistive tactile sensor for tissue characterization during catheter-based cardiac surgery," *The International Journal of Medical Robotics and Computer Assisted Surgery,* 2011.

[110] K. S. Ryu, X. Wang, K. Shaikh, and C. Liu, "A method for precision patterning of silicone elastomer and its applications," *Microelectromechanical Systems, Journal of,* vol. 13, pp. 568-575, 2004.

[111] L. Wang, T. Ding, and P. Wang, "Effects of Compression Cycles and Precompression Pressure on the Repeatability of Piezoresistivity for Carbon Black Filled Silicone Rubber Composite," *Journal of Polymer Science Part B: Polymer Physics,* vol. 46, pp. 1050-1061, 2008.

[112] W. J. Lee, J. H. Son, N. H. Kang, I. M. Park, and Y. H. Park, "Finite-Element Analysis of Deformation Behaviors in Random-Whisker-Reinforced Composite," *Scripta Materialia,* vol. 61, pp. 580-583, 2009.

[113] X. W. Zhang, Y. Pan, Q. Zheng, and X. S. Yi, "Time Dependence of Piezoresistance for the Conductor Filled Polymer Composites," *Journal of Polymer Science Part B: Polymer Physics,* vol. 38, pp. 2739-2749, 2000.

[114] R. S. Hall, G. T. Desmoulin, and T. E. Milner, "A Technique for Conditioning and Calibrating Force-Sensing Resistors for Repeatable and Reliable Measurement of Compressive Force," *Journal of biomechanics,* vol. 41, pp. 3492-3495, 2008.

[115] M. Kalantari, J. Dargahi, J. Kövecses, M. Ghanbari, and S. Nouri, "A New Approach for Modeling Piezoresistive Force Sensors Based on Semiconductive Polymer Composites," *IEEE/ASME Trans. Mechatron,* vol. PP, pp. 1–10, 2011.

[116] V. Laukhin, V. Lebedev, E. Laukhina, C. Rovira, and J. Veciana, "Piezoresistive biocompatible membranes for flexible pressure sensors," 2011, pp. 2694-2697.

[117] G. R. Ruschau, S. Yoshikawa, and R. E. Newnham, "Resistivities of Conductive Composites," *Journal of applied physics,* vol. 72, pp. 953-959, 1992.

[118] J. H. Constable, "Analysis of the Constriction Resistance in an ACF Bond," *Components and Packaging Technologies, IEEE Transactions on,* vol. 29, pp. 494-501, 2006.

[119] http://en.wikipedia.org/wiki/File:Asperities.svg, ed.

[120] A. Ranga, R. Mongrain, Y. Biadilah, and R. Cartier, "A Compliant Dynamic FEA Model of the Aortic Valve," in *12th IFToMM World Congress*, Besançon, France, 2007.

[121] J. Vossoughi, "Determination of Mooney Material Constants for Highly Nonlinear Isotropic Incompressible Materials Under Large Elastic Deformations," *Experimental Techniques,* vol. 19, pp. 24-27, 1995.

[122] C. Multiphysics, "Structural Mechanics Module User's Guide," ed, 2007, pp. 5-190.

[123] R. W. Ogden, *Non-Linear Elastic Deformations*: Dover Pubns, 1997.

[124] A. N. Gent, *Engineering with rubber: How to design rubber components*, 2nd ed.: Hanser Gardner Pubns, 2001.